NASA-CR-191771

The University of Michigan

Space Physics Research Laboratory

Ann Arbor, MI 48109

STUDIES OF DYNAMIC PROCESSES RELATED TO ACTIVE EXPERIMENTS IN SPACE PLASMAS

FINAL REPORT

GRANT: NAGW 2055

National Aeronautics and Space Administration

Washington, D.C.

For the Period:

1 August 1990 - 30 September 1992

Peter M. Banks

Principal Investigator

Torsten Neubert

Associate Investigator

SUMMARY: This is the final report for grant NAGW 2055, "Studies of Dynamic Processes Related to Active Experiments in Space Plasmas", covering research performed at the University of Michigan in the period August 1, 1990 to September 30, 1992. The grant is a continuation of grant NAGW 1566, which was awarded to the group while located at Stanford University. The grant was awarded to study (a) Theoretical and data analysis of data from the CHARGE-2 rocket experiment (1keV; 1-46 mA electron beam ejections) and the Spacelab-2 shuttle experiment (1keV; 100 mA), (b) studies of the

THE UNIVERSITY OF MICHIGAN
SPACE PHYSICS RESEARCH LABORATORY
COLLEGE OF ENGINEERING
DEPARTMENT OF ATMOSPHERIC, OCEANIC AND SPACE SCIENCES
SPACE RESEARCH BUILDING
2455 HAYWARD STREET
ANN ARBOR, MICHIGAN 48109-2143

313-936-7775
313-763-5567 (FAX)
9102407554 (TELEX)

18 January 1993

Dr. Mary Mellott
Code SSI
NASA/Headquarters
600 Independence Avenue
Washington, DC 20546

Re: Grant: NAGW 2055

Dear Dr.Mellott:

On behalf of Peter Banks and Torsten Neubert and to fulfill the requirements for the grant NAGW 2055 entitled " Studies of Dynamic Processes Related To Active Experiments In

itform, with the ambient
nputer simulation model,
eturn currents observed
consistent model for the
ized plasma and for the
were essentially finished
of Michigan. Our main
n of electron beams with
ed return fluxes to the
at the Beam Atmosphere
ol to determine not only
nts and optical emissions
el is currently used in the
th Particle Accelerators)
omagnetic and relativistic
n with Professor Oscar
versity of Iowa. The code
ics of an electron beam
f Cherenkov radiation in
lation of a plasma cloud
nd CRIT releases. This is
s. The simulations show
oud to very high energies,
as been used to study the
lar wind flow across the
features of the Earth's
ent system, the cusp, and

1. Introduction

The grant NAGW 2055 substituted NAGW 1566 when the PI and his collaborators moved from Stanford University to the University of Michigan. The period covered in this report correspond to the time at the University of Michigan namely August 1, 1990 to September 30, 1992. This period includes a one year no cost extension.

The work under this grant "Studies of Dynamic Processes Related to Active Experiments in Space Plasmas" has covered modeling and data analysis of electron beam ejections form the CHARGE-2 sounding rocket experiment (1 keV, 1-46 mA) and the Spacelab-2 experiment (1 keV, 100 mA), studies of the dynamics and radiation from plasma clouds ejected into ambient magnetized plasmas, and studies of radiation from tethered spacecraft systems. At the time of the move to Michigan, the tethered studies were completed along with the data analysis of CHARGE-2 data. Also completed was a two-stream model for the interaction of electron beams with the Earth's neutral atmosphere.

During our time at the University of Michigan, the two-stream model was applied to a range of situations, studying the effects of secondary electron fluxes on spacecraft charging, density enhancements and optical emissions in the beam column, and electron energy spectral variations with altitude. To extend the beam studies, a 3-D electromagnetic and relativistic particle code was developed. With the code we have simulated the dynamics and the radiation of an electron beam, for the first time in 3-D with a fully electromagnetic code (to our knowledge). In addition, we embarked on a study of plasma clouds propagating across a magnetic field, inspired by CRIT and CRRES results. More details on our work is given in the sections below.

2. The Beam Atmosphere Interaction

The Beam Atmosphere Interaction (BAI) has been studied by means of a two-stream code. The code solves two first-order, non-linear differential equations in the differential energy flux of particles streaming along a magnetic field. The equations couple the forward and backward fluxes, and model the transport, secondary electron generation, and the cascading in energy of primary and secondary electrons. The code has been successful in modeling the return current contribution to the CHARGE-2 rocket resulting from secondary and back scattered primary beam electrons. CHARGE-2 is the first experiment that has allowed an accurate measurement of the BAI return current contributions. The good agreement between model and observations indicate that we have a good understanding of the BAI process.

The model also produces optical emission rates, plasma density enhancements, and the energy spectrum of electrons inside the beam column as a function of altitude. This has proved very useful in the SEPAC experiment flown on the ATLAS-1 mission. One of the objectives was to generate artificial aurora by a beam ejected from the shuttle and observed by cameras in the shuttle bay. The optical emissions observed in the upper atmosphere as a result of beam ejections are currently being modeled with the code.

Our BAI results as well as other advances in the field over the past decade was published in a comprehensive review paper [Neubert and Banks, 1992]. It is included in the appendix.

3. The 3-D Particle Code

To further study the electromagnetic radiation and the dynamics of electron beams, a 3-D electromagnetic and relativistic particle code was developed. As a new feature "quiet start" conditions were approached by including the poloidal magnetic field due to the current carried by the beam electrons streaming along a background magnetic field. The complex structure of the whistler mode waves in the vicinity of the beam suggest that the transverse velocity (gyration) of the beam electrons, generated as a result of Langmuir space charge oscillations, is involved in the generation of the whistler mode. A paper describing these initial results has been submitted to Geophysical Research Letters [Nishikawa et al., 1992]. The manuscript is included in the appendix.

The code has also been applied to the problem of plasma clouds ejected across a magnetic field. The motivation was here the recent CRRES and CRIT releases. With the full 3-D configuration, it was possible to study the formation of charge layers at the sides of the cloud, and on the front and rear surfaces of the cloud, and the expansion of these layers along the magnetic field into the ambient plasma. It was found that the electrons accelerated out of the charge layers may reach very high energies and directly generate optical emission in the upper atmosphere (aurora). Results on the dynamics of plasma clouds and the electromagnetic radiation from such clouds was published in Journal of Geophysical Research [Neubert et al., 1992]. The paper is included in the appendix.

Finally the code was used to simulate a plasma flowing over a magnetic dipole, analogous to the solar wind flowing past the Earth's magnetic field. The results show the formation of a bow shock an extended tail, the Chapman-Ferraro current systems, and the penetration of solar wind particles into the cusp regions. The paper will be published in IEEE transactions on Plasma Science [Bunerman et al., 1993]. It is included in the appendix.

4. Publications

Under NAGW 2055:

Neubert, T., and P. M. Banks, Resent results from studies of electron beam phenomena in space plasmas, *Planet. Space Sci.*, *40*, 153, 1992.

Neubert, T., R. H. Miller, O. Buneman, and K.-I. Nishikawa, The dynamics of low-β plasma clouds as simulated by a 3-dimensional, electromagnetic particle code, *J. Geophys. Res.*, *97*, 12057, 1992.

Buneman, O., T. Neubert, and K. -I. Nishikawa, Solar wind-magnetosphere interaction as simulated by a 3D, EM particle codes, *IEEE Trans. Plasma Sci.*, *in press*, 1992.

Nishikawa, K.-I., O. Buneman, and T. Neubert, Simulation studies of electron beam-driven instabilities by 3-D electromagnetic particle codes, *J. Geophys. Res.*, *submitted*, 1992.

Under NAGW 1566:

Donohue, D. J., T. Neubert, and P. M. Banks, Estimating radiated power from a conducting tethered satellite system, *J. Geophys. Res.*, *96*, 21245, 1991.

Neubert, T., S. Sasaki, B. E. Gilchrist, P. M. Banks, P. R. Williamson, A. C. Fraser-Smith, and W. J. Raitt, Observation of plasma wave turbulence generated around large ionospheric spacecraft: Effects of motionally induced EMF and of electron beam emission, *J. Geophys. Res.*, *96*, 9639, 1991.

Neubert, T., P. M. Banks, B. E. Gilchrist, A. C. Fraser-Smith, P. R. Wiliamson, W. J. Raitt, N. B. Myers, and S. Sasaki, Modification of spacecraft charging and the near-plasma environment caused by the interaction of an artificial electron beam with the earth's upper atmosphere, *Proceedings of Spacecraft Charging Technology Conference, Monterey, October 1989*, R. C. Olsen Ed., 1991.

Neubert, T., and P. M. Banks, Plasma density enhancements created by the ionization of the Earth's upper atmosphere by artificial electron beams, *AGARD Conference Proceedings, No 485*, pp. 21-1-22-6, *Bergen, Norway*, 1990.

Neubert, T., P. M. Banks, B. E. Gilchrist, A. C. Fraser-Smith, P. R. Williamson, W. J. Raitt, N. B. Myers, and S. Sasaki, The interaction of an artificial electron beam with the earth's upper atmosphere: Effects on spacecraft charging and the near-plasma environment, *J. Geophys. Res.*, *95*, 12209, 1990.

Neubert, T., M. J. Mandell, B. E. Gilchrist, P. M. Banks, P. R. Williamson, W. J. Raitt, N. B. Myers, S. Sasaki, K. Oyama, and I. Katz, The sheath structure around a negatively charged rocket payload, *J. Geophys. Res., 95*, 6155, 1990.

Gilchrist, B. E., P. M. Banks, T. Neubert, P. R. Williamson, N. B. Myers, and W. J. Raitt, Electron collection enhancement arising from neutral gas jets on a charged vehicle in the ionosphere, *J. Geophys. Res., 95*, 2469, 1990.

Myers, N. B., W. J. Raitt, B. E. Gilchrist, P. M. Banks, T. Neubert, P. R. Williamson, and S. Sasaki, A comparison of current-voltage relationships of collectors in the earth's ionosphere with and without electron beam emission, *Geophys., Res. Lett., 16*, 365-368, 1989.

5. Presentations

Neubert, T., R. H. Miller, O. Buneman, K.-I. Nishikawa, and R. Roussel-Dupre, The dynamics of finite-sized, low-b plasma clouds injected at an angle to a background magnetic field, *AGU Fall meeting, San Francisco,* 1990.

Buneman, O., K.-I. Nishikawa, and T. Neubert, Interaction of solar wind and Earth's field as simulated by a 3-D particle code, *AGU Fall meeting, San Francisco,* 1990.

Neubert, T., Recent results of electron beam studies in space, *APEX experimenters meeting, Lipesk, Russia,* 1991.

Neubert, T., R. H. Miller, O. Buneman, K.-I. Nishikawa, and R. Roussel-Dupre, The dynamics of finite-sized, low-b plasma clouds injected at an angle to a background magnetic field, *ISSS-4, Nara, Japan,* 1991.

K.-I. Nishikawa, C. K. Goertz, O. Buneman, and T. Neubert, Simulation studies of the electron beam-driven instabilities by 3-D electromagnetic particle codes, *ISSS-4, Nara, Japan,* 1991.

Neubert, T., R. Miller, and O. Buneman, The Dynamics of low-β plasma clouds as simulated by 3-dimensional, electromagnetic particle code, *AGU Fall Meeting, San Francisco,* 1991.

Donohue, D. J., T. Neubert, and P. M. Banks, Estimating radiated power from a conducting tethered satellite system, *AGU Fall Meeting, San Francisco,* 1991.

Nishikawa, K.-I., O. Buneman, and T. Neubert, Simulation studies of the electron beam-driven instabilities by a 3-d electromagnetic particle code, *AGU Fall Meeting, San Francisco,* 1991.

Nishikawa, K.-I., O. Buneman, and T. Neubert, Simulation of electron beam-driven instabilities by a 3-D electromagnetic particle code, *International Conference on Plasma Physics, Innsbruck, June 29 - July 3*, 1992.

Nishikawa, K.-I., O. Buneman, and T. Neubert, Solar wind-magnetosphere interaction as simulated by a 3D, EM particle code, *Chapman Conference on Solar Wind Sources of Magnetospheric ULF Waves, Minnesota,Sep 14 - 18*, 1992.

Buneman, Neubert et al., Interaction of solar wind and Earth's field as simulated by a 3-D EM particle code, *AGU Fall meeting, San Francisco*, 1992.

Gilchrist, Neubert, et al., Spacecraft Potential Control by Neutral gas Release: Results from the CHARGE-2B electron beam rocket experiment, *AGU Fall meeting, San Francisco*, 1992.

APPENDIX
PUBLICATIONS UNDER NAGW 2055

RECENT RESULTS FROM STUDIES OF ELECTRON BEAM PHENOMENA IN SPACE PLASMAS

TORSTEN NEUBERT and PETER M. BANKS

Space Physics Research Laboratory, Department of Oceanic, Atmospheric and Space Science,
University of Michigan, Ann Arbor, MI 48109-2143, U.S.A.

Abstract— Experiments involving the ejection of beams of electrons from spacecraft have been performed for more than 2 decades in order to study fundamental plasma physical processes as well as for a range of diagnostic- and application-oriented purposes. This paper reviews some of the key issues that have been pursued in the past 10 years. These include questions regarding spacecraft charging and beam dynamics, the interaction of beams with neutral gas and plasmas, and the electromagnetic radiation generated by continuous and pulsed electron beams. It is shown how our understanding of these phenomena has matured, thereby providing a solid foundation for future experiments involving the use of electron beams.

1. INTRODUCTION

The Universe as we know it is made up of neutral and ionized matter permeated by gravitational and electromagnetic fields. It is highly dynamic and in constant change as manifested by the birth and death of stars. One of the fundamental processes that arises naturally out of this dynamic interaction between matter and fields is the generation of electric currents. As charged particles tend to flow in force-free directions, currents tend to be magnetic field-aligned in which case they are often called "Birkeland" currents after Professor Birkeland who first suggested such currents flow in the Earth's magnetosphere (Egeland and Leer, 1986). Their existence is now firmly established and it has been found that they are intimately connected to "inverted V" events, the generation of aurora, and the generation of electromagnetic radiation in the range from a few Hertz to many megahertz. It is also thought that Birkeland currents are of importance throughout the Universe on a variety of scales up to galactic scales (Faelthammar, 1986; Peratt, 1986, 1988, 1990). It is therefore not surprising that the scientific community has shown considerable interest in performing space experiments which involve the ejection of electron beams and the formation of artificially generated currents. These so-called "active experiments" allow the study of fundamental plasma physical processes, thereby gaining quantitative information that is almost impossible to obtain when observing natural phenomena. With active experiments, the charged particle source (e.g. the electron beam) characteristics are known and provide a specific stimulus to the coupled response of electromagnetic fields and plasma. In many ways,

active experiments provide an important calibration of natural phenomena.

There are a variety of additional objectives that also motivated past space experiments with charged particle beams. These include the probing of the Earth's magnetic field on a global scale by recording the echo of particles mirroring in the conjugate hemisphere as done in the *ECHO* series of sounding rockets (Winckler *et al.*, 1989; Hallinan *et al.*, 1990), probing the local electric and magnetic field as done on *GEOS* 1 and 2 (Melzner *et al.*, 1978; Junginger *et al.*, 1984), and using pulsed electron beams as a means of generating electromagnetic radiation for purposes of communication between ionospheric spacecraft and receivers on conjugate spacecraft or on the Earth (e.g. Inan *et al.*, 1984).

However, experience has shown that there are many technical problems associated with the successful ejection of charged particle beams in space and the study of these has taken considerable effort. A foremost challenge has been the charging of spacecraft platforms as a result of charged particle beam ejection. As pointed out by Linson (1982), an isolated spherical conductor of 1 m diameter will charge at a rate of 9 V μs^{-1} when a beam of 1 mA is ejected and no return currents from the ambient plasma are collected. Because of this rapid charging rate, and its influence on processes in the plasma surrounding the beam source, it is important to undertake experiments and theoretical studies aimed at understanding and mitigating the processes associated with electrical charging of the beam-emitting platform. In doing so the goal is both scientific and technical. On the one hand, to design successful space experiments with a charged particle beam apparatus it is important to understand

the underlying physical processes linked with the beam emissions. On the other hand, it is also important to be able to achieve a high quality of the emitted charged particle beam for the purpose of probing nature with a beam of well-defined characteristics. The quest for such understanding involves an exciting body of basic physical processes, including the formation of large and complicated sheath regions of charged particle and electromagnetic field fluctuations, plasma–neutral gas interactions, wave-particle interactions within plasmas, and non-linear phenomena such as plasma wave turbulence, just to name a few.

In this paper it is our aim to review selected results of the 1980s and to discuss future directions of active electron beam experiments in space. More information on beam experiments is found in the review paper by Winckler (1980), the monograph by Grandal (1982), the special issue of *Advances in Space Research*, edited by Brenning and Mendillo (1990), the special issue of *Radio Science* (1984), and the European Space Agency report by Burke (1983).

The organization of this paper is as follows: in Section 2 some basic processes associated with electron beam emissions are discussed. These are spacecraft charging, including the phenomenon of super charging and virtual cathode formation, beam–atmosphere interaction (BAI), and beam system–plasma interaction (BSPI). Then, in Section 3 we discuss the theory for electromagnetic radiation from continuous and pulsed electron beams and relate some experimental results obtained from space shuttle and sounding rocket experiments. Finally in Section 4 we discuss the current status of electron beam experiments and point out future directions for the field.

2. BASIC PROCESSES

When an electron beam is ejected from a spacecraft, the spacecraft potential will rise, drawing return current electrons from the ambient plasma. For low potentials, space charge in the plasma is small and the electrons collected by the spacecraft are those whose trajectories directly intersect the spacecraft structure. For potentials well above the ambient plasma thermal energy, an extended region of positive space charge will develop around the spacecraft. Ambient electrons that enter this sheath have a chance of reaching the payload through the combined action of the highly inhomogeneous electric field in the sheath and the ambient magnetic field. Thus, the effective current collecting area of the spacecraft is enhanced by the space charge sheath, thereby increasing the collected current.

The electron thermal current density j_{e} in an equilibrium plasma is given by:

$$j_{ve} = en\langle v_e \rangle / 4, \qquad (1)$$

where e is the elementary charge, n the plasma density, and $\langle v_e \rangle$ the average electron velocity. In a Maxwellian plasma the expression for $\langle v_e \rangle$ is:

$$\langle v_e \rangle = (8kT/\pi m_e)^{1/2}, \qquad (2)$$

where kT is the electron energy and m_e the electron mass. The ion thermal current density and ion velocity are given by similar expressions. While the temperature of the ionospheric plasma is fairly constant and approximately the same for ions and electrons to within a factor of 2–3, the densities may vary many orders of magnitude. Typical values for the particle velocities and the peak densities encountered in the ionosphere and the corresponding current densities are given in Table 1.

The electron thermal current available to a sounding rocket payload at low potentials in the ionosphere is 2–10 mA m^{-2} depending on the plasma density and temperature. Beam experiments flown in the past have carried beam accelerators ejecting beams with currents up to several hundred milliampères and individual electron energies up to 40 keV. Since current collecting areas on such platforms are seldom more than a few square meters, such payloads have often reached high positive potentials.

For most applications it is essential that the beam escapes the nearby region of the spacecraft in a well-known and coherent manner, preferably with the full electron accelerator energy and small energy, spatial or temporal dispersion. In practice, observations and theoretical simulations indicate that beam emissions are accompanied by many dynamic charging processes, both of the platform, within the beam itself, and in the surrounding medium. Thus, platform charging and beam characteristics can have large dynamic fluctuations on time-scales of the order of plasma time periods (microseconds) and physical scales of the order of Debye lengths (millimeters). These micro-scale effects have the net consequence of d.c. charging of the spacecraft, reducing the beam escape current, degrading the average beam particle energy by an amount corresponding to the average spacecraft potential, and degrading the beam coherence.

A number of effects help to enhance the emitting platform return current above the limit set by ionospheric thermal current densities and thereby reduce platform charging. These effects are associated with interactions between the ambient plasma and any neutral gases surrounding the payload and the electron

TABLE 1.

kT (eV)	n (m^{-3})	$\langle v_e \rangle$ (m s^{-1})	$\langle v_i \rangle$ (m s^{-1})	j_{oe} (A m^{-2})	j_{oi} (A m^{-2})
0.1	5×10^{11}	2.1×10^5	1.2×10^3	4.2×10^{-1}	2.4×10^{-3}

beam and charged platform. Specific effects include beam–atmosphere interactions (BAI) and beam–system plasma interactions (BSPI). The neutral gases involved may be the ambient atmosphere, outgassing from the platform, or attitude control thruster emissions. By various processes, these gases can be ionized and thereby create enhanced plasma densities in the vicinity of the payload. This component of the return current is sometimes called the "active" component to distinguish it from the "passive" component which is the current drawn to an anode immersed in a plasma. The process identified as the beam–plasma discharge (BPD), investigated in many chamber experiments (Bernstein et al., 1979), is thought to occur in space at relatively low altitudes (110–160 km) (Linson, 1982) where the neutral gas density is relatively high. It will not be covered in this review.

2.1. Passive current collection

The problem of determining the current and potential existing between two concentric electrodes in an unmagnetized plasma was first discussed by Langmuir and Blodgett (1924). In their theory, an anode immersed in a plasma will develop a positive space-charge sheath out to a distance r_s, the sheath edge, where the potential reaches the ambient plasma potential. At the sheath edge, thermal electron fluxes enter the sheath from the ambient undisturbed plasma, and the potential structure in the sheath as well as the location of the sheath edge are calculated by considering current continuity and Poisson's equation. The mixed boundary conditions are the thermal current density at the sheath edge and the potential of the conducting bodies. From this theory the current to a probe is space-charge limited. Langmuir and Blodgett (1924) gave the expression for the current to a probe at a positive potential Φ_0 in the case of spherical symmetry and no magnetic field:

$$I_{sci} = 4\pi\varepsilon_0 (32e/81m_e)^{1/2} \Phi_0^{3/2} \alpha^{-2}, \tag{3}$$

where α is a geometrical parameter. It was assumed that the current was carried by electrons to an anode. If the probe sheath radius is much larger than the probe radius, r_p, the following expression was found for α:

$$\alpha^{3/4} = 1.11 r_s/r_p. \tag{4}$$

Since the current to the probe must equal the cur-

rent across the probe sheath, we also have:

$$I_{sci} = 4\pi r_s^2 j_{oe}. \tag{5}$$

Combining equations (3)–(5) we find:

$$I_{sci} = C_e j_{oe}^{3/7} (r_p \Phi_0)^{6/7}. \tag{6}$$

The expression for the ion current to a cathode is similar. For electrons the numerical value for C_e is 6.946×10^{-3}, and for O$^+$ ions C_i is 3.674×10^{-4}, with the parameters of the equation given in SI units.

The current given in equation (6) has been found for an unmagnetized plasma. This condition can be regarded as a rather good approximation when considering ion collection by a negatively biased payload because of the large ion Larmor radius. For example, an O$^+$ ion which has just entered the sheath and obtained the energy of 1 eV will already at that point have a Larmor radius of 13 m ($B = 0.44$ G) which usually is large compared with the sheath dimension. The ions can therefore be regarded as unmagnetized in the sheath region. Electrons are, however, limited by the magnetic field in their motion perpendicular to the field, and thus the electron current that can be collected is reduced compared with the values predicted by equation (6).

Theories extending the work of Langmuir and Blodgett (1924) for the case of beam-emitting spacecraft in the ionosphere was put forward by Beard and Johnson (1961) (without magnetic field) and Parker and Murphy (1967) (with magnetic field). Parker and Murphy included the magnetic field effects by using the conservation of energy and angular momentum of particles collected by a sphere. The upper limit of electron current collection according to their results is:

$$I/I_0 < 1 + [8e\Phi_0/(m_e\omega_{ce}^2 a^2)]^{1/2}, \tag{7}$$

where I_0 is the thermal electron current to the sphere at plasma potential, ω_{ce} is the electron gyrofrequency and a is the radius of the sphere.

The space-charge limited current for an unmagnetized plasma given in equation (6) increases as $\Phi^{6/7}$ while the magnetic-field limited current in equation (7) increases as $\Phi^{1/2}$. A consequence of this and of the differing dependence of system parameters appearing in the two expressions, the predicted current collection in the presence of a magnetic field is smaller than without a field as expected.

Studies have been made in the past decade in space and in laboratory plasma chambers to test the validity of the estimates given in equations (6) and (7). For space experiments this task is not as simple as one would imagine because of the difficulty in measuring the spacecraft potential accurately during beam emissions. As we will show later, the ejection of charged particle beams has the effect of generating a turbulent region with enhanced energetic particle fluxes in the vicinity of the spacecraft. These fluxes contaminate the potential measurements, which are usually performed by measuring the potential difference between the rocket body and smaller spheres mounted on booms extending from the rocket. Furthermore, in many cases the sheaths are of such dimensions that the length of the floating probe booms is smaller than the sheath radius and thus the potential measurement does not reflect the complete potential difference between the ambient plasma and the spacecraft. Recently however, a technique has been developed which uses two payloads connected by a conducting, insulated wire. The payloads are allowed to drift apart up to many hundreds of meters and the potential of the beam-emitting payload is measured with respect to the remote tethered payload located outside of the disturbed region.

Such a technique was used in the *CHARGE* series of sounding rocket experiments (Sasaki *et al.*, 1987, 1988; Myers *et al.*, 1990). The sheath formation and the ion current collection to a negatively charged payload was studied by applying a potential difference of up to 460 V between the two tethered payloads, the mother payload biased negative and the daughter payload biased positive. The potential of each payload relative to the ambient plasma was estimated by noting that the total current to the structure must equal zero. As a consequence, the ion current to the negative mother balanced the electron current to the positive daughter. Since the thermal ion current density in the plasma is much smaller than the electron current density (Table 1) the mother charged to a large negative potential while the daughter charged to a small positive potential. In other words, by far the most of the 460 V potential drop was found in the positive ion sheath surrounding the mother payload.

The data obtained in the *CHARGE*-2 experiment was compared with computer calculations by the NASCAP/LEO code (Mandell *et al.*, 1990; Neubert *et al.*, 1990a). The code, in essence, simulated the space-charge limited current and the corresponding sheath structure as given by the theory of Langmuir and Blodgett (1924). However, the advantage of the code is that the actual shape of the spacecraft can be modelled rather than assuming an equivalent sphere

or an infinite cylinder, as must be done when treating the problem analytically. Furthermore, the velocity of the spacecraft through the plasma could be included in the calculation. This is particularly important for ion-current collection since the spacecraft velocity is of the order of the ion thermal velocity and therefore significant wake and ram asymmetries are created in the ambient plasma density and the current collection. With the computer simulation it was also possible to estimate the effects of secondary electron emission caused by the bombardment of the rocket skin by incoming ions.

A contour plot of the sheath structure around the mother payload computed by the NASCAP/LEO code is shown in Fig. 1a and b for two values of the spacecraft potential: -30 and -200 V. The contour marked with the number 2 is the -2 V contour, which is basically the sheath edge. The length of the rocket is 3.26 m and the diameter is 44 cm. Four floating probes separated by 25 cm were mounted on a boom. The influence of these was also modelled by taking into account the internal resistance of the floating probe array. The probes can be seen at $z = 9$ extending outward from the rocket.

The return current characteristic of the mother payload as a function of rocket potential was determined from the measurement of the current in the tether with gradually increased bias potentials applied between the mother and the daughter. The results are shown in Fig. 2 for two such experiments performed at 244 and 247 km altitude. Also shown are the results of the NASCAP/LEO code which show very good agreement with observations.

The study of current collection and sheath formation of payloads at negative potentials led to the following conclusions:

(1) Magnetic field effects on the ion motion in the sheath could be ignored, as expected. The sheath structure and the current collection was close to the predictions of the theory of space-charge limited flow with modifications listed below.

(2) The velocity of the rocket had the effect of increasing the ion-current collection by as much as 40% at low potentials, decreasing to 15% at higher potentials (Mandell *et al.*, 1990). At the time of the experiments the rocket velocity was 580 m s^{-1}.

(3) Laboratory experiments on secondary electron yields arising from alkali metal ions impacting on aluminum oxidized surfaces show that significant numbers of secondary electrons are emitted for potentials above a threshold of 200 V and that the yield reaches 0.5 electrons per impacting ion at 400 V (Dietz and Sheffield, 1975). To the best of our knowledge,
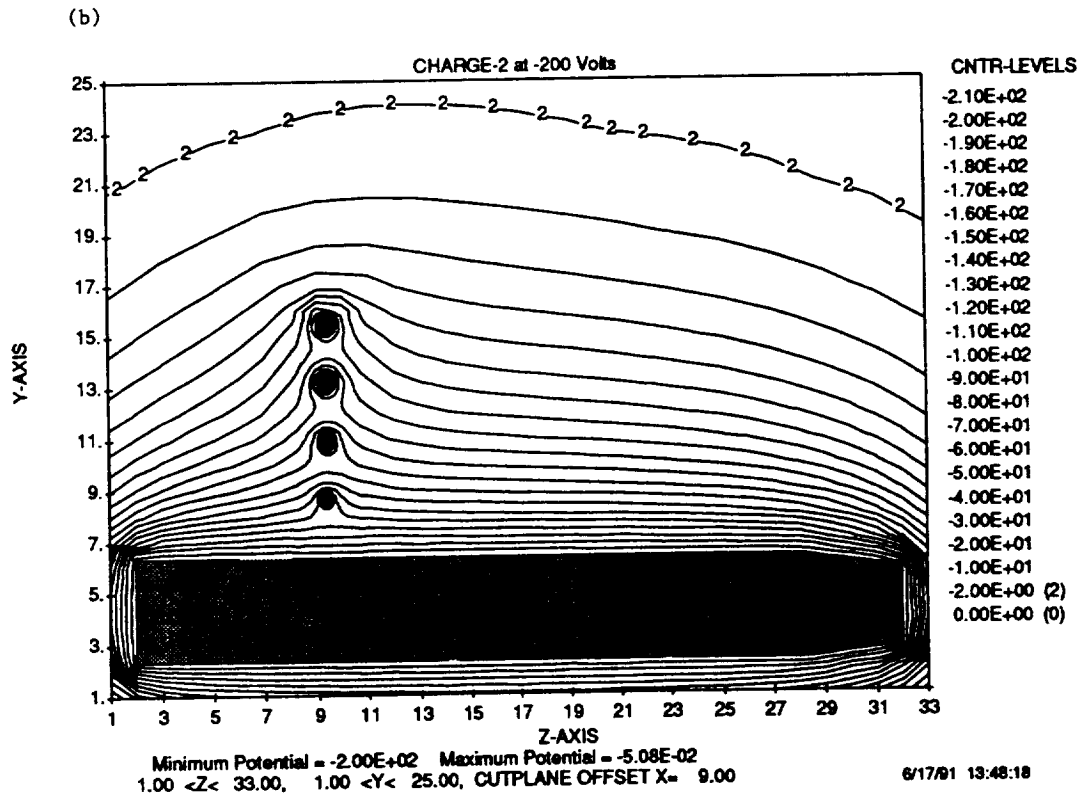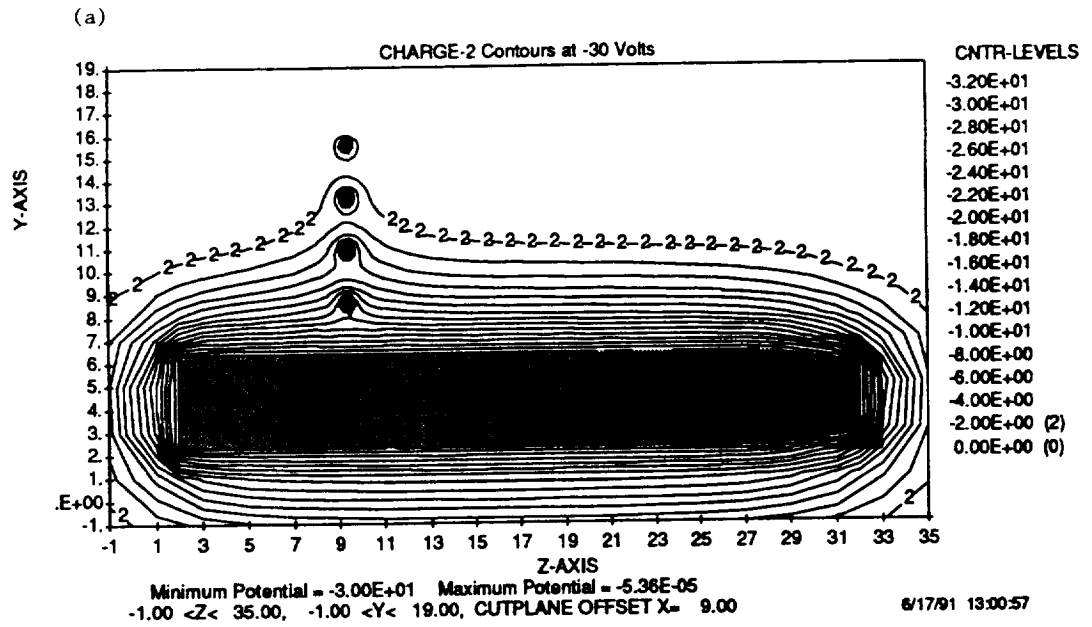
(a)

CHARGE-2 Contours at -30 Volts

CNTR-LEVELS

Y-AXIS

Z-AXIS

Minimum Potential = -3.00E+01   Maximum Potential = -5.36E-05
-1.00 <Z< 35.00,   -1.00 <Y< 19.00, CUTPLANE OFFSET X= 9.00

6/17/91 13:00:57

-3.20E+01
-3.00E+01
-2.80E+01
-2.60E+01
-2.40E+01
-2.20E+01
-2.00E+01
-1.80E+01
-1.60E+01
-1.40E+01
-1.20E+01
-1.00E+01
-8.00E+00
-6.00E+00
-4.00E+00
-2.00E+00 (2)
0.00E+00 (0)

(b)

CHARGE-2 at -200 Volts

CNTR-LEVELS

Y-AXIS

Z-AXIS

Minimum Potential = -2.00E+02   Maximum Potential = -5.08E-02
1.00 <Z< 33.00,   1.00 <Y< 25.00, CUTPLANE OFFSET X= 9.00

6/17/91 13:48:18

-2.10E+02
-2.00E+02
-1.90E+02
-1.80E+02
-1.70E+02
-1.60E+02
-1.50E+02
-1.40E+02
-1.30E+02
-1.20E+02
-1.10E+02
-1.00E+02
-9.00E+01
-8.00E+01
-7.00E+01
-6.00E+01
-5.00E+01
-4.00E+01
-3.00E+01
-2.00E+01
-1.00E+01
-2.00E+00 (2)
0.00E+00 (0)

FIG. 1. NASCAP/LEO SIMULATION OF THE POTENTIAL STRUCTURE AROUND THE *CHARGE*-2 MOTHER PAYLOAD WHEN BIASED TO (a) −30 V AND (b) −200 V.
The x and y axes are in units of 10.8 cm. The −2 V potential contour is marked with the number 2 (from Neubert *et al.*, 1990a).
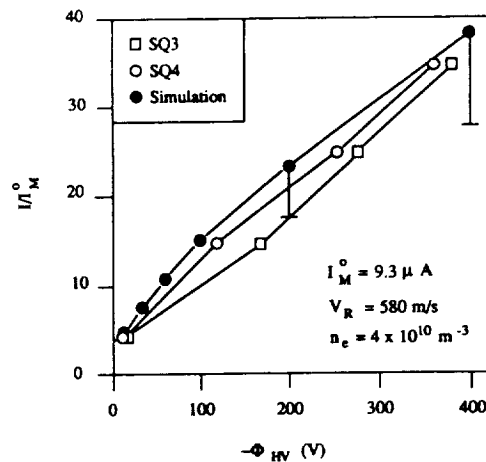
FIG. 2. THE ELECTRON RETURN CURRENT–PAYLOAD POTENTIAL CHARACTERISTIC OF THE *CHARGE*-2 MOTHER PAYLOAD (FROM NEUBERT *et al.*, 1990a).
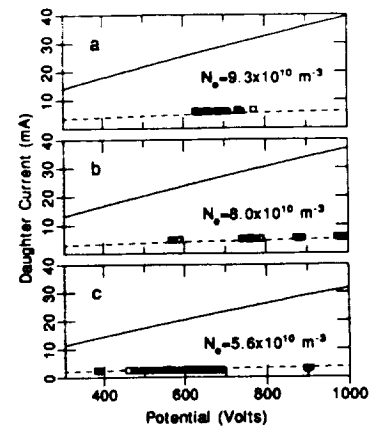
FIG. 3. CURRENT COLLECTION BY THE *CHARGE*-2 DAUGHTER PAYLOAD VS VEHICLE POTENTIAL COMPARED WITH : THE LANGMUIR AND BLODGETT MODEL (SOLID LINE) AND THE PARKER AND MURPHY MODEL (DASHED LINE) (FROM MYERS *et al.*, 1989).

no studies have been performed for O^+ ion beams bombarding oxidized metal surfaces. However, reports of other combinations of ion beams and surfaces indicate that the values given above are applicable to oxidized metal surfaces (Szapiro *et al.*, 1988; Szapiro and Rocca, 1989; Utterback and Miller, 1961; Hayden and Utterback, 1964; Amme, 1969). A review is given in Langley *et al.* (1984). The NASCAP LEO simulations and comparison with experimental data indicated that secondary electrons were emitted during the negative bias operations of *CHARGE*-2 roughly as predicted by laboratory data.

An electron beam source mounted on the *CHARGE*-2 mother payload emitted 1 keV electrons with currents up to 46 mA as measured by on-board diagnostics. The current–voltage characteristic of the daughter payload (electron collection at positive potential) was obtained for beam-emission sequences executed with low resistance in the tether circuit. Comparison of the observations and the theoretical estimates given by equations (6) and (7) was reported by Myers *et al.* (1989). The key results are shown in Fig. 3. The model estimates were found by approximating the short cylindrical daughter payload (44 cm diameter, 82 cm long) with an equivalent (equal area) sphere. As can be seen from the figure, the observed electron return current and the Parker and Murphy model estimates are in close agreement and substantially smaller than the Langmuir–Blodgett predictions.

With the assumption of current continuity (ejected current equals collected current) and beam escape, the

return current–voltage characteristic of the mother payload could also be determined. The observations were compared with the models of equations (6) and (7), again approximating the mother payload as an equivalent sphere. It was found that at high altitudes (above 240 km) the electron return current was again well below the estimate of Langmuir and Blodgett, but above the upper limit of Parker and Murphy (Myers *et al.*, 1989, 1990; Mandell *et al.*, 1990). At low altitudes, however, the return current increased above even the Langmuir and Blodgett model estimate. The reason for this is the increased influence of the ambient neutral atmosphere and the BAI process, to which we will return in the following subsection.

Mandell *et al.* (1990) studied the return current collection of the *CHARGE*-2 mother payload at high altitudes using the true shape of this body. These computer estimates were in better agreement with the observations than estimates based on the Parker and Murphy model. Mandell *et al.* concluded that the difference arose from the fact that the Parker and Murphy model assumes a spherical body. Thus, although the daughter payload was a short cylinder, it was well approximated by a sphere. The mother payload, in contrast, was a long cylinder which was oriented perpendicular to the ambient magnetic field and this significantly increased the return current over the Parker and Murphy model values.

Study of current collection during application of passive positive potentials led to the following conclusions:

(4) For spherical payloads, the electron return cur-

rent is magnetically limited and close to the Parker and Murphy limit even during simultaneous electron beam emissions, provided the experimental altitude is above 240 km. (Rocket apogee was at 260 km so no information pertaining to the topside ionosphere was obtained.)

(5) A non-spherical payload can collect electron return currents somewhat in excess of the Parker and Murphy limit, as estimated by approximating the payload with an equivalent area sphere. The difference can be attributed to the fact that the Parker and Murphy model relies on the assumption of symmetry in the ambient magnetic field.

Laboratory and rocket experiments on charging phenomena performed in Japan have been reviewed by Kawashima (1982). The observations presented there are generally in accord with the conclusions reached above, provided the system is in a regime where surrounding neutral gases are not ionized. As will be discussed in the following sections, neutral gases may, in fact, play a very important role in space-borne electron beam experiments.

2.2. Beam–atmosphere interactions

The beam–atmosphere interaction (BAI) involves the collisional ionization of the ambient atmosphere by energetic electrons. It is a process which occurs naturally on auroral field lines where electron beams precipitate into the upper atmosphere generating aurora and enhancing the ambient plasma densities. The excitation of aurora is one of the natural phenomena that can be studied with the use of artificial electron beams, as will be done in the *ATLAS*-1 space shuttle mission scheduled for early 1992 (Taylor *et al.*, 1991).

For the purpose of studying the effect of BAI on charging levels and return current collection of space craft, the *CHARGE*-2 sounding rocket experiment was the first to allow separate measurement of the active and the passive component of the return current (Neubert *et al.*, 1990b). The experimental configuration is shown in Fig. 4, which illustrates the two payloads and the current system during electron beam ejections from the mother. From the measurements of the beam current, I_{beam}, and the tether current, I_{tether}, the return currents to the payloads can be determined by assuming that the beam current escapes the near-environment of the mother:

$$I_D = I_{tether} \qquad (8)$$

$$I_M = I_{beam} - I_{tether}, \qquad (9)$$

where I_D is the return current to the daughter and I_M the current to the mother. The daughter current represents the passive current component since the
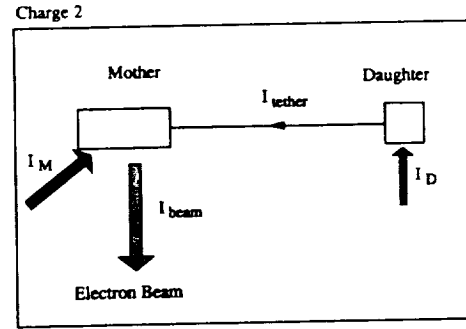

FIG. 4. CONFIGURATION OF THE *CHARGE*-2 PAYLOAD AND THE AVERAGE ELECTRON CURRENT SYSTEM AROUND THE PAYLOAD DURING AN ELECTRON BEAM EXPERIMENT (FROM NEUBERT *et al.*, 1990b).

daughter is located far from the mother and outside the disturbed region surrounding the mother and the electron beam, while the current to the mother represents the sum of the passive and active components. Since the passive component can be deduced from the daughter measurement, the active component can be extracted from the mother return current.

The observations of current collection during the *CHARGE*-2 flight are summarized in Fig. 5. This shows the fraction of the beam current collected by the daughter as function of altitude. The labels SQ2–SQ6 mark the beam-emission sequences performed
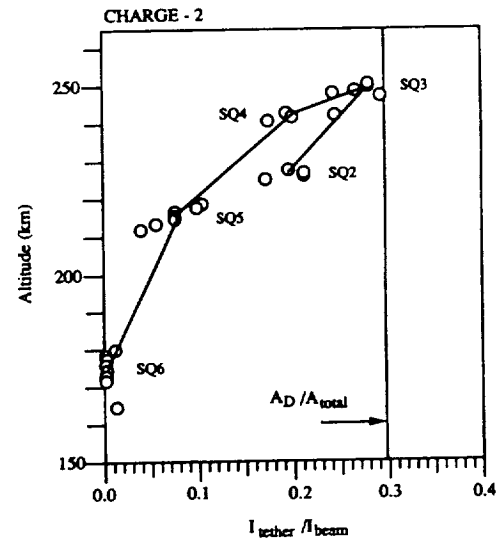

FIG. 5. *CHARGE*-2 OBSERVATIONS OF THE TETHER TO BEAM CURRENT RATIO AS A FUNCTION OF ALTITUDE.
Also indicated is the ratio of the daughter area to the total area of the two payloads (from Neubert *et al.*, 1990b).

during the flight numbered in time sequence. Also indicated is the fixed ratio of daughter current collection area to the total collecting area of the two payloads. At high altitudes, the fraction of the return current collected by the daughter is close to the ratio of the two areas. This is expected for passive current collection. At lower altitudes, a progressively smaller fraction of the total return current is collected by the daughter. Assuming that the beam escapes, this implies that progressively more current must be collected directly by the mother. This can only happen if the active component of electron current increases.

Since the active current component increases with decreasing altitude it was suggested by Neubert *et al.* (1990b) that the active component was due to ionization created in a BAI process. In order to quantify the increased current due to this process, a computer code, first developed for the study of the generation and transport of photoelectrons in the upper atmosphere (Banks and Nagy, 1970) and later for auroral electron fluxes (Banks *et al.*, 1974), was modified by Neubert *et al.* for the purpose of modelling the behavior of magnetic field-dominated electrons ejected from a spacecraft and scattered back and forth along magnetic field lines by collisions with atmospheric gases. Primary and secondary electrons scattered back to the payload would constitute the active source of return electron current.

The code solves two first-order, non-linear differential equations in the differential energy flux streaming along an ambient magnetic field. The equations coupling the forward flux, Φ^+, with the backward flux, Φ^-, are described by:

$$\Phi^{+\prime}(z,E) = -\sigma_2(z,E)\Phi^+(z,E)+\sigma_1(z,E)\Phi^-(z,E)$$
$$+Q^+(z,E)-L(E)\Phi^+(z,E) \quad (10)$$

$$\Phi^{-\prime}(z,E) = \sigma_2(z,E)\Phi^-(z,E)-\sigma_1(z,E)\Phi^+(z,E)$$
$$-Q^-(z,E)+L(E)\Phi^-(z,E). \quad (11)$$

Here Φ' denotes the derivative of Φ with respect to z, which is the dimension in the direction of the magnetic field. σ_2 is the cross-section describing the loss in the electron energy range E to $E+dE$. σ_1 is the cross-section describing the elastic backscattering of electrons. Q is the electron production rate due to ionization and cascading of electrons down in energy, and L describes the loss of flux out of the beam flux-tube induced by the motion of the spacecraft perpendicular to the magnetic field.

The problem is treated in one dimension and is applied to the situation of electrons emitted from a spacecraft by modelling the fluxes that are confined to the magnetic flux-tube encompassing the beam. It

is assumed that the beam and the secondary electrons fill a flux-tube with a certain cross-sectional dimension and that the fluxes are homogeneous within this flux-tube. From experiments, an estimate of the width of the beam flux-tube is 4 beam electron Larmor radii at 90 pitch angle (Frank *et al.*, 1989; Winckler *et al.*, 1989). The loss term L describes the loss of flux out of the sides of the flux-tube caused by the motion of the spacecraft perpendicular to the magnetic field.

To model typical conditions, equations (10) and (11) were solved numerically for a 1 keV electron beam of 100 mA current emitted downwards from an altitude of 260 km over White Sands, NM, at midnight. The MSIS/86 model (Hedin, 1987) was used for the neutral atmosphere (N_2, O_2, O) and the IRI model (Bilitza, 1986) was used for the ionosphere. The IRI model is needed to model Coulomb collisions.

The differential electron energy flux at the spacecraft altitude is shown in Fig. 6. The upward flux is the flux returning to the spacecraft from below. A portion of this flux will in general be collected by the spacecraft and form the active component of the return current, while the rest will reach locations above the spacecraft and interact with the neutral constituents here. In Figs 6 and 7 it is assumed that the portion of the flux collected by the spacecraft can be ignored relative to the total flux.
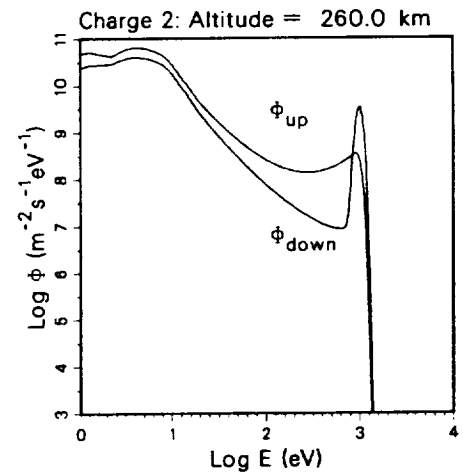
The downward flux consist of two contributions.

FIG. 6. MODEL ESTIMATES OF THE UPWARD AND DOWNWARD DIFFERENTIAL ELECTRON FLUX AS A FUNCTION OF ENERGY AT THE SPACECRAFT ALTITUDE.
The beam is emitted downward parallel to the magnetic field with an energy of 1 keV and a current of 100 mA (the fluxes scale linearly with beam current). The primary beam is seen as the peak at 1 keV in the downward flux (from Neubert *et al.*, 1990b).

One is the electron beam flux, which is modelled as Gaussian in energy around the 1 keV beam energy, and the other is the secondary electrons generated at lower energies and propagating in the same direction as the beam electrons from locations above the spacecraft. Thus, one will in general expect a hot component of electron fluxes to impinge on the spacecraft from both hemispheres. This is in accordance with observations made in the *ECHO*-2 experiment (Winckler *et al.*, 1975).

Figure 7 shows the fluxes as a function of altitude for 1 keV and 100 eV electrons. As can be explained by electron free-path considerations, energetic electron fluxes are generated along the magnetic field to considerable distances from the spacecraft. This is in accordance with optical observations in other experiments which found streaks of optical emissions aligned with the magnetic field and extending far from the payload and its sheath (O'Neil *et al.*, 1978a,b; Winckler *et al.*, 1989).

At low altitudes the flux becomes omnidirectional and approaches zero because of the progressively shorter mean free path in the lower thermosphere. Above the spacecraft, the upward flux decreases relatively slowly with altitude because of the increased mean free path which allows the electrons to escape without significant collisions. Similarly, the downward flux from above the spacecraft increases from zero at high altitudes (a boundary condition) to large values at low altitudes.

The active return current estimated to reach the *CHARGE*-2 rocket mother payload from such model calculations has been found to be consistent with the observed magnitude of the active current. Thus, there was no need to involve other processes for this experiment. However, at higher altitudes and for spacecraft velocities across the magnetic field typical of orbiting platforms, the active return current component due to BAI becomes small. In order to estimate the BAI currents to other types of ionospheric spacecraft a series of calculations were performed for a range of altitudes, spacecraft sizes, and velocities (Neubert and Banks, 1990). Noting that the BAI return current is directly proportional to the emitted beam current, the BAI effect can be quantified by a gain factor Λ which is the ratio of the return current to the ejected beam current at the spacecraft altitude. The loss to the flux-tube incurred by the motion of the spacecraft contained in the term L of equations (10) and (11) can be described by the parameter v:

$$v = r_\perp/d y.\tag{12}$$

where $v_\perp$ is the cross-field velocity of the spacecraft and $d y$ is the cross-field dimension of the beam disturbance in the direction of motion.

A summary of the BAI study is shown in Fig. 8 where the gain factor Λ is plotted as function of v for three different altitudes. The gain factor is split into two parts describing the fluxes from above and below the spacecraft. As expected, when v becomes large, Λ decreases. Similarly, when the altitude increases, Λ decreases. At the bottom of the figure is indicated the range in v that can potentially be covered by various ionospheric spacecraft. An array of 10 electron guns along the space station may, when the long axis of the station is aligned with the velocity vector, result in a large value of $d y$, say 100 m. The ionospheric orbital

A)

Charge 2: E = 1.0 keV

Altitude (km)

Φ_{down} Φ_{up}

Spacecraft Altitude

Φ_{down}

Log Φ (m^{-2}s^{-1}eV^{-1})

B)

Charge 2: E = 10.0 eV

Altitude (km)

Φ_{down} Φ_{up}

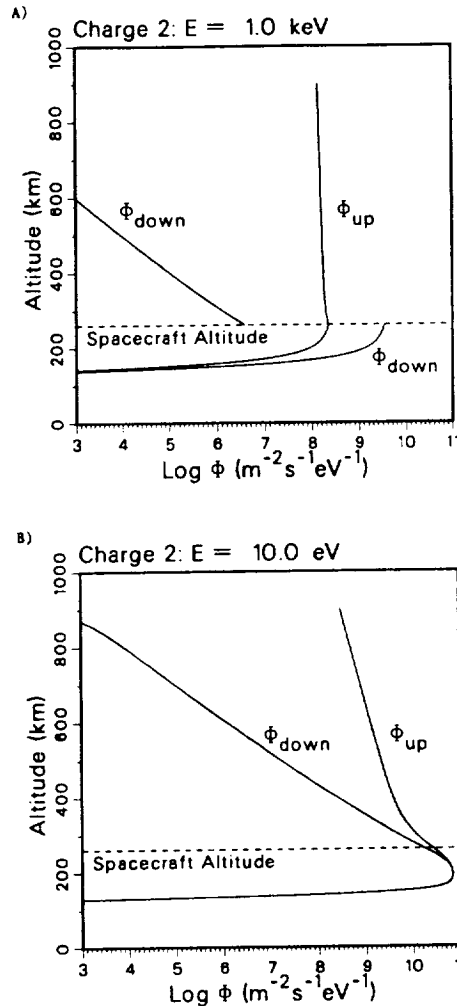Spacecraft Altitude

Log Φ (m^{-2}s^{-1}eV^{-1})

FIG. 7. MODEL ESTIMATES OF THE DIFFERENTIAL ELECTRON FLUXES AS A FUNCTION OF ALTITUDE FOR THE SAME PARAMETERS USED IN FIG. 6.
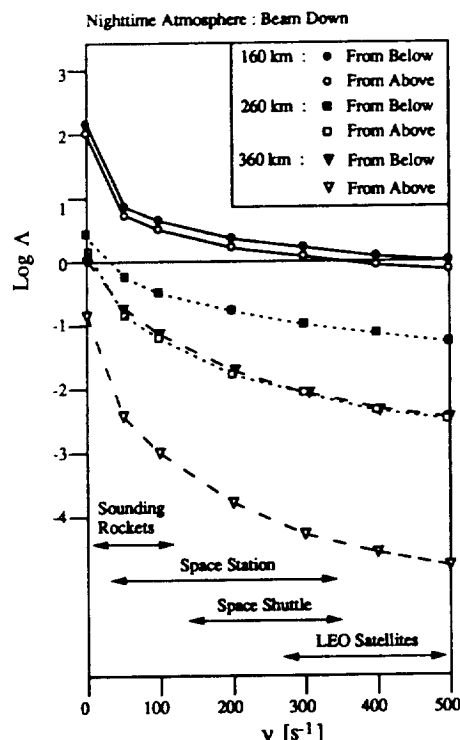(a) 1-keV electrons and (b) 10-eV electrons (from Neubert *et al.*, 1990b).

FIG. 8. MODEL ESTIMATES OF THE BEAM ATMOSPHERE INTER-
ACTION (BAI) GAIN FACTOR A AS A FUNCTION OF THE
SPACECRAFT PARAMETER ν (FROM NEUBERT AND BANKS, 1990).

velocity is typically 7 km s^{-1} with perpendicular vel-
ocities down to 3.5 km s^{-1}. The minimum ν in this
case is 35 s^{-1}.

Since the spacecraft potential sheath is generally
smaller than the beam flux-tube dimension, A must
be somewhat larger than 1 in order for the BAI return
current to balance the beam current. From Fig. 8 we
estimate that at 200 km altitude, a spacecraft with ν
of 50 s^{-1} will just be able to collect the complete return
current from the BAI.

It is also the case that an energetic electron wake
exists behind an orbiting or otherwise moving payload
emitting a steady electron beam. This wake is aligned
along the magnetic flux-tubes traversed by the beam.
The width of the region is of the order of four gyro-
radii, based on measurements by Frank et al. (1989)
and Winckler et al. (1989). The length of the wake
behind the payload depends on the time taken for the
atmospherically scattered electrons to lose their excess
kinetic energy or to escape from the atmosphere. The
energy degradation time, T, depends on the mag-
nitude of the inelastic cross-section, σ_1, the neutral
gas density, n, and the electron velocity, r_e, according

to the relation $T \simeq 5\, n\sigma_1 r_e$, assuming that about five
collisions are needed to bring an average energetic
electron down to thermal electron energies. For con-
ditions at 220 km, for example, $T \simeq 0.03$ s. For an
orbiting payload at this altitude in the ionosphere, the
energetic electron wake zone would extend approxi-
mately 1.2 km behind the vehicle. At higher altitudes,
the wake length is determined by the speed at which
electrons leave the atmosphere. In this case elastic
scattering dominates, but numerical models are
necessary to determine counteracting effects of the
atmospheric albedo for downward moving electrons
and net escape from the atmosphere.

The plasma density enhancement and optical emis-
sions from the BAI are phenomena which will be
explored in the ATLAS-1 space shuttle mission (1992)
and the CHARGE-2b sounding rocket experiment
planned for the spring of 1992. The experiments can
study auroral processes in a quantitative manner and
can in addition give new information on the physics
of plasma density structures in the lower ionosphere
and their influence on radio wave propagation (Banks
and Gilchrist, 1985). Using the model described by
equations (10) and (11), both plasma density enhance-
ments along the beam flux-tube and optical emission
rates can be calculated. Examples of the plasma den-
sity enhancement created by electron beam ejection
from 200 km altitude are shown in Fig. 9 for two
electron beam energies. The time constant for recom-
bination is inversely proportional to the electron den-
sity and is about 7.7 s for 10^6 cm^{-3} increasing to about
1 min when the density has decayed to 10^5 cm^{-3}. At
this point the density is still a factor 100 larger than
the background density.

In situ observation of plasma density enhancements
is difficult. However, observing the phase shift of the
telemetry signal between a mother and daughter pair,
where one of the payloads carries an electron accel-
erator, estimates of the local plasma density enhance-
ment can be made as was done in the MAIMIK exper-
iment (Friedrich et al., 1991). The upper estimates
found here are consistent with the estimates shown in
Fig. 9.

The results from the BAI studies were:

(6) The interaction of artificial electron beams with
the neutral atmosphere can be modelled, thereby giv-
ing quantitative estimates of enhanced return
currents, as well as plasma density enhancements,
optical emissions, electron differential energy fluxes,
etc. along the magnetic flux-tubes containing the
source electrons.

2.3. Beam/system–plasma interactions

The ejection of an electron beam from a spacecraft
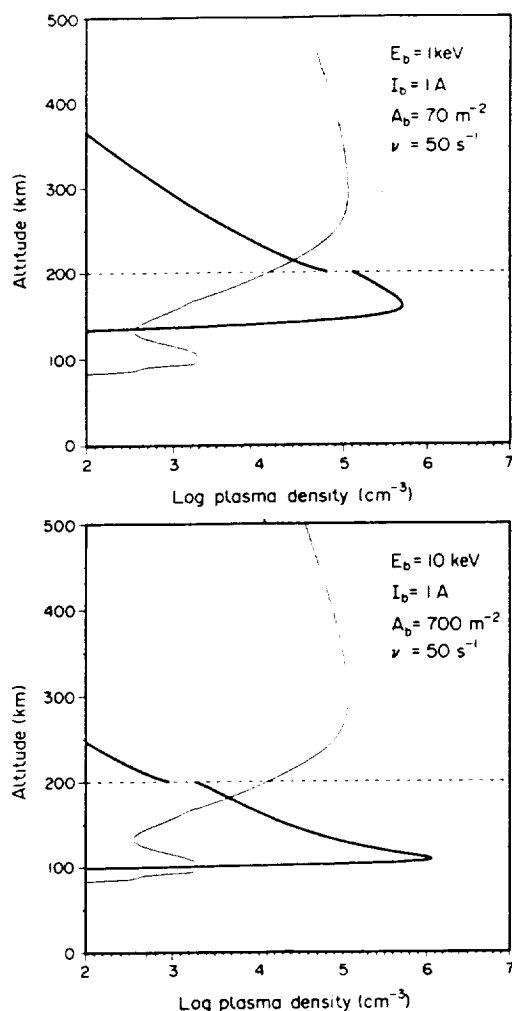strongly perturbs the local plasma environment. In

FIG. 9. MODEL ESTIMATES OF THE PLASMA DENSITY IN THE BEAM FLUX-TUBE AS A FUNCTION OF ALTITUDE (HEAVY LINE) AND AMBIENT PLASMA DENSITY (THIN LINE). The spacecraft altitude is indicated by the dashed line (from Neubert and Banks. 1990).

addition to the ionization of the ambient neutral atmosphere mentioned above, beam ejection results in plasma wave generation and plasma heating in a region surrounding the spacecraft and the beam flux-tube (Cartwright et al., 1978; Arnoldy and Winckler, 1981; Arnoldy et al., 1985). Many of the processes involved in this interaction are also found in conjunction with auroral precipitation of energetic electrons (Gurnett et al., 1986; Frank et al., 1989).

In the past, these processes have been studied in the laboratory as well as in space. The advantage of space experiments is the absence of walls and their con-

taminating effects, which allows the study of larger-scale phenomena such as the electromagnetic radiation from electron beams which usually have very long wavelengths compared with other scales in a plasma (Debye length. Larmor radius. etc.). On the other hand, a disadvantage is that it is more difficult to get detailed measurements. In the laboratory, the experiments can be repeated many times and measurements can be performed at different locations giving good temporal and spatial coverage. In space, this problem has been approached with the use of two or more separate payloads, one carrying a source and all payloads carrying a selection of plasma diagnostic instrumentation. Such configuration has proved very useful as demonstrated by the recent ECHO-6 and -7 sounding rocket experiments (Winckler et al., 1989; Erickson and Winckler. 1990) and the Spacelab-2 flight of the space shuttle which released a plasma diagnostics package to free-fly during electron beam emission from the space shuttle orbiter (Gurnett et al., 1986; Reeves et al., 1988a).

The plasma disturbances are a consequence of the sudden ejection of large amounts of charge which create charge imbalances and large transient electric fields at beam turn on and off. In addition, the drift relative to the ambient plasma of the energetic primary beam electrons and the lower energy return current electrons and secondary electrons generate plasma waves in a broad frequency range. The hot plasma region around the beam flux-tube was investigated in the ECHO-7 experiment. Here three sub-payloads were injected upwards relative to the main payload at various angles to the magnetic field. The main payload carried an electron beam accelerator ejecting beams at a range of energies and currents (up to 36 keV, 180 mA) as well as beam pitch angles. The turbulent region as observed from one of the sub-payloads, the Plasma Diagnostics Package (PDP), is shown in Fig. 10 (Winckler et al., 1989). In the figure, the floating potential of the PDP is shown as function of perpendicular distance to the beam flux-tube for a range of beam pitch angles (the floating potential is proportional to the temperature of the plasma). The dimension of the disturbed region generally increases with beam pitch angle. It is largest for 75 -85 pitch angle even though the beam in this case ejected downwards and away from the PDP. This indicates that much of the disturbance is accounted for by secondary and scattered electrons in the flux-tube rather than the primary beam electrons.

In the disturbed region around the beam flux-tube, low frequency electrostatic waves are excited in the range from essentially zero frequency and up to harmonics of the electron gyrofrequency (Shawhan et al.,
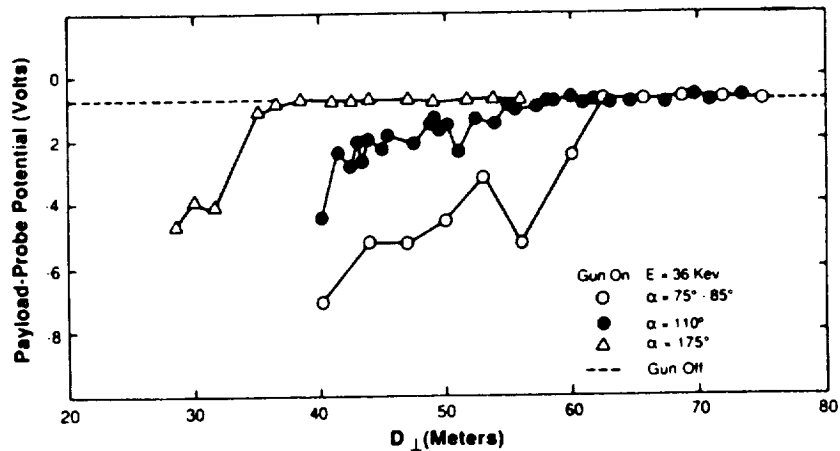
FIG. 10. *ECHO-7* OBSERVATIONS OF THE HOT PLASMA FOR THREE INJECTION PITCH ANGLES IN TERMS OF THE FLOATING POTENTIAL DECREASE OF THE *PDP* PAYLOAD BODY, PROPORTIONAL TO kT, AS A FUNCTION OF DISTANCE TRANSVERSE FROM THE BEAM INJECTION FIELD LINE, ALL FOR 36-kV, 180 mA INJECTIONS (FROM WINCKLER *et al.*, 1989).

1984; Neubert *et al.*, 1986, 1991; Abe *et al.*, 1988; Frank *et al.*, 1989). The low frequency modes have been studied in the laboratory (Gekelman and Stenzel, 1978; Stenzel, 1978a,b) and in computer simulations (Okuda and Ashour-Abdalla, 1988). The concensus is that the broad-banded noise below the lower hybrid frequency is ion acoustic noise generated by lower energy electrons flowing primarily as return currents to the payload. The disturbed region is, however, not symmetric around the magnetic field. Due to the motion of a spacecraft perpendicular to the field, there exists a turbulent wake region behind the beam (Frank *et al.*, 1989; Reeves *et al.*, 1990a). In the beam region, as in the wake, elevated electron temperatures and low frequency wave turbulence are found. The low frequency waves are then generated not just by return current electrons but, more generally, by lower energy electrons.

Electromagnetic broad-banded noise in the whistler mode extending from the lower hybrid frequency and to the electron gyrofrequency is thought to be generated by the primary beam electrons (Gurnett *et al.*, 1986). We return to this point in the following section.

Localized primarily to the turbulent beam region are waves around the electron gyrofrequency and its harmonics, the plasma frequency and the upper hybrid frequency (Cartwright and Kellogg, 1974; Gurnett *et al.*, 1986; Neubert *et al.*, 1991). Computer simulations have shown that these high frequency wave modes are generated by the primary beam electron motion as well as by the induced azimuthal $E \times B$ drift of beam electrons and ambient plasma electrons

around the beam. The electric field here is either the radial field caused by the excess negative charge in the beam column or the electric field from waves in resonance with the particles (Winglee and Kellogg, 1990; Okuda and Ashour-Abdalla, 1990). As a result, the beam electrons experience energy loss and scattering.

Computer particle simulations have proven to be very useful in studying spacecraft charging, return current collection, and beam coherence. Using 2-D simulations (three velocity components) Winglee and Pritchett (1988) studied many aspects of the dynamics of electron beams emitted from spacecraft. In Fig. 11 is shown the response of the plasma to the ejection of an electron beam at a time $\omega_{pb}t = 120$, where $\omega_{pb}t$ is the electron beam plasma frequency. The magnetic field is along the x-axis and the beam is emitted at a finite angle to B. Figure 11a shows contours of the charge density of the electron beam and the spacecraft, which is modelled as a planar conductor. The helical primary beam can be seen for about two gyrations, embedded in beam electrons scattered by electrostatic fields from the beam space charge, plasma wave noise, and the spacecraft electric fields. Figure 11b shows the ambient plasma electron density. The shaded regions are those with densities smaller than the unperturbed density. The depletion is brought about by the collection of return currents to the spacecraft as shown by the arrows. Behind the spacecraft this region is of a dimension perpendicular to B which is comparable with the spacecraft dimension. In front of the spacecraft, the region is surrounding the primary beam
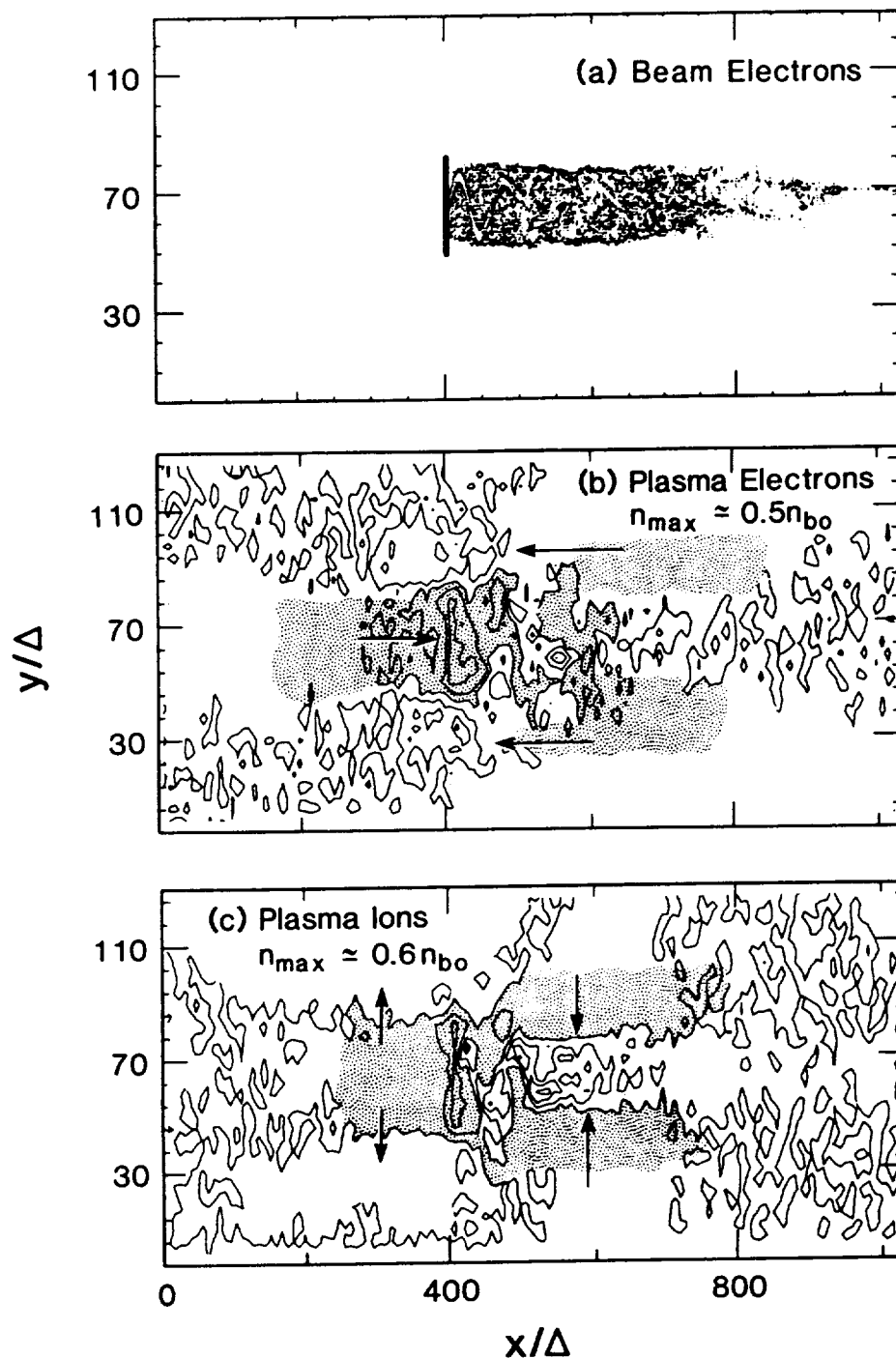
FIG. 11. PARTICLE SIMULATION OF THE INJECTION OF ELECTRON BEAMS FROM SPACECRAFT.
Contours of (a) the charge density of the beam and the spacecraft, (b) the plasma electron density, and (c) the plasma ion density at $\omega_{pb}t = 120$. Successive contours in (a) differ by a factor of 3.16 while those in (b) and (c) decrease linearly from the maximum value down to 8% of the maximum value. The arrows in (b) and (c) indicate the direction of the plasma flows in response to the beam injection. The shaded areas indicate the region where the density is smaller than in the initial plasma density (from Winglee and Pritchett, 1988).

column. Current closure is in this simulation achieved by the plasma ion motion shown in Fig. 11c, which allows ions to flow across the magnetic field to a distance limited by their Larmor radius.

The beam structure obtained in the 2-D simulation, is consistent with optical observations of the electron beam structure during the STS-3 mission of the space shuttle (Banks and Raitt, 1988). It was found that the electron beam initially moved outwards along a classical helical trajectory. However, within a short distance electrons were deflected into paths parallel and anti-parallel to the magnetic field lines threading the primary helix. This resulted in the formation of a thin-walled, hot, electron torus with a radius equal to the primary beam gyroradius.

Winglee and Pritchett (1988) also found that a build-up of negative space-charge in the beam region close to the spacecraft may occur if the beam stagnation time t_s is smaller than the plasma response time t_{rp}. For a given beam current, the ratio of the two time-scales depends on the beam density, the beam energy and the area of the spacecraft. The negative space-charge region is often referred to as a virtual cathode. The formation of a virtual cathode partially inhibits beam escape, destroys the spatial coherence of the beam, and creates additional plasma wave turbulence (Pritchett, 1990).

Early 1- and 2-D simulations gave rather restrictive values for the beam stagnation time and questions arose about beam escape from spacecraft in ionospheric beam experiments (Pritchett and Winglee, 1987; Winglee and Pritchett, 1988). However, other studies argued that experimental observations indicated beam escape, or at least that a substantial portion of the beam escaped the spacecraft (Neubert et al., 1988; Farrell, 1990). The discrepancy was resolved when 3-D simulations were performed. In three dimensions the criteria for beam escape are less restrictive because electrostatic fields decrease more rapidly with distance than in two dimensions. Simulations and experimental observations are now in agreement on this point: namely, that in most cases in past experiments, the beams were able to leave the payload environment (Okuda and Ashour-Abdallah, 1991; Pritchett, 1991).

Nevertheless, the virtual cathode effect is still important for electron beam emissions in space, and while it may not have limited the beam escape in past experiments, it certainly affects beam coherence. In addition, it is probably responsible for much of the electrostatic noise observed from the beam-emitting spacecraft both at low frequencies as observed in the SEPAC space shuttle experiment (Neubert et al., 1986; Cai et al., 1987) and at high frequencies as

suggested by Neubert et al. (1991). Furthermore, return current electrons with energies in excess of the beam accelerator energy observed in the past (Managadze et al., 1988; Wilhelm et al., 1984; Waterman et al., 1988) and optical emissions (Sasaki et al., 1985a) are probably a result of such space-charge effects in the near-environment of the spacecraft rather than caused by a beam-plasma instability or a beam-plasma discharge.

Transient excursions of the spacecraft potential to levels well above the beam energy, often called "supercharging", have occasionally been observed (Sagdeev et al., 1981; Maehlum et al., 1988). It has been suggested that these high fields are associated with the formation of a virtual cathode. It is proposed that electrons are accelerated to high energies in the cathode region and that a percentage of these escape at energies which exceed the beam energy thereby driving the spacecraft to large positive potentials (Maehlum et al., 1988; Managadze et al., 1983, 1988; Denig et al., 1990).

The results on plasma heating, wave excitation, and beam dynamics can be summarized as:

(7) The 3-D structure of the disturbed electron beam region is now explored, revealing the dimension of the disturbed region to be about 4 beam electron Larmor radii perpendicular to the magnetic field. It has also been established that there exists a turbulent wake region behind the beam flux-tube.

(8) It is clear that transients in electrostatic potentials as well as return currents, azimuthal currents around the beam, and the primary beam current are important for the generation of broad-band radiation observed during electron beam ejection.

(9) Beam dynamics including electrostatic beam expansion, return current structure, and the phenomenon of virtual cathode and other space charge effects are now better understood.

(10) The success of the past decade in the understanding of the complete beam/spacecraft system is due to the synergy of detailed observations from multiple platforms, analytical models, and computer particle simulations.

2.4. Neutral gas emissions

The normal electrical neutralization of spacecraft at high altitudes relies solely on the ability to collect sufficient current from the ambient plasma since ionization of the neutral atmosphere provides little additional plasma. While the beam–system interactions mentioned previously have been thought to increase the electron current across the magnetic field, and thereby increase the return current through wave-induced particle diffusion (Linson, 1969; Hastings,

1987), there are practical limits to the efficiency of such processes. Furthermore, while laboratory experiments indicate that such processes occur in this environment, it has not been possible to establish their importance in space experiments.

Another possibility for increasing the return current to a beam-emitting payload is through ionization of payload gases introduced accidentally through outgassing or deliberately, as in the case of attitude control thrusters. For example, in the *ECHO*-4 rocket experiment it was found that the injection of N_2 gas by attitude control thrusters on the beam-emitting payload had the effect of lowering the spacecraft potential during beam emissions (Israelson and Winckler, 1979). This was also observed in the *SEPAC* experiment (Sasaki *et al.*, 1985b) as well as in the *CHARGE*-2 experiment. In the case of *CHARGE*-2, N_2 emissions from the beam-emitting mother as well as from the tethered, but passive daughter, reduced the spacecraft potential (Gilchrist *et al.*, 1990; Banks *et al.*, 1990). The reduction in potential is thought to be brought about by the ionization of the neutral gas cloud. The ionization is not dependent on the primary beam electrons but is triggered by return current electrons energized in the sheath. This conclusion was reached from the fact that the *CHARGE*-2 daughter payload was located so far from the mother payload that the gas cloud could not have reached the beam region in the time it took the daughter to drop in potential. As a result of the decreased potential, wave turbulence was decreased (Neubert *et al.*, 1991), and the beam escaped with a larger fraction of its energy as inferred from ground-based radar observations of the plasma density enhancement caused by BAI (Gilchrist, 1991). The reduction of spacecraft potential and easier escape of the beam from the payload in the presence of ambient or thruster neutral gases have also been found in computer simulations (Winglee, 1990).

Another means of controlling the spacecraft potential involves the use of the so-called plasma contactor, or hollow cathode. It operates by creating a dense plasma cloud in the vicinity of the spacecraft which then acts as a bridge between the more dilute background plasma and the spacecraft (Patterson, 1987; Williams *et al.*, 1987; Katz and Davis, 1987). The plasma contactor in its normal mode of operation relies on the ionization within the hollow cathode of neutral gas flowing out from a pressure chamber. At positive bias potential, the contactor may operate in the so-called ignited mode in which the ionization occurs in the gas plume in the sheath region. Thus, the ignited mode is simply the ejection of neutral gas as observed in the *CHARGE*-2 experiment. The

importance of this discovery is that with this method it is fairly simple and inexpensive to control large positive potentials and that such control seems to reduce plasma wave noise and allow the beam to escape with almost its complete accelerator energy. The limits in terms of beam current that can be neutralized in this way and the gas densities and flow rates required need to be explored in future experiments.

The results given above can be summarized:

(11) Large, positive payload potentials can be reduced by the ejection and subsequent ionization of neutral gas. The limits of beam currents that can be ejected during neutral gas emissions and the gas density and flow rates required to neutralize the payload need to be quantified with accurate experiments in space.

(12) When the payload potential is reduced by neutral gas emissions, the plasma wave noise is reduced and the beam escapes with a larger fraction of its accelerator energy.

3. WHISTLER MODE RADIATION FROM ELECTRON BEAMS

3.1. *Background*

We now explore some basic features of wave generation from pulsed and d.c. electron beam experiments in space plasmas. We pay particular attention to whistler wave generation in ionospheric plasmas and to the limits on the electron beam energy for wave generation in the two principal resonances, Landau resonance and cyclotron resonance. The "standard" way of calculating the radiation from a single particle spiralling in a magnetized cold background plasma is to solve Maxwell's equations with the moving particle as the current source (Mansfield, 1967; McKenzie, 1967). In this treatment, the radiation is found to be particularly intense for waves satisfying the resonance condition:

$$R = s\omega_c^* + k_\parallel v_\parallel - \omega = 0. \tag{13}$$

In equation (13), ω_c^* is the relativistic beam particle cyclotron frequency:

$$\omega_c^* = \omega_c(1 - v^2/c^2)^{1/2}, \tag{14}$$

where v is the particle velocity and c is the velocity of light. The component of the wave vector parallel to the magnetic field, $k_\parallel$, is given by

$$k_\parallel = k \cos \theta, \tag{15}$$

where k is the wavenumber and θ the angle of the wavenumber to the magnetic field. Similarly, for the particle velocity along the magnetic field:

$$r = r \cos \chi. \tag{16}$$

where χ is the pitch angle of the particle. The wave frequency ω is related to k through the plasma dispersion relation.

The parameter s takes on the value 0 for Landau resonance where Cherenkov radiation is emitted, 1 for cyclotron resonance, and -1 for anomalous cyclotron resonance. Larger integer values denote higher order cyclotron resonances. Condition (13) is often referred to as the first-order resonance. Since the background plasma is usually inhomogeneous, waves and particles in resonance at one point will become off-resonant as they propagate away to other regions. Enhanced interaction is achieved when waves and particles are also in second-order resonance, namely when:

$$dR(z)/dz = 0, \tag{17}$$

where z is the coordinate along the background magnetic field (Neubert *et al.*, 1987).

As an example, we consider the case of whistler mode radiation. An approximate expression for the refractive index μ for $\omega > \omega_{LHR}$ and $\omega_{ce} < \omega_{pe}$ is:

$$\mu = \omega_{pe}/[\omega(\omega_{ce}\cos\theta-\omega)]^{1/2}, \tag{18}$$

where $\mu = kc \, \omega$. ω_{pe} is the electron plasma frequency, and ω_{ce} the electron gyrofrequency. The resonance cone angle is the angle at which the refractive index and the wavenumber goes to infinity:

$$\cos\theta_r = \omega/\omega_{ce}. \tag{19}$$

Real solutions to equation (18) require $\theta < \theta_r$. Figure 12 shows a sketch of the whistler mode refractive index surface as function of θ for two values of the wave frequency. Also shown is the direction of the group velocity, which is perpendicular to the surface.

For $\omega < \omega_{ce}$ 2 (satisfied by ω_1 in Fig. 12) the refractive index surface has a dimple around $\theta = 0$ such that a minimum in μ occurs for $\theta = \theta_g$, the so-called Gendrin angle. For $\omega > \omega_{ce}/2$ the dimple disappears (as is the case for ω_2 in Fig. 12) and the minimum in μ_1 occurs for $\theta = 0$. The minimum value of μ_1 found from equation (18) is:

$$\mu_{1min} = 2\omega_{pe}/\omega_{ce} \quad (\omega < \omega_{ce}) \tag{20}$$

and the Gendrin angle is:

$$\cos\theta_g = 2\omega/\omega_{ce} \quad (\omega < \omega_{ce}/2). \tag{21}$$

The relativistic expression for the electron energy, E, normalized to the electron rest mass (511 keV) is:

$$E = (1-v^2/c^2)^{-1/2}-1, \tag{22}$$

where the resonance beam electron velocity found from equation (13) is:

$$v_{\parallel}/c = g_s^*/\mu_1 \tag{23}$$

with $g_s^* = 1 - s\omega_{ce}^*/\omega$.

From equation (23) it is seen that at a given wave frequency there is a maximum beam energy for which resonance is possible. This energy corresponds to the minimum in μ_1. A minimum of the beam energy can be found by noting that small wavelength whistler waves have a very large refractive index and are primarily electrostatic in nature. As a result they are strongly damped as they propagate through a plasma. Using a wavelength of 1 m as a practical lower limit for whistler mode propagation, this corresponds to a maximum of $k = 2\pi \, \mathrm{m}^{-1}$.

The maximum and minimum electron energies for Landau resonance are shown in Fig. 13 and for cyclo-

FIG. 12. THE WHISTLER MODE REFRACTIVE INDEX SURFACE. The arrows indicate the direction of the group velocity, which is perpendicular to the surface.
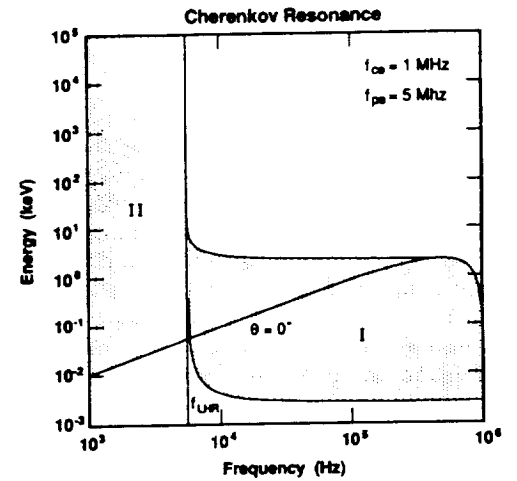

FIG. 13. MAXIMUM AND MINIMUM RESONANCE ENERGY FOR CHERENKOV RESONANCE. Shaded areas indicate regions of resonance.

tron resonance in Fig. 14. The region allowing resonance with whistler mode waves is marked with I. (Region II is discussed later.) Also shown is a curve through this region which corresponds to the resonance energy for $\theta = 0$. It is assumed that $\omega_{ce} 2\pi$ and $\omega_{pe} 2\pi$ are 10^6 s^{-1} and 5×10^6 s^{-1}, respectively, which are values representative for the peak of the ionosphere. The ion population is exclusively O$^+$. The figures show the resonance energies according to the Stix (1962) formulation of the cold plasma dispersion relation and includes relativistic effects on the beam electrons. It is assumed that the pitch angle, $\alpha = 0$.

At frequencies below one half the electron gyrofrequency and above the lower hybrid frequency, f_{LHR}, the maximum energy for Landau resonance is approximately constant in wave frequency for given background plasma parameters [from equations (20) and (23)]. In the ionosphere the ambient plasma density and therefore the plasma frequencies may have large fluctuations depending on local time, geographic location, and even small variations in altitude. As a result, the maximum energy for Landau resonance may also vary and will generally increase with decreasing density. Many electron beam experiments performed in the past have been in the range from 1 to 5 keV and were therefore expected to generate waves through Landau resonance in the whistler mode. Some experiments, in particular the ECHO series, used higher energies, up to 40 keV, and the degree to which Cherenkov radiation was generated via Landau resonance depended on the spacecraft altitude and ionospheric conditions.
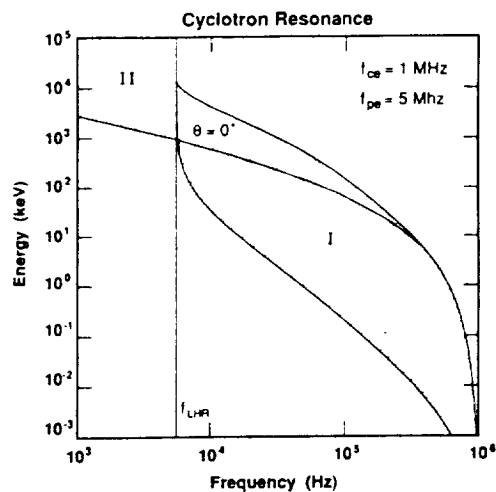
For low frequency waves in cyclotron resonance, η becomes large and, consequently, the resonance energy becomes large, as can be seen from equation (23). As the wave frequency approaches the lower hybrid frequency, the resonance cone angle approaches 90 and the maximum as well as the minimum resonance particle energy go to infinity. Because of the higher energy required for cyclotron resonance, this resonance has not been studied to the same degree as Cherenkov resonance. Future experiments with higher energy accelerators may study cyclotron resonance. It will be relatively simple to distinguish between cyclotron and Landau resonance. In the latter, the wave energy propagates in the same direction as the beam electrons, while in the former the waves propagate opposite to the beam electrons.

Below the lower hybrid resonance the topology of the wave normal surface changes. The resonance cone disappears and the wave normal surface becomes closed. The maximum in energy found for frequencies above the lower hybrid resonance becomes a minimum in energy below the lower hybrid resonance. The region of electron energies in resonance here is marked II in Figs 13 and 14.

3.2. Radiation from d.c. electron beams

On auroral field lines charged particles are accelerated by localized electric fields thought to be located at altitudes of 2–4 Earth radii. The result is the creation of an electron plasma with beam-like distributions in velocity. These electrons excite aurora as they penetrate the upper atmosphere. They also generate plasma waves over a wide frequency range. Figure 15 shows a typical frequency spectrum of the electric field intensity observed by the DE 1 satellite as it traverses the auroral oval from the polar cap and to the plasmasphere (Gurnett et al., 1983). Above the electron gyrofrequency auroral kilometric radiation (AKR) and emissions at the upper hybrid frequency are seen, while below the gyrofrequency, in the whistler mode frequency range, auroral hiss and plasmaspheric hiss are seen as the spacecraft enters the plasmasphere. In particular we point out the funnel shape of the auroral hiss as it appears on a frequency-time plot as shown in Fig. 15. This shape is consistent with the idea that the whistler wave noise is generated with wave normals close to the resonance cone through Landau resonance with energetic auroral electrons accelerated at some localized altitude below the spacecraft.

The funnel shape is a result of the propagation characteristics of whistler mode waves at the resonance cone. The higher the wave frequency, the narrower the resonance cone; because the direction of

Cyclotron Resonance

$f_{ce} = 1$ MHz
$f_{pe} = 5$ Mhz

$\theta = 0^\circ$

II

I

f_{LHR}

Energy (keV)

Frequency (Hz)

Fig. 14. MAXIMUM AND MINIMUM RESONANCE ENERGY FOR CYCLOTRON RESONANCE.
Shaded areas indicate regions of resonance.

the group velocity for waves at the resonance cone is perpendicular to k, the angle of propagation to B increases with wave frequency. Thus high-frequency emissions are first encountered as the spacecraft approaches the field line. In the case of a point source, only a V-shaped outline of the funnel will be seen. Such emissions are frequently observed and have been named "saucers" (James, 1976). A "filled-in" funnel requires a beam (or sheath) source which extends from a given point in space.

Emissions of a similar nature have been observed in artificial beam experiments. In the *Spacelab-2* experiments made with the space shuttle, a small satellite, the *Plasma Diagnostics Package* (*PDP*), was released from the shuttle and separated to distances of about 300 m during a 6 h period. During that time, the shuttle was maneuvered to provide four magnetic conjunctions of the *PDP* and the shuttle. During two of these, an electron beam (with electron energies of 1 keV, and currents of 50, 100, or 150 mA) was emitted from the shuttle. The electric field intensity observed by the *PDP* during the ejection of a continuous beam at 50 mA is shown in Fig. 16 (Gurnett *et al.*, 1986). Over frequencies between about 30 kHz and up to the electron cyclotron frequency a funnel-shaped emission is seen which bears close resemblance to the auroral hiss shown in Fig. 15. As the *PDP* approaches the beam flux-tube the high frequency emissions are observed first followed by lower frequency emissions. When the *PDP* crosses the beam, emissions are also observed close to the local upper hybrid frequency inside the beam.

The similarities of the natural and beam-generated emission led to the conclusion that they were a result of the same process. In the case of the *Spacelab-2* beam, it was found that the spectral shape on time-frequency plots as well as the electric field polarization were consistent with the assumption of Landau resonance between beam electrons and whistler waves at the resonance cone (Farrell *et al.*, 1988).
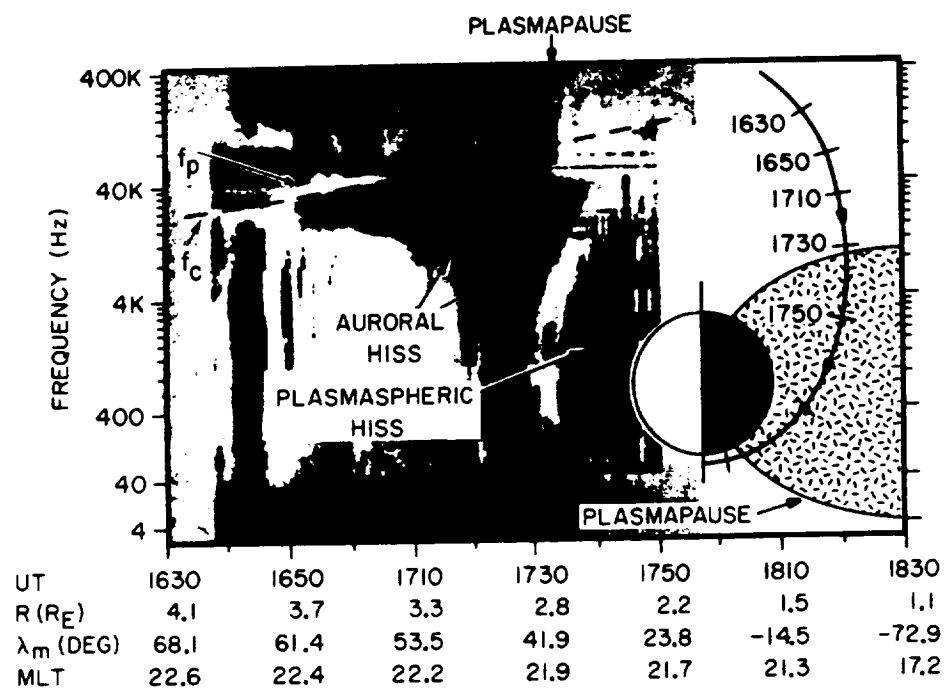
The *Spacelab-2* observations allowed the quantitative comparison of theories for wave generation by electron beams with the observations. Studies in the past of naturally occurring plasma waves and particle distributions using the formulation of Mansfield (1967) and McKenzie (1967) led to the conclusion that incoherent Cherenkov radiation (the radiation from each electron is added incoherently) was several orders of magnitude lower than observed (Taylor and Shawhan, 1974). Because the power radiated by coherent radiation is proportional to N^2, where N is the number of particles, while the power from incoherent radiation is proportional to N, an assumption of some coherency will increase the power and bring

it in agreement with observations. Similar conclusions were reached for the *Spacelab-2* electron beam (Farrell *et al.*, 1988). It was found that the radiation from the beam was orders of magnitude above expectations for an incoherent process and that some coherency must have been present. Following an idea of Bell (1968), analytical calculations and 1-D computer simulations were presented by Farrell *et al.* (1989), which demonstrated that density perturbations in the electron beam density, caused by Langmuir oscillations in the beam, as observed during magnetic conjunction, can provide the necessary coherence. The density perturbations were found to propagate with a velocity close to the beam electron velocity and could therefore radiate through the Landau resonance.

Later simulation studies in two dimensions confirmed this conclusion with minor modifications. Pritchett *et al.* (1989) found that the beam-plasma interaction creates a current structure that radiates much like an antenna through the Cherenkov radiation mechanism. In their study, the beam region carried no net current at the start of the simulation. This was achieved by giving the higher density background plasma an appropriate low energy drift velocity in the opposite direction to the beam velocity. Although the average net current is zero, radiation is still generated because of the electron current perturbations created in the beam by micro-instabilities.

Other studies of electron beam radiation include that of Wong and Lin (1990) which presents an analytical model for the modes generated inside the beam and the coupling at the beam edge of these modes to the ambient plasma. It was found that this process could generate whistler mode radiation which propagates in the ambient plasma with k close to the resonance cone as observed in the *Spacelab-2* experiments. A particle simulation of the *Spacelab-2* experimental results was presented in Omura and Matsumoto (1988). The simulation was done in two dimensions with periodic boundary conditions in the dimension along the beam. Such boundary conditions amount to simulating an infinite beam. Even so, the results showed wave spectra as a function of distance from the beam which resembled the funnel-shaped spectra of *Spacelab-2*. They suggested that the funnel was a result of frequency-dependent damping as the waves propagate away from the beam. Furthermore, they found that the wavelength of the electrostatic noise generated inside the beam column did not match the wavelength of the radiated whistler wave noise and concluded that the radiation was not caused by bunching of the beam electrons.

The results of radiation from continuous electron beams can be summarized as follows:

PLASMAPAUSE

UT   1630   1650   1710   1730   1750   1810   1830
R (R$_E$) 4.1   3.7   3.3   2.8   2.2   1.5   1.1
λ_m (DEG) 68.1   61.4   53.5   41.9   23.8   -14.5 -72.9
MLT   22.6   22.4   22.2   21.9   21.7   21.3   17.2

ELECTRIC FIELD, DE-I, OCTOBER 15, DAY 288, 1981

FIG. 15. A REPRESENTATIVE SPECTROGRAM OF THE ELECTRIC FIELD INTENSITIES FOR A NIGHT-SIDE CROSSING OF THE AURORAL FIELD LINES AS OBSERVED BY DE-1 (FROM GURNETT et al., 1983).
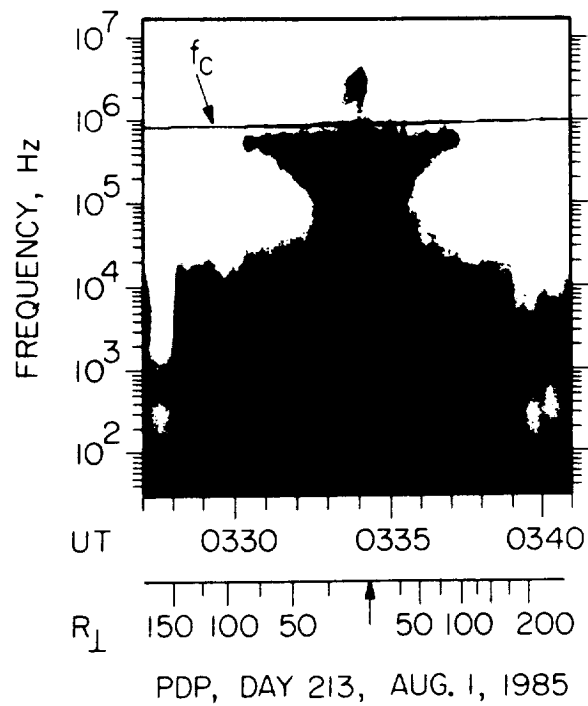
FIG. 16. A SPECTROGRAM OF THE ELECTRIC FIELD INTENSITY DURING ELECTRON BEAM EJECTIONS FROM THE SPACE SHUTTLE.

The free-flying *PDP* is in magnetic conjunction with the shuttle and in the beam region at the time indicated by the arrow (from Gurnett *et al.*, 1986).
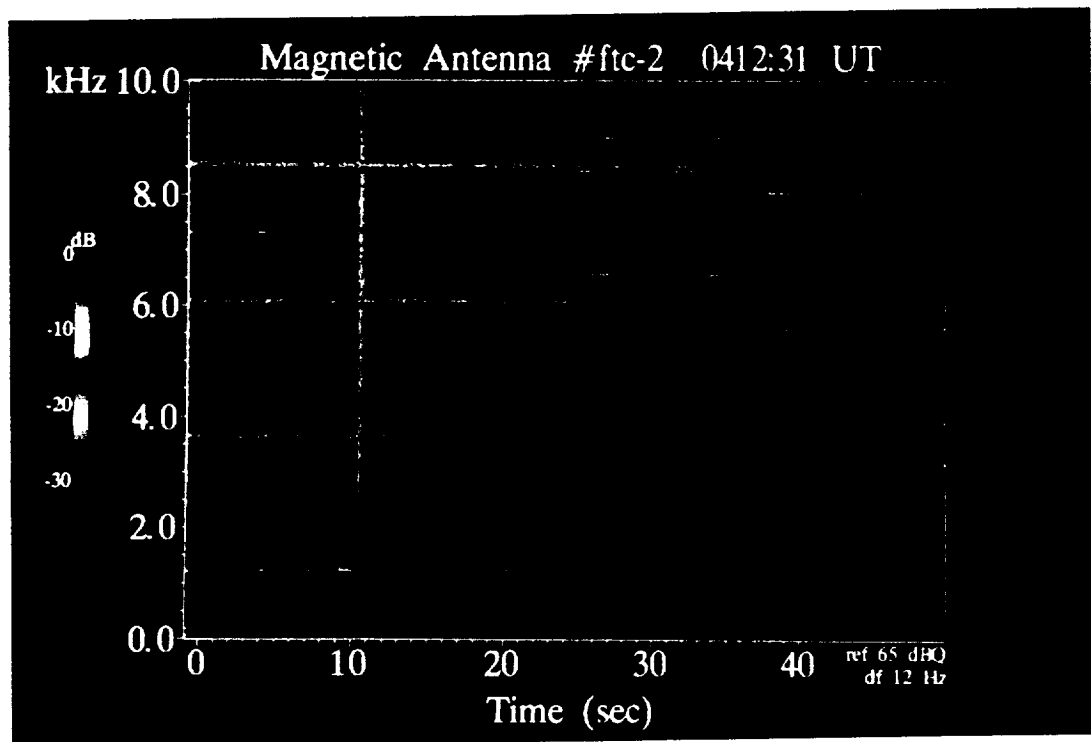
FIG. 17. THE MAGNETIC FIELD IN THE FREQUENCY RANGES 0–10, 20–10, AND 20–30 kHz AS A FUNCTION OF TIME.
The *PDP* is free-flying and the FPEG is pulsed at 1.22 kHz (from Bush *et al.*, 1987; Neubert *et al.*, 1988).

173

(13) The consensus from experiments and computer simulations is that in past experiments, employing kiloelectronvolt energy electron beams, whistler wave radiation is generated through Cherenkov resonance with beam electrons.

(14) The intensity of the radiation is between the levels expected for incoherent and coherent radiation. Micro-instabilities in the beam are found to be important for the establishment of quasi-coherency and thereby for the creation of the structure of the radiating current.

(15) The details of the formation of the radiating current structure are not well understood. It is thought that Langmuir oscillations play an important role in bunching the electrons. Spacecraft potential oscillations may also be important.

3.3. Radiation from pulsed electron beams

A pulsed electron beam generates electromagnetic radiation at the pulsing frequency and its harmonics. The radiation signature is therefore easier to distinguish from ambient plasma noise than the radiation from continuous beams. Furthermore, the spectrum of the radiation contains information on the spatial structure of the pulsed beam which can be compared with the format of the injected beam. In this way additional detailed information on beam dynamics and radiation can be obtained. Since the very first space-borne electron beam experiment (Hess et al., 1971), it has been conjectured that pulsed electron beams could be used as virtual antennas for communication purposes, for instance between space and ground or between two platforms in space. Beams have an advantage over conventional electric dipole antennas or magnetic dipole loop antennas, which is particularly important in the VLF whistler mode frequency range; because of the large wavelength of VLF waves it takes very long electric dipoles or large loops to efficiently radiate VLF waves.

The STS-3 mission of the space shuttle orbiter, flown in 1982, carried an electron beam accelerator especially designed to study the radiation from pulsed electron beams. The accelerator, the Fast Pulse Electron Generator (FPEG) emitted 1 keV energy electron beams with currents of 50, 100 or 150 mA. The beam could be square-wave modulated from d.c. and up to several hundred kilohertz with a pulse rise-time of the order of 10⁻⁶s (Banks et al., 1987). The electromagnetic radiation generated by beams pulsed at ELF and VLF frequencies was observed with wave receivers mounted on a PDP, which was either stored in the payload bay, or mounted on the Remote Manipulating System (RMS) (Shawhan et al., 1984; Reeves et al., 1988b).

Attempts were made to detect the radiation at remote locations in the magnetosphere by executing beam emission sequences coordinated with the DE 1 satellite at times when the shuttle and the satellite were in magnetic conjunction. The results were negative; however it was later shown that either the STS-3 attitude was such that the electrons hit the main body of the orbiter, or raytracings showed that it was not possible for whistler mode waves to propagate from the STS-3 location up to the vicinity of the DE 1 satellite (Inan et al., 1984). The FPEG PDP was flown again in the Spacelab-2 mission of 1985 as mentioned earlier. Radiation was observed on the PDP freeflyer out to its maximum separation distance of about 300 m (Bush et al., 1987; Reeves et al., 1988a; Neubert et al., 1988). Again no radiation was observed on the ground or on DE 1.

Results from other experiments studying the radiation characteristics of pulsed electron beam emissions are reported in Cartwright and Kellogg (1974); Reme (1980); Holzworth and Koons (1981); Winckler et al. (1984, 1985); Kellogg et al. (1986); Sasaki et al. (1987, 1988); Goerke et al. (1990); Neubert et al. (1991). In most of these experiments, attempts were made to detect the wave fields on the ground. The results to date have proved negative, and the largest distance from the beam source that VLF wave fields have been observed is of the order of 1-2 km.

In parallel with the experimental efforts involving the FPEG, a theory for the radiation from the square-wave modulated electron beam was developed. The first model considered the coherent radiation from a finite train of pulses injected into a magnetized plasma (Harker and Banks, 1983). For simplicity, each pulse was assumed to traverse an unbounded path length ($-\infty$ to $+\infty$). The beam was assumed to radiate coherently and the radiation was determined for the frequency range from the lower hybrid frequency to the electron gyrofrequency. In Harker and Banks (1985) the power radiated by a beam propagating into a half space (0 to $+\infty$) was calculated for frequencies both below and above the lower hybrid frequency. The power was found for the far-field region, which is the region at distances beyond a few perpendicular wavelengths from the beam source. Since the Spacelab-2 observations were performed in the near-field region a near-field model was developed (Harker and Banks, 1987) giving the complete polarization of the electric field. Observations showed, however, that associated with the pulsed beam injection, considerable broad-band electrostatic noise was generated just as for the case of continuous beam injection. This made it difficult at times to determine the

spectral component on the pulsing frequency or its harmonics. The magnetic field, on the other hand, was very clear and undisturbed from broad-band noise. The calculations were therefore extended to include the near-field components of the magnetic field (Neubert and Harker, 1988). Finally, the theory has been extended to allow calculations of signal levels on the ground from pulsed beam emissions in space (Harker et al., 1991).

The theory of Harker and Banks is based on the work of McKenzie (1967). It assumes that the radiating current is that of an infinitely thin electron beam spiralling around the geomagnetic field under the influence of the Lorentz force. The beam is square-wave modulated (pulsed) and the beam electrons within a pulse are assumed to radiate coherently. Effects of electrostatic expansion of the helical beam, return currents and other processes which destroy the ideal beam structure are accounted for through an attenuation factor which assumes that the ability of the beam to radiate coherently decreases exponentially with distance from the beam accelerator.

The Harker and Banks theory was developed particularly for the square-wave modulated electron beam of the FPEG. Other treatments include the radiation from pulsed electron beams at zero degree pitch angle (Lavergnat and Lehner, 1984; Ohnuki and Adachi, 1984) and sinusoidally modulated electron beams at arbitrary pitch angles (Lavergnat et al., 1984).

As a result of the assumption of a square-wave modulated current source, the radiated fields contain a factor D, the so-called duty cycle factor:

$$D = 1 \eta \sin(\eta \pi b\ d), \qquad (24)$$

where b/d is the duty cycle, b is the on-time for a pulse, and d is the total modulation period. The parameter η is the harmonic number. The factor D arises naturally from the Fourier transform of a square-wave function.

During the Spacelab-2 experiment, several predictions of the Harker and Banks theory were tested. The PDP free-flight provided observations of the electric and magnetic fields during a beam sequence in which the beam (100 mA) was pulsed with 50% duty cycle at 1.22 kHz. The PDP was located during this beam sequence at distances from a few meters to 150 m from the electron beam. A spectrogram of the magnetic field is shown in Fig. 17 (Bush et al., 1987; Neubert et al., 1988). The relative signal intensity is color coded showing the fundamental and the odd harmonics of the modulation frequency as horizontal lines. In the first half of the panel (0–25 s) the frequency band is from 0 to 10 kHz, the following quarter

(25–38 s), the band is 20–10 kHz with 20 kHz at the bottom of the frequency scale, and in the last quarter the band is from 20 to 30 kHz. During the time interval shown the distance of the PDP was 75 m perpendicular from the beam.

The Fourier transform of a square-wave function with a 50% duty cycle has vanishing even harmonics and odd harmonics with amplitudes that varies as $1/f$. Figure 18 shows the magnetic field amplitude of the narrow-band emissions observed at three different locations of the PDP relative to the beam (Reeves et al., 1988a). As can be seen, the amplitude does decrease approximately as $1/f$. Note also that even harmonics are present, although weaker by an order of magnitude. This indicates that the beam is losing some of its square-wave form within the 300 m distance of the PDP and the shuttle. However, as pointed out by Reeves et al. (1990b), the duty cycle factor is very sensitive to changes in the duty cycle. A change from 50 to 50.5% is enough to account for the amplitude of the even harmonics.

The beam resonance condition determines k_i. The dispersion relation has two roots or two values of k for given values of k and ω. In certain frequency bands one of these roots becomes imaginary, which corresponds to evanescent waves. In the near-field these waves can give important contributions to the electromagnetic field. In the theory of Harker and Banks root1 is evanescent below f_{LHR} while root2 is continuous across f_{LHR}. Above f_{LHR} root1 corresponds to waves generated at the resonance cone, while root2 corresponds to waves generated in the central hump of the refractive index surface. Studies of the amplitude of the harmonics as a function of distance from the beam show that the signal amplitude roughly follows the predictions for the root2 waves. For the Spacelab-2 free-flight, f_{LHR} was around 3 kHz, and therefore the first harmonic was below f_{LHR} while the third and higher harmonics were above f_{LHR}. The root1 solutions for the higher harmonics have, according to the theory, much larger amplitudes than observed. Furthermore, the first harmonic (which is evanescent for root1) should be strong very close to the beam, and decrease rapidly with distance until the root2 waves become dominant. This behavior was not observed in the magnetic field data. Rather, the amplitude varied with distance much as predicted for root2 waves (Reeves et al., 1990a).

As shown in Fig. 19, the first harmonic of the electric field below f_{LHR} did decrease relatively rapidly with distance (Reeves et al., 1988a). At the same time, emissions around the second and third harmonics, broad-band as well as narrow-band, became relatively dominant. It is possible that these waves are lower
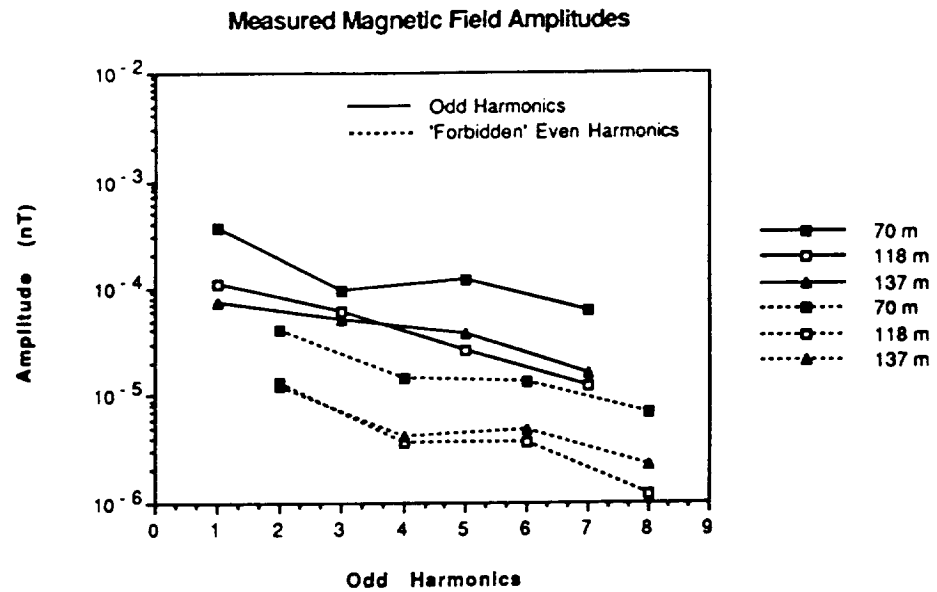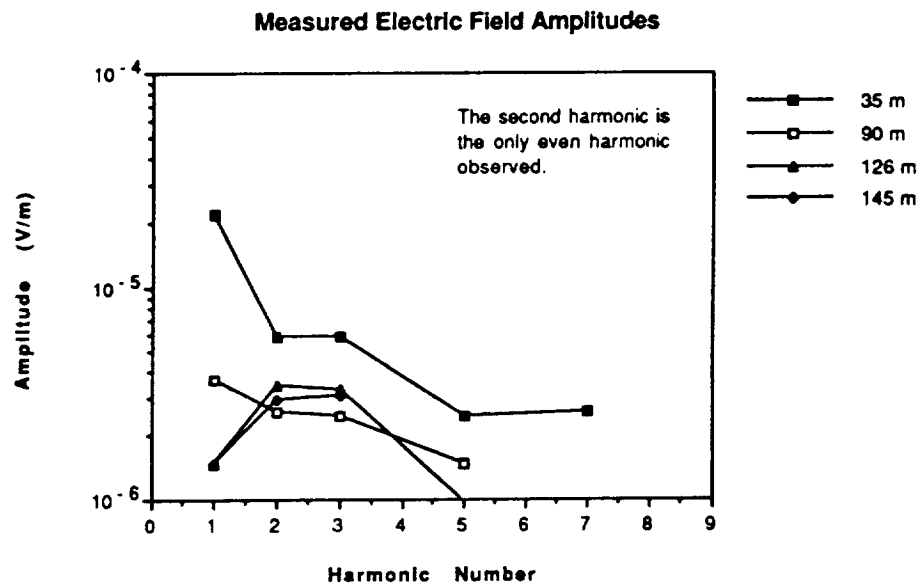
Measured Magnetic Field Amplitudes

Odd Harmonics

FIG. 18. MAGNETIC FIELD AMPLITUDE OF THE HARMONICS OF THE BEAM PULSING FREQUENCY (1.22 kHz) AT THREE DIFFERENT LOCATIONS OF THE PDP RELATIVE TO THE BEAM (FROM REEVES et al., 1988a).

hybrid waves as suggested by computer particle simulations (Matsumoto and Fukuchi, 1985; Hwang and Okuda, 1989).

The dependence of the wave field amplitude on the

duty cycle has been studied by injecting a sequence of pulses with constant pulsing frequency and varying the duty cycle. Figure 20 shows the magnetic field amplitude observed in the payload bay of the first

Measured Electric Field Amplitudes

The second harmonic is the only even harmonic observed.

Harmonic Number

FIG. 19. ELECTRIC FIELD AMPLITUDE OF THE HARMONICS OF THE BEAM PULSING FREQUENCY (1.22 kHz) AT DIFFERENT LOCATIONS OF THE PDP (FROM REEVES et al., 1988a).
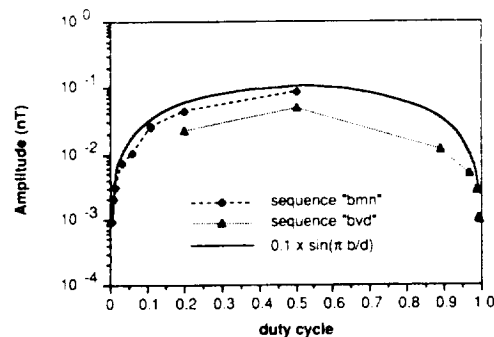
Fig. 20. Magnetic field amplitude of the fundamental
frequency as a function of duty cycle.
The solid line is the duty cycle factor D arbitrarily normalized
to 0.1 (from Reeves et al., 1990b).

Variation of Amplitude of Fundamental with Frequency

Fig. 21. The magnetic field amplitude of the fun-
damental as a function of the pulsing frequency.
Predicted curves are shown for Cherenkov root1 and root2.
The size of the markers indicate the duty cycle (from Reeves
et al., 1990b).

harmonic as a function of duty cycle (Reeves et al.,
1990b). The factor D is normalized to the arbitrary
value of 0.1 in order to enable the comparison with the
observations. As can be seen, the agreement between
observations and predictions is quite good. As the
duty cycle goes to zero, the average current goes to
zero and the field amplitude approaches some small
background level. For the duty cycle approaching
100%, the beam becomes continuous and only broad-
band noise is generated. Here, the amplitude again
approaches a very small value. One question that has
remained unanswered in the past has been whether
the sudden onset and turn-off of the beam, that is, the
leading or trailing edge of the beam or sudden changes
in the spacecraft potential were responsible for the
radiation. In this case, radiation should be inde-
pendent of the duty cycle. Thus, the Spacelab-2 study
shows that the source at least to some approximation
is square-wave modulated as predicted by theory.

The polarization of the beam-generated fields was
studied in Neubert et al. (1990c). Although only one
component of the electric and one component of the
magnetic field was measured, the spin of the PDP was
utilized to find the polarization of the fields in the spin
plane. It was found that the observed polarization did
not agree well with the predicted polarization and
that therefore the current structure departed from
the helical structure assumed in the model. Another
possibility comes from the fact that the theory pre-
sented in Harker and Banks (1987) neglects the con-
tribution from a branch cut in the integration over
k, which corresponds to ray propagation, and only
considers the simple poles which correspond to sur-
face waves. The model is, therefore, incomplete as it
stands.

A final comparison with theory is shown in Fig. 21
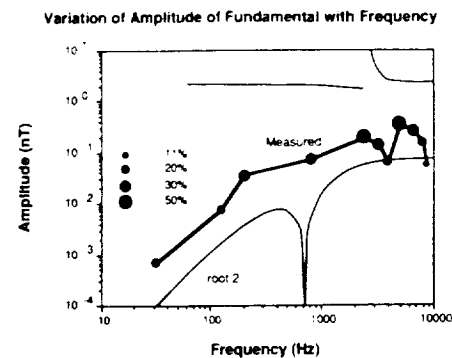(Reeves et al., 1990b). The amplitude of the fun-

damental component is plotted as function of
frequency. This coverage in frequency required a
compromise on the duty cycle. The duty cycle used is
shown by the size of the markers. 50% duty cycle
having the largest marker. At this time the PDP was
located in the payload bay. Also shown are the pre-
dictions of the model for root1 and root2. Again it
can be concluded that the model predictions for root2
are in general agreement with observations while
root1 predicts amplitudes many orders of magnitude
above observations.

The results from pulsed electron beam studies can
be summarized as follows:

(16) Observations show that the spectral structure
of the wave emissions closely follows the spectral
structure of the injected beam current. A square-wave
modulated beam generates harmonics as expected
from the Fourier transform of a square-wave func-
tion.

(17) A closer comparison with the theory of Harker
and Banks (1987) reveals that the amplitude depen-
dence of individual harmonic components with fre-
quency or distance from the beam is not as expected
from theory. In addition, the observed polarization is
not as expected. The amplitude is in general agreement
with the predictions of root2.

(18) A conclusion must be that the model does not
assume the correct structure of the radiating current.
For instance, a current structure as expected from
simulations of continuous beam emissions, when
modulated by a square wave, will give the observed
spectral structure. The amplitude and polarization
from such a model may agree better with obser-
vations.

4. DISCUSSION

From the 18 summary points given throughout this paper it is seen that a basic understanding of many processes associated with electron beam ejection in space plasmas has been achieved. This knowledge has emerged from a synthesis of experiments, analytical modelling, and computer simulations. As a result, beam ejection can now be controlled to a higher degree than before, allowing the ejection of larger currents, increasing the beam coherence and the escape energy of the beam, and reducing the plasma wave noise. These are crucial skills for some of the applications of electron beams to improving understanding of natural processes of plasma wave generation.

Experiments in the future are needed to study still unresolved issues as well as to capitalize on our ability to better control the electron beam ejection process. High time resolution observations of plasma waves and particles and potential oscillations of beam-emitting platforms are needed to understand the establishment of the payload potential and the sheath structure. Ionization processes in the sheath region due to outgas, thruster emissions or hollow cathode operations also need to be studied. Calculations indicate that instabilities may be induced by the ionization (Cook and Katz, 1988).

One of the natural processes that will need more study in the future regards the generation of electromagnetic radiation from electron beams. While the consensus is that radiation observed in past experiments is a result of Cherenkov radiation, it is still debated how the radiation current structure is formed. It is important to answer this question as it pertains to the generation of VLF waves in the ionosphere from natural processes. The VLF whistler mode is the most dominant wave mode observed in the magnetosphere, and these waves control the energetic electron population (Kennel and Petschek, 1966).

The ideas and experiences of the past will be put to practice in the ATLAS-1 space shuttle mission (1992) which will fly the SEPAC electron beam experiment (7 kV, 1.6 mA). For the first time in ionospheric beam experiments, a hollow cathode will be used to control the spacecraft potential. Thus the beam should escape with almost its complete and known energy. Optical emissions from the natural aurora as well as from the SEPAC electron beam, as it ionizes the Earth's upper atmosphere, will be observed by the sensitive on-board cameras and spectrographs of the AEPI experiment. The dynamics of the ionization structures created in the upper atmosphere by the beam will be studied by ground-based radars, and attempts will be made to observe VLF radiation on the ground. (The beam can be modulated up to 5 kHz.)

The structure of the radiating beam electron current can possibly be deduced from detailed observations of the electromagnetic field in the vicinity of the beam. Such measurements are planned for the CHARGE-2b sounding rocket experiment (1992). The electromagnetic radiation from the beam will be observed from a sub-payload equipped with a sophisticated wave experiment measuring simultaneously three electric and three magnetic field components. The experiment will also allow the study of the limits to vehicle neutralization by thruster emissions.

Finally we point out that the recent development of comparatively small electron linear accelerators now makes possible a whole new class of ionospheric modification experiments (Banks et al., 1991). With electron beams in the megaelectronvolt range it is possible to create substantial ionization from the source altitude down to an altitude of 40 km. In the region from 40 to 60 km, the modification of the fair weather electric potential may result in electric fields of a sufficient magnitude to cause breakdown and discharge in the beam column. The result is the initiation of lightning discharges along the initial beam column and associated VLF wave generation.

REFERENCES

Abe, Y., Erickson, K. N. and Winckler, J. R. (1988) ELF electric turbulence near an electron beam-emitting rocket in the auroral ionosphere. *Planet. Space Sci.* **36**, 235.

Amme, R. C. (1969) Origin of secondary electrons ejected from gas-covered surfaces by fast neutral beams. *J. chem. Phys.* **50**, 1891.

Arnoldy, R. L., Pollock, C. and Winckler, J. R. (1985) The energization of electrons and ions by electron beams injected in the ionosphere. *J. geophys. Res.* **90**, 5197.

Arnoldy, R. L. and Winckler, J. R. (1981) The hot plasma environment and floating potentials of an electron-beam-emitting rocket in the ionosphere. *J. geophys. Res.* **86**, 575.

Banks, P. M., Chappell, C. R. and Nagy, A. F. (1974) A new model for the interaction of auroral electrons with the atmosphere: spectral degradation, backscatter, optical emission, and ionization. *J. geophys. Res.* **79**, 1459.

Banks, P. M., Fraser-Smith, A. C. and Gilchrist, B. E. (1991) Ionospheric modification using relativistic electron beams. *AGARD Conference Proceedings*, No. 785, pp. 22-1 22-17, Bergen, Norway.

Banks, P. M. and Gilchrist, B. E. (1985) Artificial plasma

density structures produced by energetic electron beams from rockets and spacecraft. *Geophys. Res. Lett.* **12**, 175.

Banks, P. M., Gilchrist, B. E., Neubert, T., Myers, N., Raitt, W. J., Williamson, P. R., Fraser-Smith, A. C. and Sasaki, S. (1990) *CHARGE-2* rocket observations of vehicle charging and charge neutralization. *Adv. Space Res.* **10**, 133.

Banks, P. M. and Nagy, A. F. (1970) Concerning the influence of elastic scattering upon photoelectron transport and escape. *J. geophys. Res.* **75**, 1902.

Banks, P. M. and Raitt, W. J. (1988) Observations of electron beam structure in space experiments. *J. geophys. Res.* **93**, 5811.

Banks, P. M., Raitt, W. J., White, A. B., Bush, R. I. and Williamson, P. R. (1987) Results from the vehicle charging and potential experiment on *STS-3*. *J. Spacecraft Rockets* **24**, 138.

Beard, D. B. and Johnson, F. S. (1961) Ionospheric limitations on attainable satellite potential. *J. geophys. Res.* **66**, 4113.

Bell, T. F. (1968) Artificial production of VLF hiss. *J. geophys. Res.* **73**, 4409.

Bernstein, W., Leinbach, H., Kellogg, P. J., Monson, S. J. and Hallinan, T. (1979) Further laboratory measurements of the beam-plasma discharge. *J. geophys. Res.* **84**, 7271.

Bilitza, D. (1986) International reference ionosphere: recent developments. *Radio Sci.* **21**, 343.

Brenning, N. and Mendillo, M. (Editors) (1990) Active experiments critical ionization velocity. *Adv. Space Res.* **10**, No. 7.

Burke, W. R. (Editor) (1983) *Active experiments in space* (*Alpach Symposium*) European Space Agency Scientific and Technical Publications *SP*-195. Noordwijk, Netherlands.

Bush, R. I., Reeves, G. D., Banks, P. M., Neubert, T., Williamson, P. R., Raitt, W. J. and Gurnett, D. A. (1987) Electromagnetic fields from pulsed electron beam experiments in space: *Spacelab-2* results. *Geophys. Res. Lett.* **14**, 1015.

Cai, D., Neubert, T., Storey, L. R. O., Banks, P. M., Sasaki, S., Abe, K. and Burch, J. L. (1987) ELF oscillations associated with electron beam injections from the space shuttle. *J. geophys. Res.* **92**, 12,451.

Cartwright, D. G. and Kellogg, P. J. (1974) Observations of radiation from an electron beam artificially injected into the ionosphere. *J. geophys. Res.* **79**, 1439.

Cartwright, D. G., Monson, S. J. and Kellogg, P. J. (1978) Heating of the ambient ionosphere by an artificially injected electron beam. *J. geophys. Res.* **83**, 16.

Cooke, D. L. and Katz, I. (1988) Ionization-induced instability in an electron-collecting sheath. *J. Spacecraft Rockets* **25**, 132.

Denig, W. F., Maynard, N. C., Burke, W. J. and Maehlum, B. M. (1990) Electric field measurements during supercharging events on the *MAIMIK* rocket experiment. *J. geophys. Res.* **96**, 3601.

Dietz, L. A. and Sheffield, J. C. (1975) Secondary electron emission induced by 5–30 keV monoatomic ions striking thin oxide films. *J. appl. Phys.* **46**, 4361.

Egeland, A. and Leer, E. (1986) Professor Kr. Birkeland: his life and work. *IEEE Trans. Plasma Sci.* **PS-14**, 666.

Erickson, K. N. and Winckler, J. R. (1990) A study of plasma heating, electric fields and plasma flow near an electron beam-emitting rocket system in the polar ionosphere. *J. geophys. Res.* (submitted).

Faelthammer, C.-G. (1986) Magnetosphere–ionosphere interactions—near-earth manifestations of the plasma universe. *IEEE Trans. Plasma Sci.* **PS-14**, 616.

Farrell, W. M. (1990) Comments on "Pulsed electron beam emission in space", by Neubert *et al.*, 1988. *J. Geomagn. Geoelec.* **42**, 57.

Farrell, W. M., Gurnett, D. A., Banks, P. M., Bush, R. I. and Raitt, W. J. (1988) An analysis of whistler mode radiation from the *Spacelab-2* experiment. *J. geophys. Res.* **93**, 153.

Farrell, W. M., Gurnett, D. A. and Goertz, C. K. (1989) Coherent Cerenkov radiation from the *Spacelab 2* electron beam. *J. geophys. Res.* **94**, 443.

Frank, L. A., Paterson, W. R., Ashour-Abdalla, M., Schreiver, D., Kurth, W. S., Gurnett, D. A., Omidi, N., Banks, P. M., Bush, R. I. and Raitt, W. J. (1989) Electron velocity distributions and plasma waves associated with the injection of an electron beam into the ionosphere. *J. geophys. Res.* **94**, 6995.

Friedrich, M., Torkar, K. M., Trøim, J. and Mæhlum, B. N. (1991) Plasma observations of the active mother-daughter payload *Maimik* in the lower thermosphere. *Planet. Space Sci.* **39**, 453–468.

Gekelman, W. and Stenzel, R. (1978) Ion sound turbulence in a magnetoplasma. *Phys. Fluids* **21**, 2014.

Gilchrist, B. E. (1991) Ph. D. thesis, Stanford University.

Gilchrist, B. E., Banks, P. M., Neubert, T., Williamson, P. R., Myers, N. B., Raitt, W. J. and Sasaki, S. (1990) Electron collection enhancement arising from neutral gas jets on a charged vehicle in the ionosphere. *J. geophys. Res.* **95**, 2469.

Goerke, R. T., Kellogg, P. J. and Monson, S. J. (1990) An analysis of whistler mode radiation from a 100 mA electron beam. *J. geophys. Res.* **95**, 4277.

Grandal, B. (Editor) (1982) *Artificial particle Beams in Space Plasma Studies* (*Geilo Symposium*). Plenum Press, New York.

Gurnett, D. A., Kurth, W. S., Steinberg, J. T., Banks, P. M., Bush, R. I. and Raitt, W. L. (1986) Whistler-mode radiation from the *Spacelab-2* electron beam. *Geophys. Res. Lett.* **13**, 225.

Gurnett, D. A., Shawhan, S. D. and Shaw, R. R. (1983) Auroral hiss, Z mode radiation, and auroral kilometric radiation in the polar magnetosphere: *DE* 1 observations. *J. geophys. Res.* **88**, 329.

Hallinan, T. J., Winckler, J. R., Malcolm, P., Stenbaek-Nielsen, H. C. and Baldridge, J. (1990) Conjugate echoes of artificially injected electron beams detected optically by means of new image processing. *J. geophys. Res.* **95**, 6519.

Harker, K. J. and Banks, P. M. (1983) Radiation from pulsed electron beams in space plasmas. *Radio Sci.* **19**, 454.

Harker, K. J. and Banks, P. M. (1985) Radiation from long pulse train electron beams in space plasmas. *Planet. Space Sci.* **33**, 953.

Harker, K. J. and Banks, P. M. (1987) Near fields in the vicinity of pulsed electron beams in space. *Planet. Space Sci.* **35**, 11.

Harker, K. J., Neubert, T., Banks, P. M., Fraser-Smith, A. C. and Donohue, D. J. (1991) Ground level signal strength of electromagnetic waves generated by pulsed electron beams in space. *Planet. Space Sci.* **39**, 1527–1536.

Hastings, D. E. (1987) Enhanced current flow through a plasma cloud by induction of plasma turbulence. *J. geophys. Res.* **92**, 7716.

Hayden, H. C. and Utterback, N. G. (1964) Ionization of helium, neon, and nitrogen by helium atoms. *Phys. Rev. A* **135**, 1575.

Hedin, A. E. (1987) MSIS-86 thermospheric model. *J. geophys. Res.* **92**, 4649.

Hess, W. N., Trichel, M. C., Davis, T. N., Beggs, W. C., Kraft, G. E., Stassinopoulos, E. and Maier, E. J. R. (1971) Artificial aurora experiment: experiment and principal results. *J. geophys. Res.* **76**, 6067.

Holzworth, R. H. and Koons, H. C. (1981) VLF emissions from a modulated electron beam in the auroral ionosphere. *J. geophys. Res.* **86**, 853.

Hwang, Y. S. and Okuda, H. (1989) Low-frequency electrostatic instabilities excited by injections of an electron beam in space. *J. geophys. Res.* **94**, 10103.

Inan, U. S., Pon, M., Banks, P. M., Williamson, P. R., Raitt, W. J. and Shawhan, S. D. (1984) Modulated beam injection from the space shuttle during magnetic conjunctions of STS 3 with the DE 1 satellite. *Radio Sci.* **19**, 487.

Israelson, G. A. and Winckler, J. R. (1979) Effect of a neutral N₂ cloud on the electrical charging of an electron beam-emitting rocket in the ionosphere: ECHO IV. *J. geophys. Res.* **84**, 1442.

James, H. G. (1976) VLF saucers. *J. geophys. Res.* **81**, 501.

Junginger, H., Geiger, G., Haerendel, G., Melzner, F., Amata, E. and Higel, B. (1984) A statistical study of dayside magnetospheric electric field fluctuations with periods between 150 and 600 s. *J. geophys. Res.* **89**, 5495.

Kawashima, N. (1982) Experimental studies of the neutralization of a charged vehicle in space and in the laboratory in Japan, in *Artificial Particle Beams in Space Plasma Studies* (Edited by Grandal, B.), p. 573. Plenum Press, New York.

Katz, I. and Davis, V. A. (1987) On the need for space tests of plasma contactors as electron collectors, paper presented at the 2nd Annual Conference on Tethers in Space, PSN NASA ESA, Venice, Italy, 4-8 October.

Kellogg, P. J., Monson, S. J., Bernstein, W. and Whalen, B. A. (1986) Observations of waves generated by electron beams in the ionosphere. *J. geophys. Res.* **91**, 12,065.

Kennel, C. F. and Petschek, H. E. (1966) Limit on stably trapped particle fluxes. *J. geophys. Res.* **71**, 1.

Langley, R. A., Bohdansky, J., Eckstein, W., Mioduszewski, P., Roth, J., Taglauer, E., Thomas, E. W., Verbeek, H. and Wilson, K. L. (1984) Data compendium for plasma surface interactions. *Nucl. Fusion, Special Issue* **27**, 99.

Langmuir, I. and Blodgett, K. B. (1924) Current limited by space charge flow between concentric spheres. *Phys. Rev.* **24**, 49.

Lavergnat, J. and Lehner, T. (1984) Low frequency radiation characteristics of a modulated electron beam immersed in a magnetized plasma. *IEEE Trans. AP-32*, 177.

Lavergnat, J., Lehner, T. and Matthieussent, G. (1984) Coherent spontaneous emission from a modulated beam injected in a magnetized plasma. *Phys. Fluids* **27**, 1632.

Liemohn, H. B. (1965) Radiation from electrons in a magnetoplasma. *J. Res. natn. Bur. Stand. D* **69**, 741.

Linson, L. M. (1969) Current voltage characteristics of an electron emitting satellite in the ionosphere. *J. geophys. Res.* **74**, 2368.

Linson, L. M. (1982) Charge neutralization as studied experimentally and theoretically, in *Artificial Particle Beams in Space Plasma Studies* (Edited by Grandal, B.), p. 573. Plenum Press, New York.

Maehlum, B. M., Troim, J., Maynard, N. C., Denig, W. F., Friedrich, M. and Torkar, K. M. (1988) Studies of the electrical charging of the tethered electron accelerator

mother daughter rocket MAIMIK. *Geophys. Res. Lett.* **15**, 725.

Managadze, G. G., Riedler, W., Balebanov, B. M., Friedrich, M. F., Gagua, T. I., Kios, Z., Lalashvili, N. A., Leonov, N. A., Lyakhov, S. B., Martinson, A. A. and Mayorov, A. D. (1983) Plasma processes in the region of electron beam injection from a high-altitude payload. *Active Experiments in Space (Alpbach Symposium)* (Edited by Burke, W. R.), European Space Agency Scientific and Technical Publications SP-195, Noordwijk, Netherlands.

Managadze, G. G., Riedler, W. K., Friedrich, M. F., Balebanov, V. M., Lalashvili, A. A., Leonov, N. A., Lyakhov, S. B., Martinson, A. A., Mayorov, A. D., Klos, Z., Zbyszynski, Z. and Torkar, K. M. (1988) Potential observations of an electron emitting rocket payload and other related plasma measurements. *Planet. Space Sci.* **36**, 399.

Mandell, M. J., Lilley, J. R., Jr., Katz, I., Neubert, T. and Myers, N. B. (1990) Computer modelling of current collection by the CHARGE 2 mother payload. *Geophys. Res. Lett.* **17**, 135.

Mansfield, V. N. (1967) Radiation from a charged particle spiralling in a cold magnetoplasma. *Astrophys. J.* **147**, 672.

Matsumoto, H. and Fukuchi, K. (1985) Computer simulation of particle acceleration and wave excitation by electron beam injection from space shuttle. *Geophys. Res. Lett.* **12**, 61.

McKenzie, J. F. (1967) Radiation losses from a test particle in a plasma. *Phys. Fluids* **10**, 2680.

Melzner, F., Metzner, G. and Antrack, D. (1978) The Geos electron beam experiment S 329. *Space Sci. Instrum.* **4**, 45.

Myers, N. B., Raitt, W. J., Gilchrist, B. E., Banks, P. M., Neubert, T., Williamson, P. R. and Sasaki, S. (1989) A comparison of current voltage relationships of collectors in the earth's ionosphere with and without electron beam emission. *Geophys. Res. Lett.* **16**, 365.

Myers, N. B., Raitt, W. J., White, A. B., Banks, P. M., Gilchrist, B. E. and Sasaki, S. (1990) Vehicle charging effects during electron beam emission from the CHARGE 2 experiment. *J. Spacecraft Rockets* **27**, 25.

Neubert, T. and Banks, P. M. (1990) Plasma density enhancements created by the ionization of the Earth's upper atmosphere by artificial electron beams. *AGARD Conference Proceedings, No. 485*, pp. 21-1-21-6, Bergen, Norway.

Neubert, T., Bell, T. F. and Storey, L. R. O. (1987) Resonance between coherent whistler mode waves and electrons in the topside ionosphere. *J. geophys. Res.* **92**, 255.

Neubert, T. and Harker, K. J. (1988) Magnetic fields in the vicinity of pulsed electron beams in space. *Planet. Space Sci.* **36**, 469.

Neubert, T., Hawkins, J. G., Reeves, G. D., Banks, P. M., Bush, R. I., Williamson, P. R., Gurnett, D. A. and Raitt, W. J. (1988) Pulsed electron beam emission in space. *J. Geomagn. Geoelect.* **40**, 1221.

Neubert, T., Mandell, M. J., Sasaki, S., Gilchrist, B. E., Banks, P. M., Williamson, P. R., Raitt, W. J., Myers, N. B., Oyama, K. I. and Katz, I. (1990a) The sheath structure around a negatively charged rocket payload. *J. geophys. Res.* **95**, 6155.

Neubert, T., Banks, P. M., Gilchrist, B. E., Fraser-Smith, A. C., Williamson, P. R., Raitt, W. J., Myers, N. B. and Sasaki, S. (1990b) The interaction of an artificial electron beam with the earth's upper atmosphere: effects on spacecraft charging and the near-plasma environment. *J. geophys. Res.* **95**, 12,209.

Neubert, T., Harker, K. J., Banks, P. M., Reeves, G. D.

and Gurnett, D. A. (1990) Waves generated by pulsed electron beams. *Adv. Space Res.* **10**, 137.

Neubert, T., Sasaki, S., Gilchrist, B. E., Banks, P. M., Williamson, P. R., Fraser-Smith, A. C. and Raitt, W. J. (1991) Observation of plasma wave turbulence generated around large ionospheric spacecraft: effects of motionally induced EMF and of electron beam emission. *J. geophys. Res.* **96**, 9639.

Neubert, T., Taylor, W. W. L., Storey, L. R. O., Kawashima, N., Roberts, W. T., Reasoner, D. L., Banks, P. M., Gurnett, D. A., Williams, R. L. and Burch, J. L. (1986) Waves generated during electron beam emissions from the space shuttle. *J. geophys. Res.* **91**, 11,321.

O'Neil, R. R., Bien, F., Burt, D., Sandock, J. A. and Stair, A. T. Jr. (1978a) Summarized results of the artificial auroral experiment. Precede. *J. geophys. Res.* **83**, 3273.

O'Neil, R. R., Shepherd, O., Reidy, W. P., Carpenter, J. W., Davis, T. N., Newell, D., Ulwick, J. C. and Stair, A. T. Jr. (1978b) *Excede* 2 test, an artificial auroral experiment: ground-based optical measurements. *J. geophys. Res.* **83**, 3281.

Ohnuki, S. and Adachi, S. (1984) Radiation of electromagnetic waves from an electron beam antenna in an ionosphere. *Radio Sci.* **19**, 925.

Okuda, H. and Ashour-Abdalla, M. (1988) Ion-acoustic instabilities excited by the injection of an electron beam in space. *J. geophys. Res.* **93**, 2011.

Okuda, H. and Ashour-Abdalla, M. (1990) Propagation of a nonrelativistic electron beam in three dimensions. *J. geophys. Res.* **95**, 2389.

Okuda, H. and Ashour-Abdalla, M. (1991) Injection of an overdense electron beam in space. *J. geophys. Res.* **95**, 21,307.

Omura, Y. and Matsumoto, H. (1988) Computer experiments on whistler and plasma wave emissions for the *Spacelab*-2 electron beam. *Geophys. Res. Lett.* **15**, 319.

Parker, L. W. and Murphy, B. L. (1967) Potential buildup on an electron-emitting satellite in the ionosphere. *J. geophys. Res.* **74**, 1631.

Patterson, M. (1987) Hollow cathode-based plasma contactor experiments for electrodynamic tether. *AIAA, AIAA-87-0571*.

Peratt, A. L. (1986) Evolution of the plasma universe: 1. Double radio galaxies, quasars, and extragalactic jets. *IEEE Trans. Plasma Sci.* **PS-14**, 639.

Peratt, A. L. (1988) The role of particle beams and electrical currents in the plasma universe. *Laser Particle Beams* **6**, 471.

Peratt, A. L. (1990) The evidence for electrical currents in cosmic plasma. *IEEE Trans. Plasma Sci.* **PS-18**, 26-32.

Pritchett, P. L. (1990) Spatial coherence during pulsed injection of electron beams. *J. geophys. Res.* **95**, 10671.

Pritchett, P. L. (1991) A three-dimensional simulation model for electron beam injection experiments in space. *J. geophys. Res.* **96**, 13,781.

Pritchett, P. L., Karamabadi, H. and Omidi, N. (1989) Generation mechanism of whistler waves produced by electron beam injection in space. *Geophys. Res. Lett.* **16**, 883.

Pritchett, P. L. and Winglee, R. M. (1987) The plasma environment during particle beam injection into space plasmas. 1. Electron beams. *J. geophys. Res.* **92**, 7673.

Reeves, E. G. D., Banks, P. M., Neubert, T., Bush, R. I., Williamson, P. R., Fraser-Smith, A. C., Gurnett, D. A. and Raitt, W. J. (1988a) VLF wave emissions by pulsed and DC electron beams in space 1: *Spacelab*-2 observations. *J. geophys. Res.* **93**, 14,699.

Reeves, G. D., Banks, P. M., Fraser-Smith, A. C., Neubert, T., Bush, R. I., Gurnett, D. A. and Raitt, W. J. (1988b) VLF wave stimulation by pulsed electron beams injected from the space shuttle. *J. geophys. Res.* **93**, 162.

Reeves, G. D., Banks, P. M., Neubert, T., Harker, K. J. and Gurnett, D. A. (1990a) VLF wave emissions by pulsed and DC electron beams in space 2: analysis of *Spacelab*-2 results. *J. geophys. Res.* **95**, 6505.

Reeves, G. D., Banks, P. M., Neubert, T., Harker, K. J., Gurnett, D. A. and Raitt W. J. (1990b) *Spacelab*-2 electron beam wave stimulation: studies of important parameters. *J. geophys. Res.* **95**, 10,655.

Reme, H. (Editor) (1980) Special issue on the results of the active French-Soviet Araks experiments. *Ann. Geophys.* **36**, 3.

Sagdeev, R. Z., Managadze, G. G., Mayorov, A. D., Kyakov, S. B., Martinson, A. A., Romanovsky, Yu. A., Adeiskvily, T. G., Leonov, N. A. and Gagua, T. I. (1981) Peculiarities of the environment disturbance during the electron beam injection from the rocket. *Adv. Space Res.* **1**, 77.

Sasaki, S., Kawashima, N., Kuriki, K., Yanagisawa, M., Obayashi, T., Roberts, W. T., Reasoner, D. L., Taylor, W. W. L., Williamson, P. R., Banks, P. M. and Burch, J. L. (1985a) Ignition of beam plasma discharge in the electron beam experiment in space. *Geophys. Res. Lett.* **12**, 647.

Sasaki, S., Kawashima, N., Kuriki, K., Yanagisawa, M., Obayashi, T., Roberts, W. T., Reasoner, D. L., Taylor, W. W. L., Williamson, P. R., Banks, P. M. and Burch, J. L. (1985b) An enhancement of plasma density by neutral gas injection observed in *SEPAC Spacelab*-1 experiment. *J. Geomagn. Geoelec.* **37**, 883.

Sasaki, S., Oyama, K. I., Kawashima, N., Watanabe, Y., Obayashi, T., Raitt, W. J., White, A. B., Banks, P. M., Williamson, P. R., Sharp, W. F., Yokota, T. and Hirao, K. (1987) Results from a series of tethered rocket experiments. *J. Spacecraft Rockets* **24**, 444.

Sasaki, S., Oyama, K. I., Kawashima, N., Obayashi, T., Hirao, K., Raitt, W. J., Myers, N. B., Williamson, P. R., Banks, P. M. and Sharp, W. F. (1988) Tethered rocket experiment (*CHARGE* 2): initial results on electrodynamics. *Radio Sci.* **23**, 975.

Shawhan, S. D., Murphy, G. B., Banks, P. M., Williamson, P. R. and Raitt, W. J. (1984) Wave emissions from dc and modulated electron beams on *STS*-3. *Radio Sci.* **19**, 471.

Stenzel, R. L. (1978a) Experiments on current-driven three-dimensional ion sound turbulence. Part 1: return-current limited electron beam injection. *Phys. Fluids* **21**, 93.

Stenzel, R. L. (1978b) Experiments on current-driven three-dimensional ion sound turbulence. Part 2: wave dynamics. *Phys. Fluids* **21**, 99.

Stix, T. H. (1962) *The Theory of Plasma Waves*. McGraw-Hill, New York.

Szapiro, B. and Rocca, J. J. (1989) Electron emission from glow-discharge cathode materials due to neon and argon bombardment. *J. appl. Phys.* **65**, 3713.

Szapiro, B., Rocca, J. J. and Prabhuram, T. (1988) Electron yield of glow discharge cathode material under helium ion bombardment. *Appl. Phys. Lett.* **53**, 358.

Taylor, W. W. L., Roberts, W. T., Reasoner, D. L., Chappell, C. R., Watkins, J. R., Baker, B. B., Burch, J. L., Gibson, W. C., Black, R. K., Tomlinson, W. M., Ferguson, G. A., Bounds, J. R., Womack, W. M., Banks, P. M., Williamson, P. R., Neubert, T., Williamson, W. S., Obayashi, T., Nagamoto, M., Kawashima, N., Kuriki, K., Ninomayo, K., Sasaki, S., Yanagisawa, M., Ejiri, M. and Kudo, I. (1991)

Space experiments with particle accelerators. *J. Spacecraft Rockets* (in press).

Taylor, W. W. L. and Shawhan, S. D. (1974) A test of incoherent Cerenkov radiation for VLF hiss and other magnetospheric emissions. *J. geophys. Res.* **79**, 105.

Utterback, N. G. and Miller, G. H. (1961) Fast molecular nitrogen beam. *Rev. Sci. Instrum.* **32**, 1101.

Waterman, J., Wilhelm, K., Torkar, K. M. and Riedler, W. (1988) Space shuttle charging or beam-plasma discharge: What can electron spectrometer observations contribute to solving the question? *J. geophys. Res.* **93**, 4134.

Wilhelm, K., Stuedmann, W. and Riedler, W. (1984) Electron flux intensity distributions observed in response to particle beam emissions. *Science* **225**, 186.

Williams, J. D., Wilbur, P. J. and Monheiser, J. M. (1987) Experimental validation of a phenomenological model of the plasma contacting process, paper presented at the 2nd Annual Conference on Tethers in Space. PSN NASA ESA, Venice, Italy, October 4–8.

Winckler, J. R. (1980) The application of artificial electron beams to magnetospheric research. *Rev. Geophys. Space Phys.* **18**, 649.

Winckler, J. R., Arnoldy, R. L. and Hendrickson, R. A. (1975) *Echo* 2: a study of electron beams injected into the high-latitude ionosphere from a large sounding rocket. *J. geophys. Res.* **80**, 2083.

Winckler, J. R., Erickson, K. N., Abe, Y., Steffen, J. E. and Malcolm, P. R. (1985) ELF wave production by an electron beam emitting rocket system and its suppression on auroral field lines: evidence for Alfvén and drift waves. *Geophys. Res. Lett.* **12**, 457.

Winckler, J. R., Malcolm, P. R., Arnoldy, R. L., Burke, W. J., Erickson, K. N., Ernstmeyer, J., Franz, R. C., Hallinan, T. J., Kellogg, P. J., Monson, S. J., Lynch, K. A., Murphy, G. and Nemzek, R. J. (1989) *Echo* 7: an electron beam experiment in the magnetosphere. *EOS* **70**, 657.

Winckler, J. R., Steffen, J. E., Malcolm, P. R., Erickson, K. N., Abe, Y. and Swanson, R. L. (1984) Ion resonances and ELF wave production by an electron beam emitting rocket in the ionosphere: *ECHO* 6. *J. geophys. Res.* **89**, 7565.

Winglee, R. M. (1990) Electron beam injection during active experiments: 2. Collisional effects. *J. geophys. Res.* **95**, 6191.

Winglee, R. M. and Kellogg, P. J. (1990) Electron beam injection during active Experiments: 1. Electromagnetic wave emissions. *J. geophys. Res.* **95**, 6167.

Winglee, R. M. and Pritchett, P. L. (1988) Comparative study of cross-field and field-aligned electron beams in active experiments. *J. geophys. Res.* **93**, 5823.

Wong, H. K. and Lin, C. S. (1990) Plasma instabilities of a finite-radius beam in a uniform plasma. *Radio Sci.* **25**, 277.

Yeh, K. C. (Editor) *Radio Science* (1984) Special issue on emissions from particle beams in space **19**, 453. (Guest Editor E. R. Schmerling).

The Dynamics of Low-β Plasma Clouds as Simulated by a Three-Dimensional, Electromagnetic Particle Code

T. Neubert and R. H. Miller

Space Physics Research Laboratory, University of Michigan, Ann Arbor

O. Buneman

STAR Laboratory, Department of Electrical Engineering, Stanford University, Stanford, California

K.-I. Nishikawa

Department of Physics and Astronomy, University of Iowa, Iowa City

The dynamics of low-β plasma clouds moving perpendicular to an ambient magnetic field in vacuum and in a background plasma is simulated by means of a three-dimensional, electromagnetic, and relativistic particle simulation code. The simulations show the formation of the space charge sheaths at the sides of the cloud with the associated polarization electric field which facilitate the cross-field propagation, as well as the sheaths at the front and rear end of the cloud caused by the larger ion Larmor radius, which allows ions to move ahead and lag behind the electrons as they gyrate. Results on the cloud dynamics and electromagnetic radiation include the following: (1) In a background plasma, electron and ion sheaths expand along the magnetic field at the same rate, whereas in vacuum the electron sheath expands much faster than the ion sheath. (2) Sheath electrons are accelerated up to relativistic energies. This result indicates that artificial plasma clouds released in the ionosphere or magnetosphere may generate optical emissions (aurora) as energetic sheath electrons scatter in the upper atmosphere. (3) The expansion of the electron sheaths is analogous to the ejection of high-intensity electron beams from spacecraft: a stagnation point is reached where the expansion is halted, allowing only a fraction of the electrons to escape. These electrons may have energies exceeding the initial beam energy (sheath electrostatic potential energy). (4) Second-order and higher-order sheaths are formed which extend out into the ambient plasma. These sheaths are curved, the curvature increasing with the order of the sheath. (5) The formation of the sheaths and the polarization field reduces the forward momentum of the cloud. Furthermore, as the cloud moves across the field, sheath particles are peeled off and left behind, while fresh particles continue to drift into the sheaths in order to maintain these. This process requires continued energy supply which further decelerates the cloud. (6) The coherent component of the particle gyromotion (the particles are born with a coherent component at $t=0$) is damped in time as the particles establish a forward directed drift velocity. In addition, particles undergo orbital phase mixing associated with the establishment of the polarization electric field. For a dense cloud in vacuum the damping occurs very quickly, while for clouds in a background plasma the polarization fields are shorted, leaving the particles to gyrate as single particles. In this case, the coherent component is almost undamped. (7) The coherent particle gyrations generate electromagnetic radiation. The simulations indicate that artificial plasma clouds released in space will radiate close to the cloud electron or ion cyclotron/upper hybrid frequencies.

1. Introduction

The interaction of plasma clouds, or streams of plasma, with ambient magnetized plasmas is a basic process found in areas ranging from astrophysics to laboratory plasma physics. Examples of such interactions include galactic plasma jets [*Yusef-Zadeh et al.*, 1984; *Arp*, 1986; *Perley et al.*, 1984], the expansion of cometary plasmas into the solar wind [*Haerendel*, 1987], the dynamics of artificial comets [*Mende et al.*, 1989; *Baker et al.*, 1989; *Winske*, 1989], and heating of tokamak plasmas by the injection of plasma beams [*Wickman and Robertson*, 1983]. Plasma cloud dynamics are also important in experiments studying the criti-

cal ionization velocity (CIV) phenomenon [*Alfvén*, 1954; *Papadopoulos*, 1985; *Torbert*, 1990] recently performed in the Earth's ionosphere and magnetosphere as part of the CRIT I program [*Brenning et al.*, 1991] and the CRRES program [*Reasoner*, 1992]. Additional areas of cloud physics include the phenomenon of outgassing from large, manned space structures. Observations indicate that a large contaminant, partly ionized, water vapor cloud travels with the space shuttle [*Kurth and Frank*, 1990]. The ionization of the water vapor comes about through charge exchange with ambient O^+. The cloud dimension is many H_2O^+ Larmor radii perpendicular to the shuttle velocity vector and extends at least 300 m behind the shuttle [*Paterson and Frank*, 1989]. For many experiments the outgased plasma cloud represents a serious contamination. Thus one of the issues raised by observations is to what extent the plasma cloud moves with the shuttle [*Katz et al.*, 1984; *Eccles et al.*, 1989].

PRECEDING PAGE BLANK NOT FILMED

The examples listed above cover a wide range of plasma parameters, and consequently theories have been developed in the past for various parameter regimes. It has been found that plasma beams can propagate in the case where the transverse beam width is wide compared to the beam ion Larmor radius and $\beta \gg 1$ (β is the ratio of the beam pressure to the magnetic field pressure) [Chapman, 1960]. This regime can be described by MHD theory. The case of high-β narrow beams also allows some cross-field propagation according to hybrid simulations [Papadopoulos et al., 1988]. However, space and laboratory experiments concur in finding that the magnetic diffusion of the magnetic field back into the beam is much above its classical value. It has been suggested that the high diffusion rate is caused by anomalous resistivity associated with electrostatic wave instabilities [Mishin et al., 1986]. Finally low-β beams have been shown to cross-field propagate for narrow beams provided their density is above some threshold [Peter and Rostocker, 1982].

In this paper we study the propagation of a low-β cloud with a transverse dimension that is larger than the ion Larmor radius. When a low-β cloud of plasma is made to stream perpendicular to a magnetic field $\vec{B}_o$ with a bulk velocity $\vec{v}_o$, one's first guess is that the field will arrest the cloud. However, ions and electrons will attempt to rotate in opposite directions, with the result that charge layers are formed at the sides of the cloud. The electric polarization field $\vec{E}_p$ created inside the cloud by these lateral charge layers is oriented such that the $\vec{E}_p \times \vec{B}_o$ drift of the cloud particles is in the same direction as the initial bulk velocity.

A simplified condition for cross-field propagation can be found by noting that the cross-field drift velocity v_1 induced by the electric polarization field is given by

$$\vec{v}_1 \simeq \vec{E}_p \times \vec{B}_o/B_o^2 \tag{1}$$

The magnitude of the electric field depends on the charge accumulated in the sheaths on the sides of the cloud. For an infinite slab of plasma, an estimate of the polarization field can be found from Poisson's equation

$$E_p = e n^c \Delta L_y / \epsilon_o \tag{2}$$

where e is the elementary charge, n^c is the cloud particle density, and ΔL_y is the thickness of the charge layers. Assuming the maximum possible sheath thickness to be one ion Larmor radius r_{Li}, a condition for cross-field propagation is found from (1) and (2) as

$$q_i \equiv \frac{\omega_{pi}^c}{\omega_{ci}^c} \geq 1 \tag{3}$$

where ω_{pi}^c is the cloud ion plasma frequency and ω_{ci}^c the cloud ion cyclotron frequency. The parameter q_i is also equal to c/v_A where c is the velocity of light and v_A the Alfvén velocity. As will be shown later, a one-dimensional cloud (an infinite slab of plasma) with $q_i = 1$ is able to cross-field propagate with half the initial velocity. Large values of q_i allow even a three-dimensional cloud to maintain its motion across B_o with almost the full initial velocity.

The stability of the charge layers has been studied analytically and by means of one- and two-dimensional parti-

cle simulations by Cai et al. [1990] and references therein. The cross-field propagation and electromagnetic radiation from plasma beams have been studied analytically [Schmidt, 1960; Borovsky, 1987; Roussel-Dupré and Miller, 1992a,b], while two-dimensional, electrostatic particle simulations have been undertaken in order to determine particle diffusion [Okuda and Hiroe, 1987] and beam dynamics [Livesey and Pritchett, 1989]. The dynamics of plasma clouds has been explored by one-dimensional electrostatic particle simulations [Galvez, 1987] and two-dimensional electrostatic simulations [Galvez et al., 1989; Galvez and Borovsky, 1992]. Results from these studies include the rapid expansion of the polarization charge layers formed at the sides of the cloud along the magnetic field, which tend to deplete the charge layers and inhibit the motion of the cloud across the magnetic field, as well as the erosion of the front of the cloud and the peeling off of the charge layers as the cloud propagates across the field.

It is clear, however, that the problem inherently is three-dimensional and that the presence of a background plasma dramatically modifies the dynamics. While much of the physics is electrostatic in nature, internal currents as well as external currents between the cloud charge layers and the ambient plasma generate electromagnetic radiation. The radiation from the external currents is analogous to the radiation from large conductors in space where the cross-field motion induces a potential difference between the two ends of the structure which, in turn, collect currents from the ambient plasma [Donohue et al., 1991]. Electromagnetic radiation from plasma clouds is important from an observational point of view in the sense that remote observations of wave emissions can serve as a diagnostic tool probing the cloud dynamics provided the radiation properties of clouds are understood. This argument applies both to artificial and natural occurring plasma clouds.

We have therefore extended the simulations referenced above by performing fully three-dimensional, electromagnetic, and relativistic particle simulations of clouds propagating both in vacuum and in a background plasma. This allows the simultaneous study of the loss of cloud momentum in the direction of propagation (x direction), the formation of charge layers at the sides of the cloud with the associated polarization electric field (y direction), and the expansion of the charge layers along the magnetic field (z direction). In addition to the particle dynamics, we also explore the radiation properties of clouds. For this first study, a simple cloud geometry and initial conditions have been chosen, namely a rectangular box of uniform density which is given a push across the magnetic field at $t = 0$. This choice has been made in order to better understand some of the fundamentals of cloud dynamics and to evaluate our results relative to one- and two-dimensional electrostatic simulations using a similar geometry and initial conditions [Galvez, 1987; Galvez et al., 1989; Galvez and Borovsky, 1992]. In section 2 we present the simulation results while section 3 contains a discussion.

2. Simulation Results

2.1 Simulation Parameters

The simulation code used in this study is a further development of the TRISTAN code [Buneman et al., 1980; Peratt et al., 1980] originally created for the CRAY-1 and CRAY-

XMP. Several new features have been implemented in order to increase the speed and versatility of the code. These include the elimination of Poisson's equation and its time-consuming solution. Instead, the fields are directly updated through current deposition of the particles [*Villasenor and Buneman*, 1992]. Furthermore, radiating boundary conditions for the fields are introduced at all boundaries using a first-order Lindman approximation [*Lindman*, 1975], and finally, Fourier transforms are completely eliminated by processing and filtering the fields locally. The particles have periodic boundary conditions. These are not consistent with the field boundary conditions; however, as will be clear later, this is a problem mainly when the cloud sheath electrons hit the boundaries or when the ambient plasma currents to the sheaths are exhausted. When the boundary conditions interfere with the physics, the simulations are stopped.

The simulations are performed on the CRAY-2 located at the National Center for Supercomputing Applications, University of Illinois. The simulation domain with the plasma cloud is shown in Figure 1. The domain is a mesh of size $92\Delta \times 46\Delta \times 185\Delta$ where Δ is the grid unit. The cloud dimension is $40\Delta \times 12\Delta \times 12\Delta$. The magnetic field is in the z direction, and at $t=0$ the cloud is pushed across the field with a velocity v_o in the x direction.

Four cases are simulated, corresponding to two sets of cloud and background plasma parameters. The background is either a vacuum or a plasma. For the cloud we have chosen two plasma densities corresponding to $q_i = 1.25$ and 2.50. The densities relate to the background plasma density as $n^c/n^b = 2$ and 8, respectively. The cloud electron thermal velocity normalized to the velocity of light, v_{th}^c/c, equals 0.02 for the rarefied cloud and 0.04 for the dense cloud. This choice ensures that the cloud Debye length λ_d^c is 0.25Δ for both clouds. The cloud ions have the same mass as the background plasma ions, and the ion to electron mass ratio is $m_i/m_e = 16$. Ions and electrons have equal thermal energy. For the background plasma, $v_{th}^b/c = 0.02$, where v_{th}^b is the electron thermal velocity. The cloud is given an initial bulk velocity v_o at $t=0$ in addition to the thermal velocity. The magnitude of this velocity is $v_o/v_{th}^b = 1.6$. From the above

parameters it can be seen that the rarefied, cold cloud has a drift velocity in excess of the thermal velocity while the reverse is true for the dense, hot cloud. The ratio of the particle pressure (thermal+dynamic) to the magnetic field pressure β is 2.2×10^{-3} for the rarefied cloud and 1.6×10^{-2} for the dense cloud. The dimension of the cloud is such that the ion Larmor radius due to the drift velocity is $r_{Li} = 2\Delta$. The above parameters lead to the following values of characteristic plasma periods: the ion cyclotron period $T_{ci} = 785$ time steps, the electron cyclotron period $T_{ce} = 49$, and the background electron plasma period $T_{pe}^b = 222$. For the rarefied cloud we have $T_{pi}^c = 628$ and $T_{ih}^c = 490$, where T_{pi}^c is the ion plasma period and T_{ih}^c is the ion upper hybrid period, while for the dense cloud, $T_{pi}^c = 314$ and $T_{ih}^c = 233$. The ion upper hybrid period is defined from the ion upper hybrid frequency $\omega_{ih}^c = \sqrt{\omega_{ci}^2 + \omega_{pi}^{c2}}$.

2.2 Sheath Formation

The charge sheaths as they have formed at $t = T_{ci}/4$ are shown in Plate 1 for the case of $q_i = 1.25$ and vacuum. The top panel shows the space charge in the center four layers in the xy plane. Negative charge is blue, and positive charge is red. The arrows indicate the direction of the electric field in that plane. The lengths of the arrows have been scaled in a way which enhances the weaker fields in order to see the field structure at some distance from the cloud. The background magnetic field is pointing out of the plane, and the cloud is moving toward higher x values. As the ions have gyrated clockwise and electrons counterclockwise, a positive charge layer is created on the right side of the cloud (right side as defined relative to the direction of motion of the cloud, i.e., low y values), and a negative layer on the left side (high y values). In addition, a positive layer has formed at the head of the cloud, and a negative layer at the tail. These layers are a result of the larger ion Larmor radius, which allows ions to move ahead of electrons across the magnetic field. The electric field inside the cloud is pointing predominantly in the y direction, while the field outside of the cloud has a twisted, dipolarlike structure arising from the L-shaped charge layers. Inside the cloud some smaller modulation of the space charge density has formed.

The charge density in the xz plane is shown in the bottom left panel. The cloud is moving horizontally and in the positive x direction, and the magnetic field is vertical and in the z direction. At the front of the cloud is seen the positive ion sheath developed by ions moving ahead of electrons, and in the tail the negative electron sheath resulting from electrons lagging behind ions. The electron sheath has at this point started to expand along the ambient magnetic field as a result of the acceleration by the parallel component of the electric field. Because of the higher ion mass, the ion sheath has expanded much less.

Close to the cloud the electric field structure is dipolar in nature, while at larger distances the field changes character and periodically changes orientation. As we will show later, the oscillating fields are those of an outward propagating, right-hand electromagnetic wave generated by the current induced from the coherent motion of electrons in the cloud. A dipole electric field decreases with distance r as r^{-3} while radiation fields decrease as r^{-2}. Therefore the radiation fields dominate over the electrostatic field at some distance from the cloud.

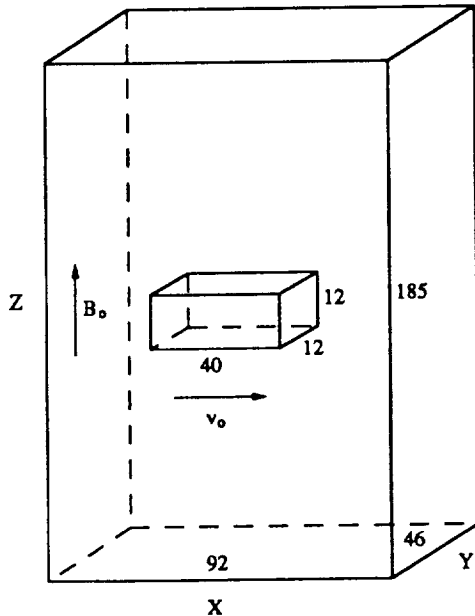The charge density in the yz plane is shown in the bottom
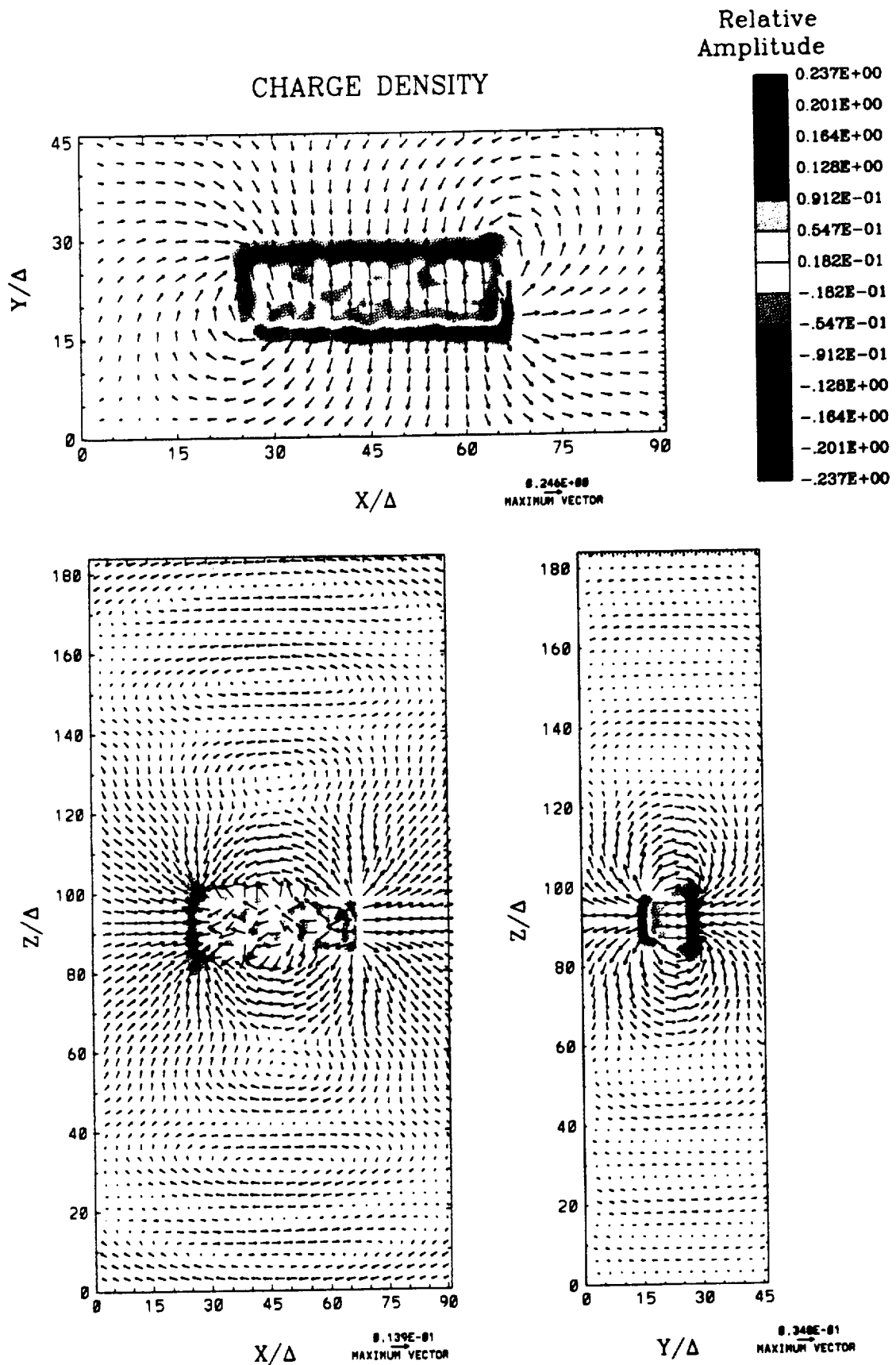

Fig. 1. The simulation domain.

CHARGE DENSITY

Relative
Amplitude

Plate 1. The charge density and electric field in the center four layers of the xy, xz, and yz planes at $t = T_{ci}/4$ for the rarefied cloud ($q_i = 1.25$) in vacuum. Positive space charge is red, and negative is blue.
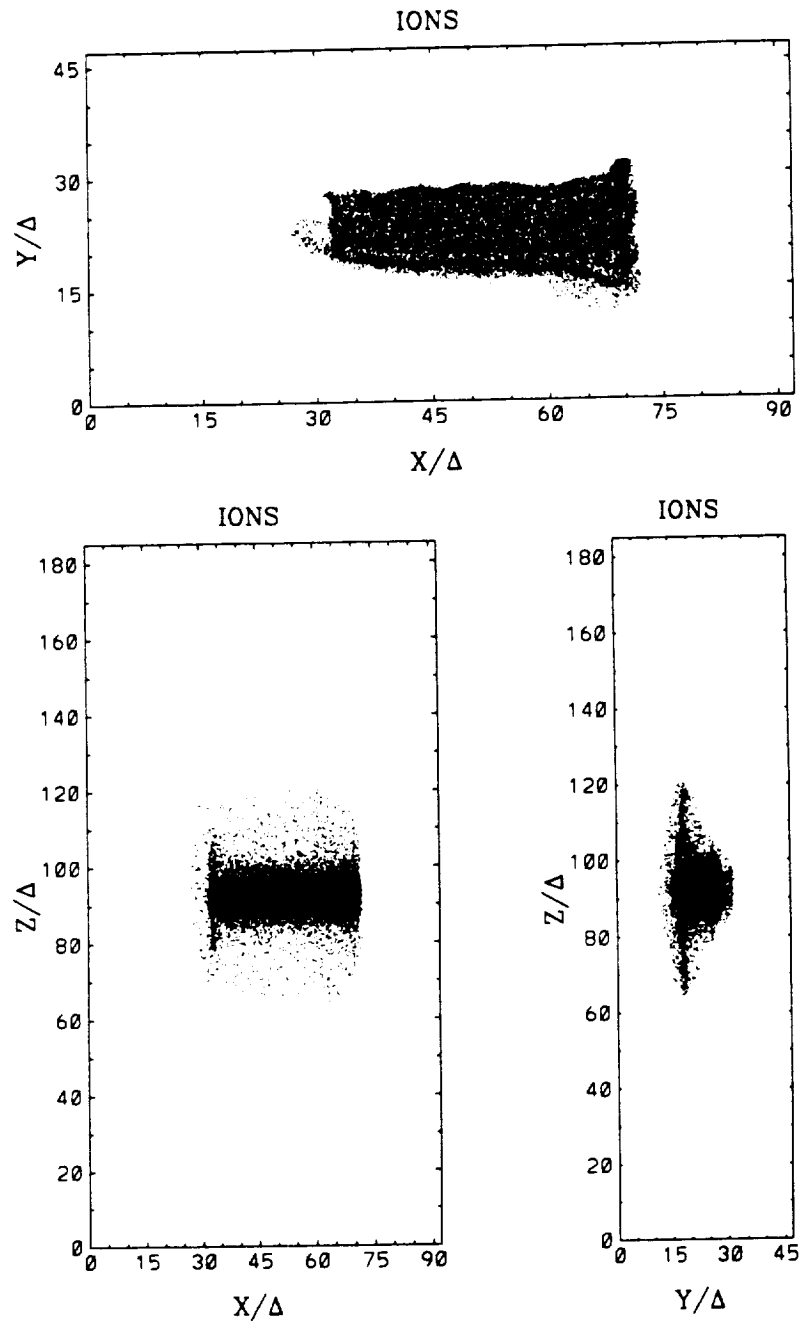
IONS

IONS   IONS

Fig. 2. The location of cloud ions projected onto the xy, xz, and yz planes at $t = T_{ci}$ for the dense cloud (q_i=2.50) in vacuum.

right panel. In this perspective, the cloud is moving out of the plane with the magnetic field vertical and in the z direction. The electric field is approximately dipolar outside of the cloud. As was the case for the electron tail sheath, electrons have begun their expansion along the magnetic field, which elongates the negative charge layer in the z direction. Note that the strongest parallel electric fields are found at the tips of the charge layers. Thus electrons located here will experience the most rapid acceleration.

The evolution of the dense cloud in vacuum at a time $t = T_{ci}$ is illustrated in Figure 2, which shows the ion positions projected onto the xy plane (top), the xz plane (bottom left), and the yz plane (bottom right). As seen from the top frame, the cloud has broadened at the head, and the ion

sheath is beginning to peel off at the tail of the cloud. The polarization electric field decreases through the sheaths from its full value at the inner edge to zero at the outer edge of the sheaths. Therefore the average drift velocity of the particles in the sheaths decrease from the bulk velocity at the inner edge to zero at the outer edge [Borovsky, 1987; Cai et al., 1990]. Notice, also, that a region of ion density depletion has developed which is close to and aligned with the primary ion sheath. As we shall see later, secondary space charge sheaths develop within the cloud and, in the case of a finite background plasma density, also in the background plasma.

The expansion of the ion sheaths along the ambient magnetic field is shown in the bottom frames. In the bottom left frame the expansion at the tail end of the cloud is par-

ticularly noticeable. As will be shown later, the bulk of the ions oscillate approximately with the ion upper hybrid period. From the values of the characteristic time constants given earlier it is seen that the ions at this time have experienced more than three oscillations (for the dense cloud, $T_{ih}^c/T_{ci} = 0.30$). Ions have therefore been ahead and behind electrons several times, and thus positive and negative charge layers have been formed alternately at the head and tail of the cloud. The expanding ion layer seen in the tail is at a location of the rear edge of the bulk of the cloud and corresponds to the narrow layer of ion density enhancement seen in the top frame. The ions that have peeled off the ion sheath are seen as a diffuse distribution behind the expanding tail layer.

The expansion of ions in the ion sheath at the side of the cloud is seen in the bottom right panel. The ion layer has a small dispersion, with ions far from the cloud located at y values closer to the center y coordinate of the cloud. These ions were the first to leave the cloud in their expansion along the magnetic field, and their location in y indicates the position where the charge layer first forms. With time, the cloud has broadened, in particular in the front portion.

The electron spatial distribution is shown in Figure 3. In the top panel is seen the peeling off of electrons in much the same way as was observed for the ions. Most noticeable, however, is the expansion of the electrons in the negative electron charge layer out to the edge of the simulation domain shown in the bottom two panels. In the process the most energetic electrons reach relativistic energies. The expansion of the lateral electron charge layer is in qualita-
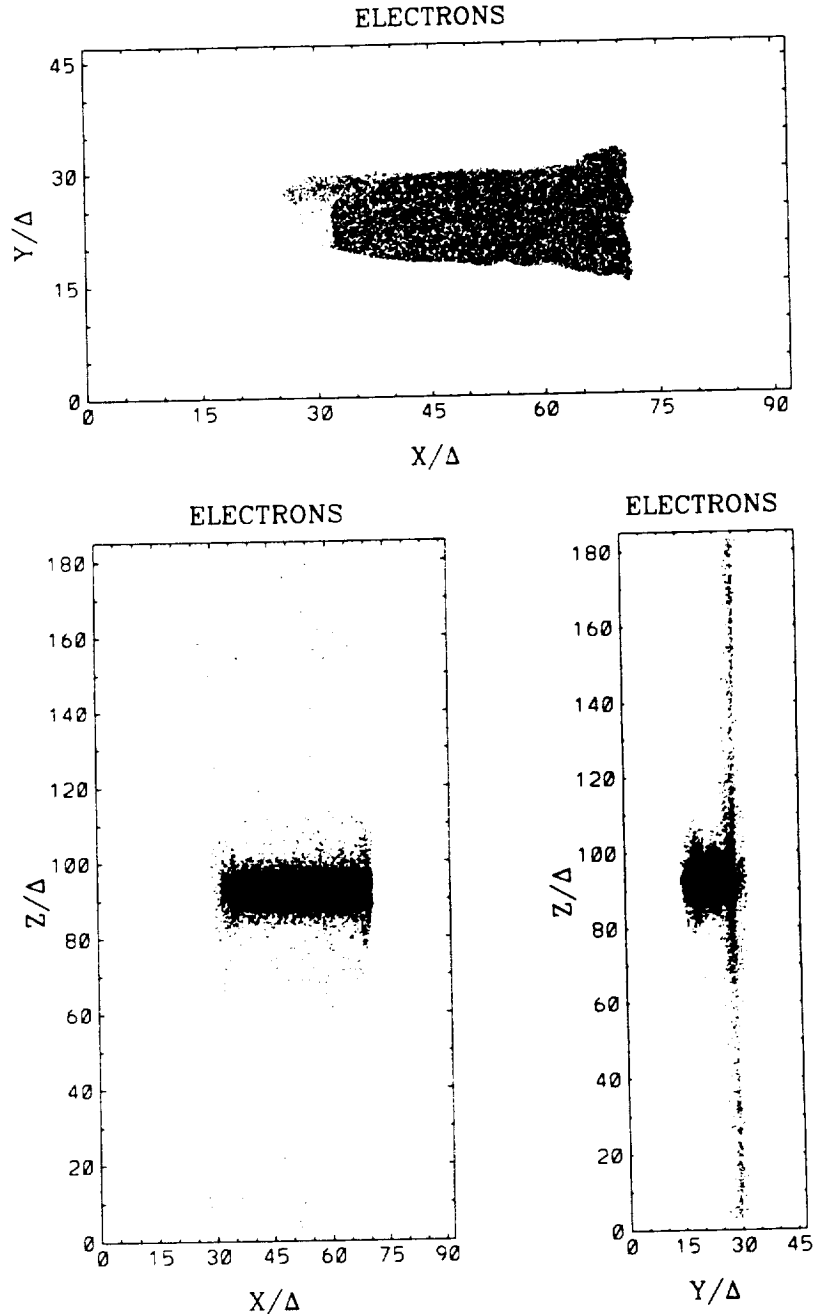
Fig. 3. The location of cloud electrons projected onto the xy, xz, and yz planes at $t = T_{ci}$ for the dense cloud in vacuum.

tive agreement with two-dimensional, electrostatic simulations [Galvez and Borovsky, 1992]. Notice also (bottom right frame) that electrons have accumulated in the ion layer in their attempt to neutralize the ion positive space charge. Furthermore, a secondary electron layer has formed close to the center of the cloud. The interior of the cloud is then expected to be quite dynamic with large-amplitude density and space charge oscillations.

The bottom left frame of Figure 3 gives a side view of the cloud and the electron sheath. The sheath exhibits a small dispersion, the outermost electrons lagging behind the cloud. The result is the formation of an electron "wing" slanted with an amount corresponding to the cross-field motion of the cloud and the field-aligned motion of the electrons.

Results from two-dimensional simulations (our xy plane) of clouds with $q_i^2 = 0.5$, 10, and 32 at a time around one ion cyclotron period are reported by Galvez et al. [1989]. These results are comparable to those shown in Figures 2 and 3 in the sense that they exhibit a broadening of the pulse front and the peeling off of the charge layers. Furthermore, Galvez et al. find the development of vortices at the front end of the cloud at the edge of the electron sheath, and vortices in the tail end of the cloud. The front vortex was found to be charge neutral and a result of a bulk plasma drift at the head of the cloud in a direction toward the main negative charge layer. This motion is an $\vec{E} \times \vec{B}$ drift due to the electric field component antiparallel to the direction of motion generated by the positive space charge at the head of the cloud. The vortices at the tail of the cloud were not charge neutral but a result of the peeling process. In addition, for the high-density cloud they found the development of the diocotron instability [Buneman, 1961] in the electron sheath.

The tendency to develop these vortices and instabilities as studied by Galvez et al. [1989] increased with plasma density. In our own simulations, with $q_i^2 = 6.25$, these phenomena were suggested, but little developed at $t = T_{ci}$. We propose that this is because our simulations are three-dimensional, which allow for a more rapid decrease of the electrostatic fields with distance. Furthermore, since the simulations by Galvez et al. [1989] were performed in a plane perpendicular to the magnetic field, electrons were not allowed to expand out of the charge layers.

For cloud propagation in a background plasma the plasma currents are able to short the space charge sheaths for both the rarefied and the dense cloud. Thus space charge layers are formed to a lesser extent, and the cross-field motion is inhibited. As a result, the features seen in Figures 2 and 3 are much less developed.

The charge distribution in the yz plane at $t=T_{ci}$ is shown in Plate 2, left panel, for the rarefied cloud in vacuum. The charge layers at the sides of the cloud have expanded to the extent indicated by the spatial particle distributions. The ion sheath has expanded very little, while the electron sheath has almost reached the boundary of the simulation domain. The electric field structure has now departed from the dipolarlike structure seen in Plate 1 at $t = T_{ci}/4$. The field orientation is such that electrons in the electron sheath located at y values between about 30Δ and 150Δ now are decelerated, while electrons further from the cloud continue to be accelerated. While the longer time duration dynamics of the sheaths cannot be studied with this simulation because of limitations on the size of the simulation domain, we suggest nevertheless that the outermost electrons may escape the cloud while some of the electrons closer to the

cloud eventually will return to the sheath. The situation is similar to the case of electron beam emission from spacecraft. Simulations find here that for beam currents that are large compared to the plasma currents, a beam stagnation point will develop, allowing some electrons to escape with energies in excess of the beam accelerator energy, while the bulk of the electrons are returned to the spacecraft [Winglee and Pritchett, 1988; Pritchett, 1991].

When a background plasma is present, currents are drawn to the sheaths, thereby reducing the polarization field. In Plate 2, right panel, is shown the charge distribution for the rarefied cloud in a background plasma. The two main sheaths are present as for the cloud in vacuum. However, the electron sheath is less developed, and the ion sheath has now expanded to the same degree as the electron sheath. The increased ion sheath is a result of electrons being collected from the background plasma to the sheath. This electron current leaves behind a positive space charge which has the effect of elongating the ion sheath. In addition to the two primary sheaths, several secondary electron and ion sheaths develop. The outermost of these seen on Plate 2 are negative electron sheaths which are curved rather than aligned with the magnetic field. In fact, the higher the order of the sheath, the more curved it is. For instance, next to the primary electron sheath, and at higher y values, is a slightly curved ion sheath. We may for convenience call this the second-order sheath. Next to this is found the third-order electron sheath which is highly curved, and similarly for the primary ion sheath, which has a slightly curved (in the opposite sense) second-order electron sheath. The third-order ion sheath is not visible.

The higher-order sheaths are developed by electrostatic field component is not at a y value corresponding to the location of the charge layers, but at y values which are somewhat further from the cloud. As a consequence, ambient plasma located further from the sheath is accelerated the most, and the curvature mentioned above is created, with a higher degree of curvature for higher-order sheaths. As an example, consider the field from an electric dipole oriented with its axis $\vec{l}$ perpendicular to an ambient magnetic field $\vec{B}_o$. Let $\vec{r}$ be the vector from the center of the dipole to the point of observation and θ the angle $(\vec{l}, \vec{r})$. It can be shown that at a given distance r from the dipole center, the electric field component parallel to $\vec{B}_o$ maximizes for $\theta = 45°$. If the dipole is immersed in an ambient plasma, the charged particles located along the line $\theta = 45°$ in the plane defined by $\vec{l}$ and $\vec{B}_o$ will experience the strongest acceleration along $\vec{B}_o$. As these particles respond to the fields, a new curved layer is formed. The fields from this layer in turn create an even more curved layer, and so on.

The cloud electrons in the negative charge layers are accelerated to relativistic energies. The strong acceleration is caused by the sudden push of the cloud across B_o at $t = 0$ and the associated impulsive formation of the charge layers and electric fields. An estimate of the maximum energy of electrons accelerated along the magnetic field due to the electrostatic forces in the electron sheath can be found by noting that the maximum potential energy of an electron in the sheath is

$$w_{pot} = \frac{1}{2}ev_oB_oL_y \qquad (4)$$

where L_y is the dimension of the cloud in the direction along

CHARGE DENSITY

CHARGE DENSITY
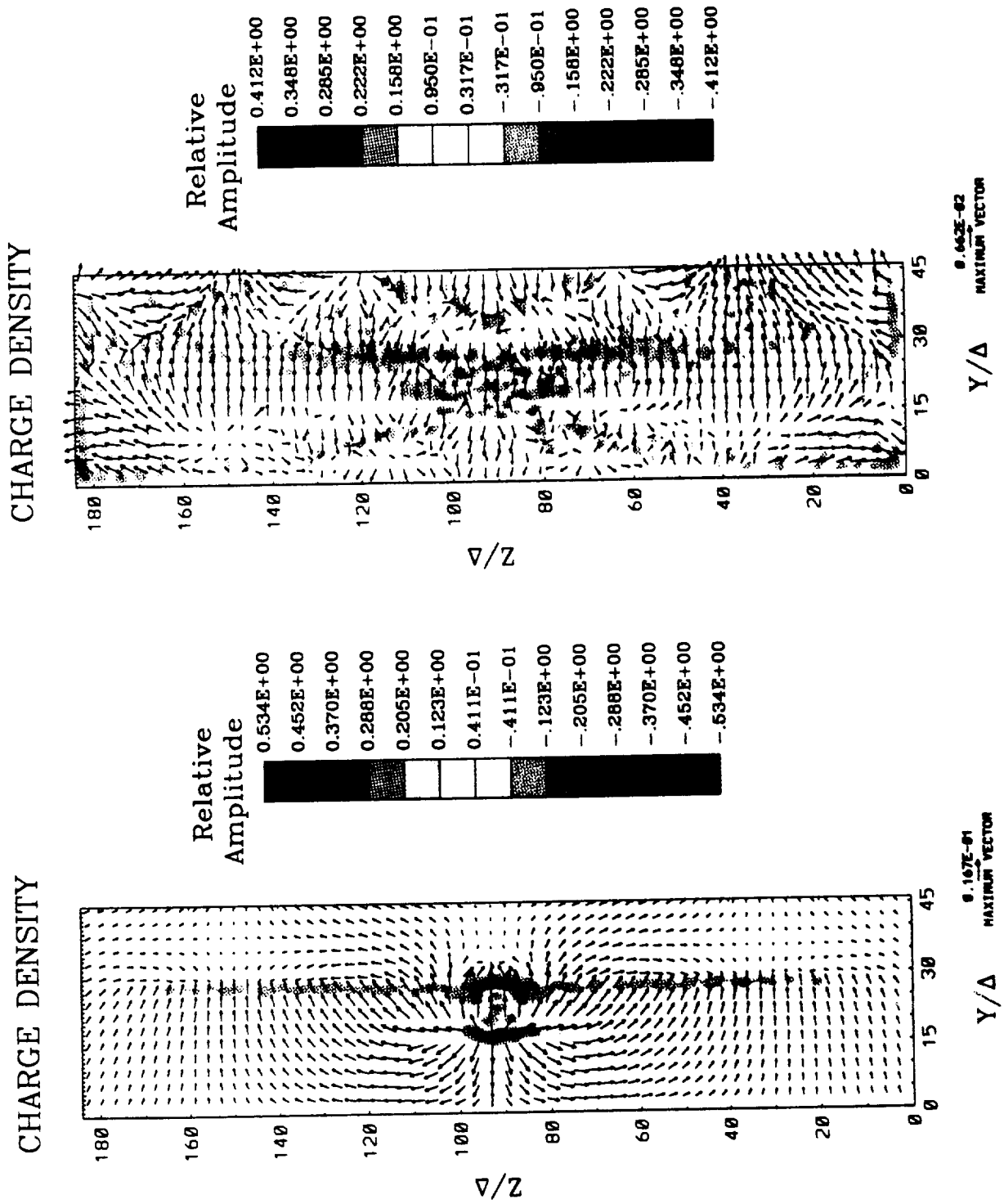
Relative
Amplitude

Relative
Amplitude

Plate 2. The charge density and electric field in the center four layers of the yz plane at $t = T_{ci}$ for the rarefied cloud ($q_i = 1.25$) in vacuum (left) and in a background plasma (right). Positive space charge is red, and negative blue.

the polarization field. Equating the kinetic energy of an electron accelerated out of the sheath with the potential energy in the sheath, the maximum kinetic energy becomes

$$\frac{w^c_{max}}{w^c_o} \simeq \frac{m_i L_y}{m_e r_{Li}} \qquad (5)$$

where $w^c_o = \frac{1}{2} m_e v^2_o$. The acceleration out of the sheath results according to (5) in electron energies which are equivalent to the ion bulk kinetic energy multiplied by a geometric factor. For clouds which are wide compared to the ion Larmor radius, very large energies can be achieved.

The maximum energy given by (5) is 89.1 for the dense cloud and 75.0 for the rarefied cloud. These values are of the same order of magnitude as found in the simulations. The energy of the fastest electron relative to the initial drift energy was for the dense cloud 80.7 and 241.3 in a background plasma and vacuum, respectively, while it was 21.9 and 100.9 for the rarefied cloud. They are lower than the vacuum cases and higher than the background plasma cases. When deriving (5), the expansion of the electron charge layer and the continuous supply of charge from the cloud, which supply a constant push, were not accounted for. Again we point out the analogy with electron beam experiments. Electrons at forces from lower-order sheaths. As pointed out by *Galvez and Borovsky* [1992], the maximum of the parallel electric the beam front are accelerated by electrostatic forces to energies which exceed the initial accelerator energy. Therefore the maximum energy in the vacuum case is expected to be in excess of the predictions of (5). With a background plasma, the fields are partly shorted by ambient plasma currents, and the acceleration is less.

2.3 Cloud Energy and Momentum

The generation of electric and magnetic fields and the energization of sheath particles require energy which is sup-

plied from the cloud kinetic energy. As a consequence the cloud slows down from its initial velocity v_o. The loss rate of particle energy density can be found from

$$\frac{dW}{dt} = \vec{J} \cdot \vec{E} - R \qquad (6)$$

where $\vec{J}$ is the current density and $\vec{E}$ the electric field. The energy loss due to electromagnetic radiation from the cloud, R, is relatively small compared to the energy loss incurred in establishing the charge sheaths and will be discussed later.

The current required to supply the charge layers at the sides of the cloud and the associated polarization electric field are dominant in this energy transfer. The polarization electric field is oriented in the positive y direction while the current supplying the charge layers at the sides is oriented in the negative y direction. The process of forming and sustaining these layers therefore reduces the cloud kinetic energy. The charge layers at the head and tail of the cloud alternate in polarity during an ion oscillation. The current in the x direction supplying these layers is 90° out of phase with the field, and the energy will therefore transfer both from the cloud kinetic energy to the fields as well as back again. This, together with the smaller area of the head and tail surfaces of the cloud relative to the sides, results in a comparatively small effect on the cloud energy budget from these layers.

The coherent components of the cloud ion and electron velocities are found by averaging the velocities of all cloud ions and electrons. The x components of the coherent velocities are shown as a function of time in Figure 4, left frame, for the rarefied cloud in vacuum. In the figure, the velocities have been normalized with the initial drift velocity v_o in the x direction. The ion velocity (dashed curve) oscillates with a period between the ion upper hybrid period ($T^c_{ih}/T_{ci} = 0.62$) and the ion cyclotron period. The oscillations are damped in
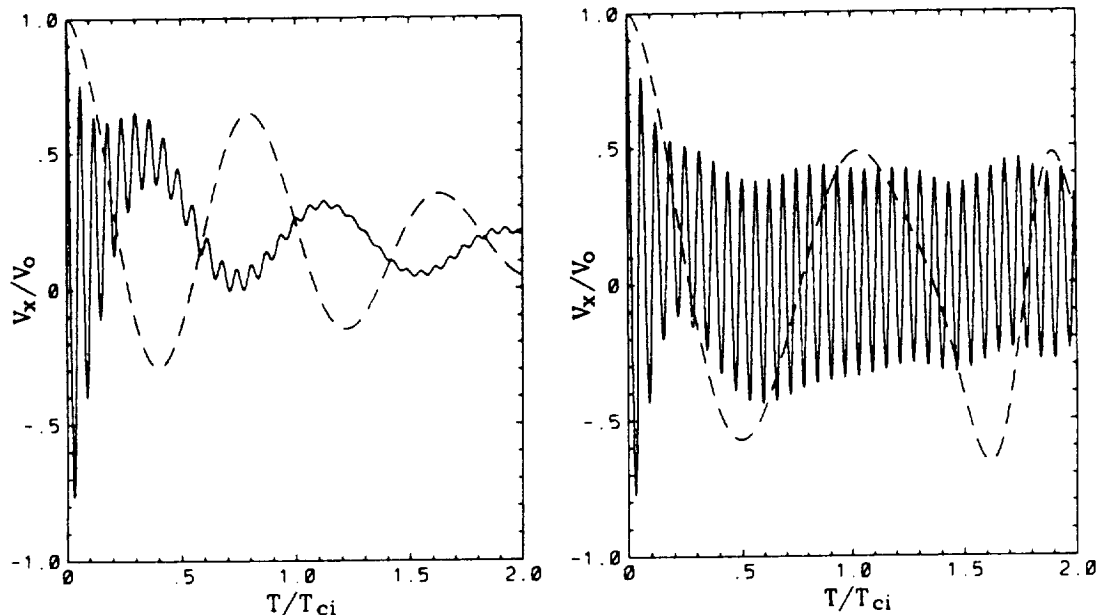

Fig. 4. The average cloud ion velocity (dashed line) and cloud electron velocity (solid line) in the x direction as a function of time for the rarefied cloud in vacuum (left) and in a background plasma (right). The velocities are normalized to the initial drift velocity.

time, and the average velocity approaches 0.2 at the end of the run. The electrons oscillate at the electron cyclotron frequency, these oscillations also being damped in time. Note that since $\omega_{ce} \gg \omega_{pe}^c$ we cannot distinguish between the electron cyclotron period and the electron upper hybrid period. The oscillations in the velocities are damped partly because individual ions and electrons gyrate less as the polarization field is getting established, and partly because the particles lose phase coherence.

The characteristics seen in Figure 4, left frame, are to be expected from a cloud that is marginally able to cross-field propagate as defined by (3) and are in qualitative agreement with two-dimensional simulations performed in the past. A cloud as defined initially in our simulations will pass from an initial stage where it is given a push across B_o, through a transitory stage where the charge layers are being established and the cloud particles undergo significant coherent gyrations, to a relaxed stage where the layers are established and the cloud ions and electrons drift with a common (lower) velocity across B_o with very little or no coherent gyrations. For a cloud that is marginally able to cross-field propagate, the bulk velocity in the final stage is much smaller than the initial velocity. As mentioned in the introduction, a one-dimensional cloud (slab) will in the latter stage cross-field propagate with a velocity that is half the initial velocity if $q_i = 1$. For the case shown in Figure 4, left frame, $q_i = 1.25$, which in the one-dimensional case should result in a final drift velocity slightly above 0.5 v_o. However, in three dimensions, the charge layers are allowed to expand, which, as we will show, leads not only to a smaller final drift velocity, but also to a steady, slow decrease of this velocity.

The coherent velocities for the rarefied cloud in a background plasma are shown in Figure 4, right frame. After an initial damping, electrons continue undamped oscillations at the electron cyclotron frequency with very little net drift across the field. Ions oscillate at first with the ion cyclotron period, and at about $t = 1.4\ T_{ci}$, ions begin to oscillate with

a period closer to T_{ih}^c. The reduction of the polarization electric field inside the cloud due to the currents from the ambient plasma to the charge layers makes the cloud particles oscillate at the cyclotron frequencies much as single particles. In other words, the shorting of the polarization electric field reduces collective effects. The oscillation period of the ions changes from the cyclotron period to the upper hybrid period because the ambient plasma currents have been exhausted. These currents flow in thin sheaths along the magnetic field, and at the time of change in periodicity, little charge is left because of the finite extent of the simulation domain. At this point the cloud ions start to oscillate as if in vacuum. The effect of the boundaries sets the limit in time that the simulations can be run.

The velocity for the dense cloud in vacuum is shown in Figure 5, left frame. The electron oscillations at the electron cyclotron frequency are strongly damped and disappear after a few oscillations. The low-frequency oscillation in the ion and electron velocities is now close to the ion hybrid period ($T_{ih}^c/T_{ci} = 0.3$), and the loss of forward momentum is less than for the rarefied cloud. After an initial decrease within the first half of an oscillation period, the ion velocity oscillation is slowly damped while oscillating around a slowly decreasing average value which reaches about 0.4 at the end of the run.

Finally, the velocity for the dense cloud in a background plasma is shown in Figure 5, right panel. The ions now oscillate much slower and closer to the cyclotron period. At about $t = 1.1\ T_{ci}$ the ambient plasma currents are exhausted, and the oscillation period decreases, as was the case for the rarefied cloud. After an initial damping, electrons continue their almost undamped oscillations at the electron cyclotron frequency. The oscillations are of a smaller amplitude than was the case for the rarefied cloud. The simulation is terminated shortly after the influence of the boundaries is noted in the cloud velocities.

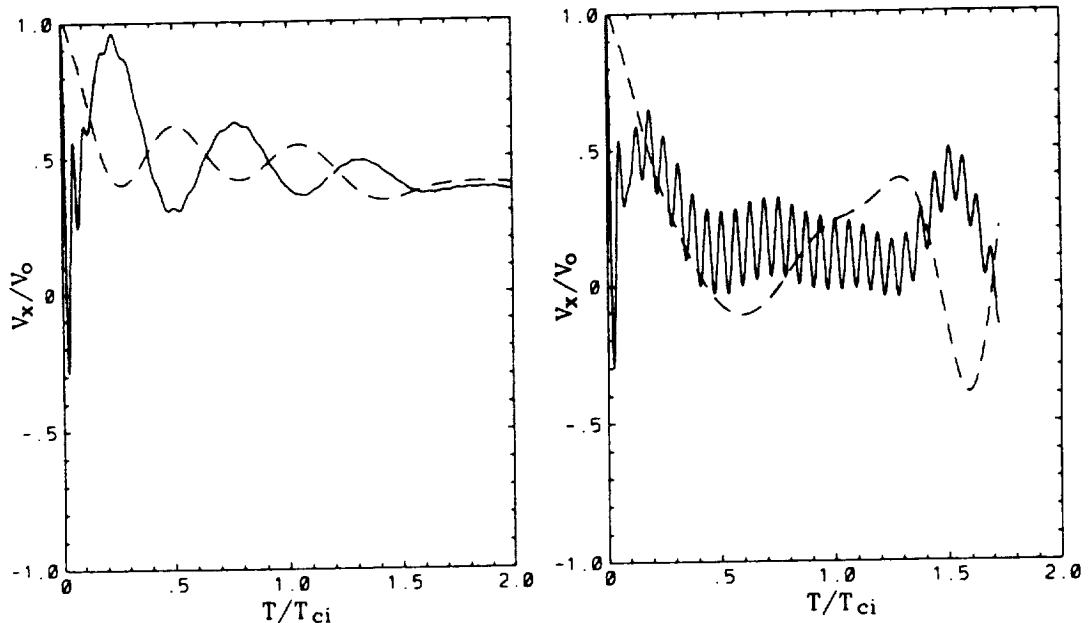Some of the characteristics seen in Figures 4 and 5 can

Fig. 5. The average cloud ion velocity (dashed line) and cloud electron velocity (solid line) in the x direction as a function of time for the dense cloud in vacuum (left) and in a background plasma (right). The velocities are normalized to the initial drift velocity.

be understood from considerations of the energy budget of the clouds. To simplify the situation we estimate the energy flow associated with the formation and maintenance of the primary charge layers at the sides of a cloud in vacuum. First we note that the electron charge layer rapidly expands. While some of the first and fastest electrons accelerated out of the sheath may be able to escape the cloud completely, the electric field structure as shown in Plate 2 seems to indicate that there may be a stagnation point in the expansion where $E_{\parallel} = 0$. It is not known if the stagnation point is stationary or if it oscillates by contracting and expanding in time. However, the slow decrease of ion momentum after the initial drop mentioned above seems to indicate a steady loss of momentum. In the following we then assume that the layer reaches some quasi-steady, average position in the direction along B_o.

Let the original cloud dimension be L_x, L_y, L_z in the x, y, z directions, and let the dimension of the extended electron layer along the z direction be M_z. As this layer is being formed, the charge required to increase the thickness of the layer by dL_y is $dQ = neL_x dL_y M_z$, where n is the electron density in the layer. This charge can be expressed in terms of the associated increment of the polarization electric field in the cloud dE'_p by using (2) and the assumption of an infinite slab:

$$dQ = \epsilon_o dE'_p L_x M_z \tag{7}$$

The current density in the cloud required to supply this charge flows in the negative y direction and is given by

$$J_{\perp} = \epsilon_o \frac{dE'_p}{dt} \frac{M_z}{L_z} \tag{8}$$

The corresponding energy density flow is then

$$\frac{dW}{dt} = \frac{1}{2}\epsilon_o \frac{dE'^2_p}{dt} \frac{M_z}{L_z} \tag{9}$$

where we have used (6). The total energy density required to establish the sheaths then becomes

$$W = \frac{1}{2}\epsilon_o E_p^2 \frac{M_z}{L_z} \tag{10}$$

where E_p is an average, quasi-steady polarization field at the time when the cloud has established its main polarization layers.

In the hypothetical case of no expansion of the charge layer, $M_z/L_z = 1$ and (10) becomes the familiar expression for the energy density of an electric field in vacuum. Assuming that most of the energy flow goes into establishing the lateral charge layers, conservation of energy then requires

$$\frac{1}{2}(m_i + m_e)v_o^2 n^c \simeq \frac{1}{2}(m_i + m_e)v_1^2 n^c + \frac{1}{2}\epsilon_o E_p^2 \frac{M_z}{L_z} \tag{11}$$

Substituting $v_1 B_o$ for E_p and rearranging the terms, one finds

$$\left(\frac{v_1}{v_o}\right)^2 \simeq \frac{q^2}{q^2 + M_z/L_z} \tag{12}$$

where $q^2 = q_i^2 + q_e^2 = c^2/v_A^2$.

The expression for v_1 has been derived under the assumption that the particles contain little gyrational energy and thus constitutes an upper limit for the cross-field drift at a time after the establishment of the charge layers. However, particles do retain some gyromotion. A second estimate of the final cross-field velocity comes from arguments of conservation of canonical momentum of the cloud particles. From Lorentz' equation one finds that $m_i dv_x/dt = eB_o dy/dt$. The y-ward displacement of the ions is then associated with a reduction in velocity in the x direction. The same is true for electrons, which are displaced to the opposite side. The displacement exposes charge layers of thickness $dv_x(m_i + m_e)/eB_o$ on the two sides and results in a polarization electric field $E_p = n^c(m_i + m_e)dv_x/B_o\epsilon_o$. The final drift velocity is then

$$v_x = \frac{dv_x n^c(m_i + m_e)}{\epsilon_o B_o^2} \tag{13}$$

or

$$\frac{v_x}{v_o} = \frac{q^2}{q^2 + 1} \tag{14}$$

Here the influence of the expansion of the electron charge layer has been ignored, while the loss of forward momentum is more rigorously accounted for.

We propose now that the initial decrease of momentum of the cloud primarily is a result of the energy required to push charge into the lateral charge layers during the first half ion oscillation. We also propose that the later, slower deceleration of the cloud is caused by the current flow in the cloud required to maintain the layers as the cloud moves across the magnetic field. Some energy is also radiated from the cloud, in particular in the transition phase, as will be discussed below; however, it constitutes a relatively small energy loss. From (12) an estimate of the degree of expansion of the electron charge layer (M_z/L_z) can be found. Although difficult in the case of the rarefied cloud, we volunteer an estimate of the initial velocity decrease of this cloud in vacuum (Figure 4, left frame), namely, $v_1/v_o \simeq 0.4$, which leads to $M_z/L_z \simeq 8.1$. The extent of the charge layer along B_o is then 97.2Δ, which compares favorably with the distance between the two stagnation points ($E_{\parallel} = 0$) seen in Plate 2. For the dense cloud, $v_1/v_o \simeq 0.6$, which gives $M_z/L_z \simeq 11.1$.

As the cloud moves across the magnetic field, the sheaths peel off as seen in Figures 2 and 3. The average current density required to maintain the sheaths is given by

$$J_{\perp} = \frac{1}{2}\epsilon_o E_p \frac{v_1 M_z}{L_x L_z} \tag{15}$$

The factor $\frac{1}{2}$ comes from the fact that the forward velocity of the electrons in the sheath decreases roughly linearly from a value of v_1 at the inner edge of the sheath to 0 at the outer edge. The time constant associated with the deceleration of the cloud due to the maintenance of the layers becomes

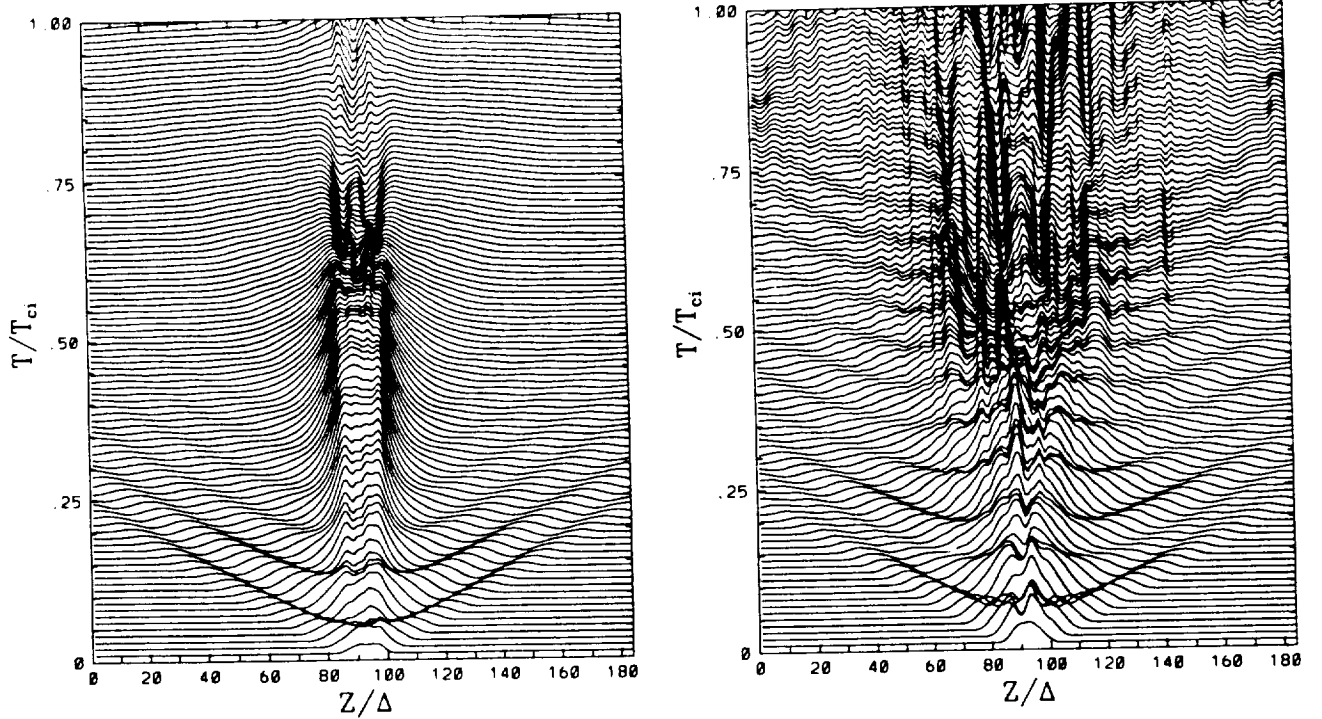$$\tau = \frac{q_i^2}{\pi} \frac{L_x L_z}{r_{Li} M_z} \frac{v_o}{v_1} T_{ci} \tag{16}$$

Fig. 6. Relative amplitude of the y component of the electric field along an axis in the z direction through the center of the rarefied cloud in vacuum (left frame) and in a background plasma (right frame). Along the vertical axis is amplitude and time, and along the horizontal axis is z.

where r is defined as $r = v_1/(\partial v_1/\partial t)$. For the rarefied cloud, $v_1/v_o \simeq 0.2$ and $M_z/L_z \simeq 8$, which gives $r \simeq 6.1 \, T_{ci}$. For the dense cloud, $v_1/v_o \simeq 0.5$ and $M_z/L_z \simeq 11$, which gives $r \simeq 7.3 \, T_{ci}$. These numbers are in reasonable agreement with the observed deceleration. With our assumption of the initial velocity decrease mentioned earlier, both clouds decelerate by 0.2 in the remaining time up to $2 \, T_{ci}$. Assuming that this second slower decrease begins at a time when the ions have completed 180° rotation, this corresponds to $r = 8.25T_{ci}$ for the rarefied cloud and $r = 8.74T_{ci}$ for the dense cloud.

2.4 Electromagnetic Radiation

We now turn to the electromagnetic radiation from the clouds. In Figure 6, left frame, is shown the amplitude of the y component of the electric field E_y along an axis in the z direction through the center of the rarefied cloud in vacuum. The vertical axis represents both relative amplitude and time. In the center of the frame is seen the growth and later decay of the polarization electric field inside the cloud. Electromagnetic radiation at the electron cyclotron frequency is also generated, which propagates into the vacuum from the cloud with the velocity of light. These waves are generated fairly strongly in the initial phase but are damped out relatively quickly. In Figure 6, right frame, is shown E_y for the rarefied cloud in a background plasma. The amplitude is here again relative, but scaled in the same manner in order to be directly comparable to the values shown in the left frame. The polarization field inside the cloud is now much more structured and with time extending out into the ambient plasma. Recall that the initial cloud dimension L_z is 12Δ. These structures may be associated with the higher-order sheaths which are formed in the cloud

as well as in the plasma, as mentioned earlier. The electromagnetic radiation continues to be generated throughout the time shown on the frame in contrast to the case of the cloud in vacuum.

We propose that the radiation from the cloud is generated by the ion and electron currents flowing in the cloud, which act as virtual antennas. The z component of the currents can be found from the average cloud particle velocities shown in Figures 4 and 5. For the cloud in vacuum, the average electron velocity oscillates strongly at the electron cyclotron frequency early in the run, but is later damped out, while for the cloud in a plasma, the electrons continue to oscillate coherently. This is consistent with the high-frequency radiation seen in Figure 6, which is damped in time for the cloud in vacuum and continues to be generated for the cloud in a background plasma. We note at this point that the initial conditions imposed on the particle velocities are important for the level of radiation. The particles are created instantaneously with a common velocity across the magnetic field; thus the cloud particles are born with a large coherent velocity component. This issue will be discussed further in the next section. Electromagnetic radiation is also generated in the low-frequency regime at the ion oscillation period; however, longer simulations in time and a different scaling for the display of the field amplitudes are needed to see these waves.

In order to examine the radiation fields further, the radiation magnetic field was sampled at $z = 140\Delta$ on the axis in the z direction passing through the center of the cloud. Figure 7 shows a hodogram of the magnetic field in the x, y plane for the rarefied cloud in vacuum around a time $t = T_{ci}/4$. A value is plotted for every 5 time steps from step 150 to step 250. The field is rotating in the same sense as the electrons and is therefore the field of a right-hand polar-
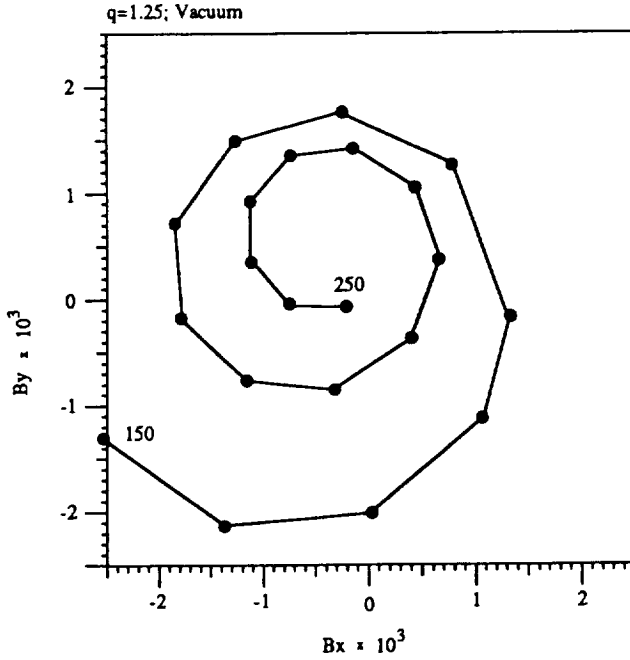
q=1.25; Vacuum

Fig. 7. Hodogram of the magnetic field amplitude (relative) in the xy plane for the rarefied cloud in vacuum. The location is center-x, center-y, and $z=140\Delta$. A value is plotted every 5 time steps from step 150 to step 250.

ized wave. As noted earlier, the electron oscillation period is about 49 time steps. During the 100 time steps shown in Figure 7, the field has undergone a little more than two complete rotations and thus oscillates at the electron cyclotron frequency. Because of the finite velocity of light the source current generating the fields is the current at earlier time steps around 50 to 150. As we will show below, the coherent electron current in the cloud constitutes the source current. Thus the source current of the fields shown in Figure 7 is associated with the second and the third electron oscillation seen in Figure 4, left frame.

The radiation from the cloud in vacuum has been estimated analytically by assuming a source current of the form

$$\vec{J} = J_e e^{i\omega_{ce}t}\vec{x} + J_e e^{i(\omega_{ce}t-\pi/2)}\vec{y} \qquad (17)$$

where J_e is estimated from the coherent motion of the electrons seen in Figures 4 and 5 (the oscillation amplitude is roughly the same in the y direction). The vectors $\vec{x}$ and $\vec{y}$ are unit vectors in the x and y directions. The vector potential $\vec{A}$ is found from

$$\vec{A} = \int_{V_c} J\frac{e^{i\vec{k}\cdot\vec{r}}}{4\pi r}d\vec{V} \qquad (18)$$

where the integration is over the cloud volume and $\vec{k}$ is the wave vector associated with the dominant wave oscillation frequency ω_{ce}; $\vec{k}$ is parallel to the position vector $\vec{r}$, which is the vector from the volume element dV to the point of observation. The magnitude of $\vec{k}$ is given the vacuum dispersion relation $\omega_{ce}/k = c$.

The electromagnetic fields are given by

$$\vec{E} = -\frac{\partial\vec{A}}{\partial t} \qquad (19)$$

and

$$\vec{H} = \sqrt{\frac{\epsilon_o}{\mu_o}}\vec{E} \qquad (20)$$

and the Poynting flux is found from

$$\vec{S} = \frac{1}{2}Re[\vec{E}\times\vec{H}^*] \qquad (21)$$

As mentioned above and shown in Figure 7, the fields for the rarefied cloud in vacuum have been sampled in the simulation at $z = 140\Delta$ on an axis in the z direction through the center of the cloud at $t = T_{ci}/4$. At this time, the charge layers have not undergone significant expansion, and the dominant fields are those of the radiation fields generated from the currents in the cloud. The vector potential at this time has been found by estimating the current from the coherent motion of the electrons in the second and third oscillation shown in Figure 4, left frame. Assuming the normalized amplitude of the velocity oscillation is 0.38, the vector potential has been found by integrating the associated current density numerically. The z component of the Poynting vector estimated from the vector potential has been compared to the z component found directly from the sampled fields. The agreement is within 10% with $S_z = 3.27 \times 10^{-7}$ when estimated from the vector potential calculation and 3.0×10^{-7} from the direct sampling of the fields (in simulation units). This good agreement substantiates our hypothesis that the fields are generated by the coherent electron current.

The loss of momentum due to radiation can be estimated by integrating the Poynting flux over a surface around the cloud. Assuming the average Poynting flux is of the order of 1×10^{-7} through an area $2 \times 92\Delta \times 46\Delta$, the energy loss rate due to radiation is of the order of 1×10^{-5} (in simulation units). The time constant of the braking of the cloud associated with radiation losses defined as $\tau_{rad} = v/(\partial v/\partial t)$ is then about $3 \times 10^3 T_{ci}$, which is much longer than the time constant found for the maintenance of the charge sheaths.

Finally we show the dispersion of the radiation from the rarefied cloud in Plate 3. The amplitude of the magnetic field component B_x in decibels is shown as a function of frequency and wave number k_z for vacuum (left frame) and a background plasma (right frame). The plot has been created by performing a two-dimensional Fourier transform (one space and one time) of B_x along the z axis through the center of the cloud for the first 500 time steps. The radiation maximizes as expected around ω_{ce} with additional lower-amplitude radiation generated along a line with a slope corresponding to the velocity of light. The radiation from the cloud in a background plasma shown in the right panel is also primarily generated close to ω_{ce}, with lower-intensity additional radiation along a line with a slope corresponding to the velocity of light. In this case, however, radiation is damped right at ω_{ce} with the result that two branches appear. The one coming from low frequencies goes to large k_z as the frequency approaches ω_{ce} (a resonance), while the second branch starts at low k_z values right above ω_{ce} (a cutoff) and approaches the slope for the velocity of light for higher frequencies. These are the characteristics of the right-hand mode in a plasma with $\omega_{ce} \gg \omega_{pe}$. The cutoff and resonance
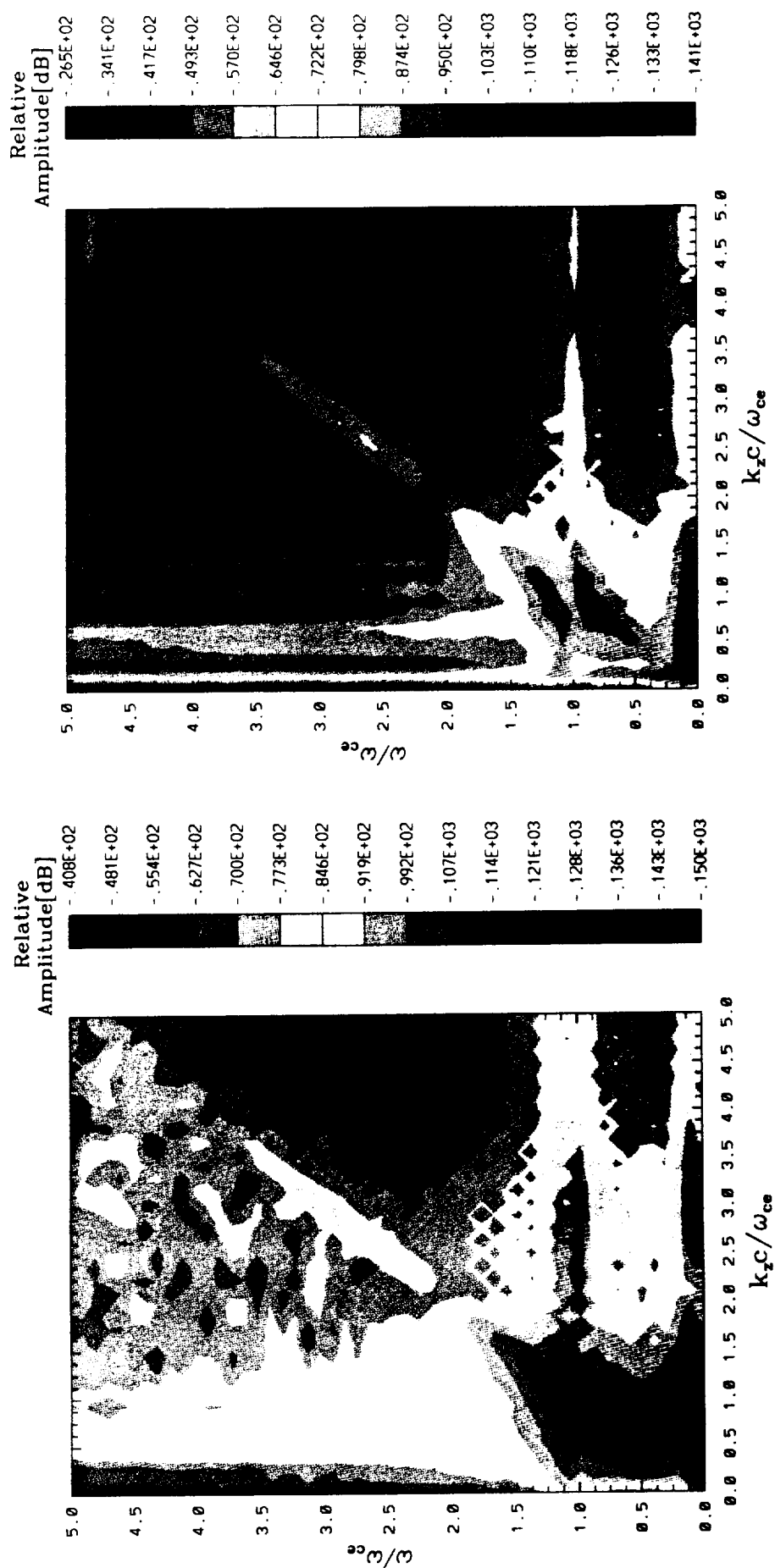
Plate 3. Wave intensity as function of ω and k_z for the rarefied cloud in vacuum (left) and in a background plasma (right).

are in this case both at ω_{ce}. Note that the amplitudes of the cyclotron frequency radiation are comparable in the two cases although they appear to be of different amplitude due to the color coding. This is caused by the difference in dynamic range used in the two plots.

3. Discussion

The shapes of the clouds investigated have been chosen as simple as possible in order to be able to differentiate between the processes and forces acting in different spatial directions. Natural or artificial plasma clouds will in general have smoothly varying density through the cloud, and the effect of the charge layers at the sides of such clouds will be less dramatic. The initial conditions were also chosen simple, namely the sudden push at $t=0$. This condition has as a consequence a sudden acceleration of electrons out of the sheath and a burst of radiation generated by the phase-coherent particles. In this regard the clouds are not in equilibrium initially but relax toward an equilibrium state at the end of the runs.

Given our initial conditions the simulations suggest that the deceleration of the clouds in vacuum occurs in two steps: The first step is a rapid deceleration within the first half of a cloud ion hybrid oscillation period caused by the transfer of cloud kinetic energy into the formation of the charge layers. In the case of the electron charge layer this layer extends out to some stagnation distance from the cloud. The second stage is the continuous deceleration caused by the current in the cloud needed to maintain the charge layers as these are peeled off when the cloud moves across the magnetic field. A third stage, which includes the expansion of the ion charge layers, has not been studied due to limitations in the length of a simulation run.

Associated with the formation of the electron charge layers, electrons are initially accelerated to energies which exceed the ion drift kinetic energy. In the case of clouds that are large compared to the ion Larmor radius, analytical considerations indicate that the energy may be considerably larger than the ion kinetic energy. This acceleration is caused by the sudden push of particles across the field. In the case of CIV experiments, or other cloud experiments in space plasmas, the ionization rate, or cloud formation rate, is slow compared to an electron cyclotron period, and the acceleration is likely to be smaller. Analytical estimates indicate, though, that if a cloud is wide compared to the ion Larmor radius and dense enough to cross-field propagate in the presence of a background plasma, electrons may be accelerated to energies which are comparable to or exceed the electrostatic sheath potential energy. In this respect the electron sheath expansion has much in common with electron beam ejections from spacecraft. For dense beams a virtual cathode will form in the beam at a point where the beam electrons stagnate as their velocity away from the spacecraft is reduced, due to the electrostatic forces in the beam and the spacecraft, which charges to positive potentials [*Winglee and Pritchett*, 1988; *Pritchett*, 1991]. The virtual cathode allows only a fraction of electrons to escape the spacecraft; however, some of the escaping electrons may have energies that exceed the beam accelerator energy. Clouds released in the ionosphere or magnetosphere may then directly excite optical emissions (aurora) in the upper atmosphere.

Both inside a cloud and in the plasma surrounding it, sec-

ondary and higher-order curved charge layers are generated extending out into the ambient plasma. These layers have been discussed qualitatively in terms of the acceleration of ambient and cloud electrons in the vicinity of lower-order layers. However, the characteristics in terms of spatial separation, expansion velocity into the ambient plasma, effects on cloud breakup, etc., have not been determined and will require longer-duration and more detailed simulations.

A cloud that is pushed suddenly across a magnetic field (or a neutral gas cloud that is instantaneously ionized) will initially radiate close to the cloud electron and ion hybrid frequencies. If the ionization is slow compared to the particle gyration period, particles will gyrate incoherently, and the radiation from the cloud will be of a smaller magnitude. Thus radiation at ion frequencies is more likely to be generated through a gyrophase-coherent process than radiation at electron frequencies. Even when particles are random in phase, electromagnetic radiation will be generated at the gyration frequencies. Our results indicate that a cloud where the polarization field is effectively shorted will be halted quickly and the particles will gyrate as individual particles with almost their full initial perpendicular velocity. Recent observations in the CRIT 1 sounding rocket experiment of the CIV process [*Brenning et al.*, 1991] included strong oscillations on the cloud ion cyclotron frequency and have been interpreted along the same lines as given above.

In addition to the radiation from internal currents, currents to the charge layers from the ambient plasma are expected to radiate. In the Earth's environment, the whistler mode should be generated through either Cherenkov resonance or cyclotron resonance. For the radiation to be significant, the cloud dimension perpendicular to the velocity (y direction) must be large compared to a perpendicular wavelength. In this case radiation should be observed as in artificial beam ejection experiments [*Gurnett et al.*, 1986] and naturally occurring beams in the auroral zone [*James*, 1976]. We note here that wave observations are potentially strong diagnostic tools for the probing of cloud dynamics provided the radiation aspects of clouds are well understood. The advantage is that the observations can be made from remote locations and do not need to be in situ.

Finally we point out the analogy of the electrodynamics of large conductors in space to cloud electrodynamics. For an insulated, perfect conductor with exposed conducting end surfaces, the total electrostatic potential difference distributed between the two end surfaces and the ambient plasma is $(\vec{v} \times \vec{B}) \cdot \vec{L}$, where $\vec{v}$ is the velocity of the conductor and $\vec{L}$ is the vector from one end of the conductor to the other. This is the same expression as (4), which was used to calculate the electrostatic potential of the electron charge layer. The electromagnetic radiation and the current systems generated in the ambient plasma as a result of large orbiting structures and large plasma clouds have therefore much in common. The radiation from large space structures have been studied by *Donohue et al.* [1991], current closure and radiation for large clouds have been treated analytically by *Borovsky* [1987], and current closure and wave generation for large space structures have been studied in laboratory plasma tanks by *Stenzel and Urrutia* [1990].

REFERENCES

Alfvén, H., *On the Origin of the Solar System*, Oxford at the Clarendon Press, London, 1954.

Arp, H., The persistent problem of spiral galaxies, *IEEE Trans. Plasma Sci.*, *PS-14*, 748, 1986.

Baker, D. N., T. A. Fritz, and P. A. Bernhard, A small-scale plasmoid formed during the May 13, 1985, AMPTE magnetotail barium release, *J. Geophys. Res.*, *94*, 17084, 1989.

Borovsky, J. E., Limits on the cross-field propagation of streams of cold plasma, *Phys. Fluids*, *30*, 2518, 1987.

Brenning, N., M. C. Kelley, J. Providakes, H. C. Stenbaek-Nielsen, and C. Swenson, Barium swarm: An ionospheric alternating current generator in CRIT I, *J. Geophys. Res.*, *96*, 9735, 1991.

Buneman, O., Symmetrical states and their breakup, in *Cross-Field Microwave Devices*, vol. 1, *Principle Elements of Cross-Field Devices*, edited by E. Okress, Academic, San Diego, Calif., 1961.

Buneman, O., C. W. Barnes, J. C. Green, and D. E. Nielsen, Review: Principles and capabilities of 3-d, E-M particle simulations, *J. Comput. Phys.*, *38*, 1, 1980.

Cai, D., O. Storey, and T. Neubert, Kinetic equilibria of plasma shear layers, *Phys. Fluids B*, *2*, 75, 1990.

Chapman, S., Idealized problems of plasma dynamics relating to geomagnetic storms, *Rev. Mod. Phys.*, *32*, 919, 1960.

Donohue, D. J., T. Neubert, and P. M. Banks, Estimating radiated power from a conducting tethered satellite system, *J. Geophys. Res.*, *96*, 21245, 1991.

Eccles, J. V., W. J. Raitt, and P. M. Banks, A numerical model of the electrodynamics of plasma within the contaminant gas cloud of the space shuttle orbiter at low Earth orbit, *J. Geophys. Res.*, *94*, 9049, 1989.

Galvez, M., Computer simulation of a plasma streaming across a magnetic field, *Phys. Fluids*, *30*, 2729, 1987.

Galvez, M., and J. E. Borovsky, The expansion of polarization charge layers into a magnetized vacuum: Theory and computer simulations, *Phys. Fluids B*, in press, 1992.

Galvez, M., G. Gisler, and C. Barnes, Computer simulations of finite plasma streams convected across a magnetized vacuum, *Phys. Fluids B*, *1*, 2516, 1989.

Gurnett, D. A., W. S. Kurth, J. T. Steinberg, P. M. Banks, R. I. Bush, and W. J. Raitt, Whistler-mode radiation from the Spacelab-2 electron beam, *Geophys. Res. Lett.*, *13*, 225, 1986.

Haerendel, G., Plasma transport near the magnetic cavity surrounding comet Halley, *Geophys. Res. Lett.*, *14*, 673, 1987.

James, H. G., VLF saucers, *J. Geophys. Res.*, *81*, 501, 1976

Katz, I., D. E. Parks, D. L. Cooke, and J. R. Lilley, Jr., Polarization of spacecraft generated plasma clouds, *Geophys. Res. Lett.*, *11*, 1115, 1984.

Kurth, W. S., and L. A. Frank, Spacelab 2 plasma diagnostics package, *J. Spacecr. Rockets*, *27*, 70, 1990.

Lindman, E. L., Free-space boundary conditions for the time dependent wave equation, *J. Comput. Phys.*, *18*, 66, 1975.

Livesey, W. A., and P. L. Pritchett, Two-dimensional simulations of a charge-neutral plasma beam injected into a transverse magnetic field, *Phys. Fluids B*, *1*, 914, 1989.

Mende, S. B., G. R. Swenson, S. P. Geller, J. H. Doolittle, G. Haerendel, A. Valenzuela, and O. H. Bauer, Dynamics of a

barium release in the magnetospheric tail, *J. Geophys. Res.*, *94*, 17063, 1989.

Mishin, E. V., R. A. Trueman, and V. Ya. Kapanitanov, Anomalous diffusion across the magnetic field-plasma boundary: The Porcupine artificial plasma jet, *J. Geophys. Res.*, *91*, 10183, 1986.

Okuda, H., and S. Hiroe, Diffusion of a plasma subject to neutral beam injection, *Phys. Fluids*, *30*, 1160, 1987.

Papadopoulos, K., On the physics of the critical ionization velocity phenomena, *Advances in Space Plasma Physics*, edited by B. Buti, p. 33, World Science, Singapore, 1985.

Papadopoulos, K., A. Mankofsky, and A. Drobot, Long-range cross-field ion-beam propagation in a diamagnetic regime, *Phys. Rev. Lett.*, *61*, 94, 1988.

Paterson, W. R., and L. A. Frank, Hot ion plasmas from the cloud of neutral gases surrounding the space shuttle, *J. Geophys. Res.*, *94*, 3721, 1989.

Peratt, A. L., J. Green, and D. Nielsen, Evolution of colliding plasmas, *Phys. Rev. Lett.*, *44*, 1767, 1980.

Perley, R. A., J. W. Drehner, and J. J. Cowan, The jets and filaments in Cygnus A, *Astrophys. J.*, *285*, L35, 1984.

Peter, W., and N. Rostoker, Theory of plasma injection into a magnetic field, *Phys. Fluids*, *25*, 730, 1982.

Pritchett, P. L., A three-dimensional simulation model for electron beam injection experiments in space, *J. Geophys. Res.*, *96*, 13781, 1991.

Reasoner, D. L., The chemical release mission of CRRES, *J. Spacecr. Rockets*, in press, 1992.

Roussel-Dupré, R., and R. H. Miller, Radiative properties of a plasma moving across a magnetic field, 1, Theoretical analysis, *Phys. Fluids B*, in press, 1992*a*.

Roussel-Dupré, R., and R. H. Miller, Radiative properties of a plasma moving across a magnetic field, 2, Numerical results, *Phys. Fluids B*, in press, 1992*b*.

Schmidt, G., Plasma motion across a magnetic field, *Phys. Fluids*, *3*, 961, 1960.

Stenzel, R. L., and J. M. Urrutia, Currents between tethered electrodes in a magnetized laboratory plasma, *J. Geophys. Res.*, *95*, 6209, 1990.

Torbert, R., Review of ionospheric CIV experiments, *Adv. Space Res.*, *10(7)*, 47, 1990.

Villasenor, J., and O. Buneman, Rigorous charge conservation for local electromagnetic field solvers, *Comput. Phys. Commun.*, in press, 1992.

Wickman, M., and S. Robertson, Cross field injection and trapping of a continuous plasma beam in a magnetic mirror, *Plasma Phys.*, *25*, 103, 1983.

Winglee, R. M., and P. L. Pritchett, Comparative study of cross-field and field-aligned electron beams in active experiments, *J. Geophys. Res.*, *93*, 5823, 1988.

Winske, D., Development of flute modes on expanding plasma clouds, *Phys. Fluids B*, *1*, 1900, 1989.

Yusef-Zudeh, F., M. Morris, and D. Chance, Large highly organized radio structures near the galactic center, *Nature*, *310*, 557, 1984.

O. Buneman, STAR Laboratory, Department of Electrical Engineering, Stanford University, Stanford, CA 94305-4055.

R. H. Miller and T. Neubert, Space Physics Research Laboratory, Department of Oceanic, Atmospheric and Space Sciences, University of Michigan, Ann Arbor, MI 48109-2143.

K.-I. Nishikawa, Department of Physics and Astronomy, University of Iowa, Iowa City, Iowa 52242-1479.

CUSTOMER'S PROOF

Solar Wind-Magnetosphere Interaction as Simulated by a 3-D EM Particle Code

Oscar Buneman, Torsten Neubert, and Ken-Ichi Nishikawa

Abstract— We present here our first results of simulating the solar wind-magnetosphere interaction with a new three-dimensional electromagnetic particle code. Hitherto such global simulations were done with MHD codes while lower-dimensional particle or hybrid codes served to account for microscopic processes and such transport parameters as have to be introduced ad hoc in MHD. Our kinetic model attempts to combine the macroscopic and microscopic tasks. It relies only on the Maxwell curl equations and the Lorentz equation for particles, which are ideally suited for computers. The preliminary results shown here are for an unmagnetized solar wind plasma streaming past a dipolar magnetic field. The results show the formation of a bow shock and a magnetotail, the penetration of energetic particles into cusp and radiation belt regions, and dawn-dusk asymmetries.

I. INTRODUCTION

THE solar wind interaction with the earth's magnetic fields gives rise to a number of important and intriguing phenomena, many of which are only partially understood. These include reconnection between the solar wind magnetic field at the day-side magnetopause and flux transfer events, the drag of the solar wind exerted on the magnetotail and associated instabilities at the magnetopause, plasma convection in the magnetosphere/ionosphere, and the generation of field-aligned current systems. Reviews of these and other phenomena can be found in [1]–[4]. The range of physical processes involved in the solar wind-magnetosphere system is quite overwhelming, and consequently a wide array of methods have been used to study these, ranging from detailed studies of select phenomena with the assumption of, for instance, a specific field geometry or set of boundary conditions, to fully three-dimensional simulations with less spatial resolution but self-consistent particle or field geometries and with no (little) influence of the boundary conditions.

The first three-dimensional (3-D), global magnetohydrodynamic (MHD) simulations of the solar wind-magnetosphere system were reported in [5]–[7]. Since then, global 3-D

MHD simulations have been used with some success to study a range of processes including reconnection in the tail [8]–[9], reconnection at the day-side magnetopause [10], the dependence on the interplanetary magnetic field (IMF) orientation of magnetospheric convection and field-aligned currents [11]–[13], the solar wind-magnetosphere-ionosphere current-voltage relationship [14], the self-excitation of auroral arcs [15], and the reconnection voltage between the closed geomagnetic field and the IMF as a function of the IMF clock angle [16].

In MHD codes the microprocesses are represented by statistical (macroscopic) constants such as diffusion coefficients, anomalous resistivity, viscosity, temperature, and the adiabatic constant. Recent studies have pointed out that results from MHD codes are sensitive to the choice of these parameters, as well as to the accuracy of the iteration scheme and have cast doubt on some results obtained in the past. Thus it has been found that in ideal MHD simulations using a high-precision code, no Kelvin-Helmholtz instability is generated along the magnetopause and there is no entry of mass, energy, and momentum through the magnetopause, contrary to conventional knowledge [17].

To include particle dynamics explicitly, a number of simulations have been performed using hybrid codes (fluid electrons, particle ions) and full particle codes in one and two dimensions. With such codes local problems have been investigated such as shocks formed in the solar wind as it encounters the magnetosheath [18]–[23] and the current layer at the day-side magnetopause [24]–[25]. Recently also global problems have been investigated in three dimensions with hybrid codes, namely the solar wind interaction with the day side of Venus [26] and the solar wind interaction with Mars and Venus [27].

With the model presented here, we intend to take the full step, namely the global simulation of the solar wind interaction with a planetary magnetic field using a particle code which contains the complete particle dynamics. As will be shown below, the advantage is that the model contains the complete physics. The price to be paid is that some scaling of plasma parameters must be done.

II. A NEW 3-D EM PARTICLE SIMULATION MODEL

Our code is a successor to the TRISTAN code [28], [29]. Its new features are that (1) Poisson's equation and Fourier transforms have been eliminated by updating the fields locally from the curl equations and depositing the particle currents according to charge-conserving formulas [30]; (2) radiating boundary conditions are applied to the fields using a first-order

Lindman approximation [31]; (3) filtering is done locally; (4) localization makes the code ideally suited to modern parallel machines which call for minimizing data paths; and (5) the code is in Fortran and is fully transportable: modest versions run on PC's and on workstations. In the past, the TRISTAN code has successfully simulated large-scale space plasma phenomena such as the formation of systems of galaxies [32]. The new version of the code has been applied to the study of the dynamics of low-β plasma clouds [33] and a tutorial on the code will appear in the proceedings of the ISSS-4 (International School of Space Simulation) held in Kyoto, Japan, in 1991 [34].

For the simulation of solar wind-magnetosphere interaction the following boundary conditions were used for the particles: (1) Fresh particles representing the incoming solar wind (in our test run unmagnetized) are continuously injected across the yz plane at $x = x_{min}$ with a thermal velocity plus a bulk velocity in the $+x$ direction; (2) thermal solar particle flux is also injected across the sides of our rectangular computation domain; and (3) escaping particles are arrested in a buffer zone and redistributed there more uniformly by making the zone conducting in order to simulate their escape to infinity. They are then written off.

For the fields, boundary conditions were imposed just outside these zones: radiation is prevented from being reflected back inward, following Lindman's ideas [31]. The lowest order Lindman approximation was found adequate: radiation at glancing angles was no problem. However, special attention was given to conditions on the edges of the computational box.

In order to bring naturally disparate time and space scales closer together in this simulation of phenomena dominated by ion inertia and magnetic field interaction, the natural electron mass was raised to 1/16 of the ion mass and the velocity of light was lowered to twice the incoming solar wind velocity. This means that charge separation and anomalous resistivity phenomena are accounted for qualitatively but perhaps not with quantitative certainty. Likewise, radiation related phenomena (e.g. whistler modes) are covered qualitatively only.

III. RESULTS OF FIRST TESTS

While on a CRAY-2, with 100 M word core memory, a 200^3 grid simulation with some 10 million particles would be possible in principle, our tests were run on the CRAY-YMP at NCAR using a modest 105 by 55 by 55 grid and only 200 000 electron-ion pairs. Initially, these fill the entire box uniformly and drift with a velocity $v_D = 0.5c$ in the $+x$ direction, representing the solar wind. The electron thermal velocity is $v_{th} = 0.02c$ while the magnetic field is initially zero. A circular current generating the dipole magnetic field is increased smoothly from 0 to a maximum value reached at time step 65 and kept constant at the value for the rest of the simulation. The center of the current loop is located at (40.5, 27.5, 28) with the current in the xy plane and the axis in the z direction. The initial expansion of the magnetic field cavity is found to expel a large fraction of the initial plasma. The solar wind density is about 0.7 electron-ion pairs per cell, the mass ratio is $m_i/m_e = 16$, and $\omega_{pe} \Delta t = 0.84$.

In Fig. 1 is shown the ion density in the center xz layer containing the dipole center at time step 785. (Data were recorded at 128 or 256 step intervals and while no fully steady state was approached, no major change was seen between steps 768 and 1024.) The ion density is color coded and the magnetic field component in the plane is shown with arrows at every third grid point. The magnitude of the field has been scaled in order to see the field direction for weak fields. Thus the length of the vectors is not a true representation of the field magnitude. The plasma is flowing through the simulation domain from left to right (low to high x values). In the process the dipolar field is compressed at the side facing the plasma wind and is extended to a long tail on the downwind side, just as the earth's magnetic field in the solar wind. Note, that in these simulations the current in the loop creating the dipole is such that the orientation of the dipole is opposite to that of the earth's field. Or, the orientation of the plane of representation is different for what is normally used, with the North Pole down and the South Pole up.

Some particles have entered the cusp regions, and on the downwind side (night side), particles have gathered on closed field lines in what could be equivalent to the radiation belt. The particles at the upwind magnetopause are forming a bow shock. The temperature of these particles is much elevated from the background temperature. Also seen upwind from the magnetopause is what could be a second shock or a foreshock. The magnitude of both shocks has a minimum at the subsolar point and is increasing to a maximum at some distance from the sun-earth line.

The current density associated with the electron and ion fluxes and the magnetic field are shown in Fig. 2. The current density component shown is perpendicular to the xz plane (J_y), with current into the plane (the positive y direction) colored red and current out of the plane colored blue. Again, the values are for the center layer containing the center of the dipole. The current densities have been determined from the y component of the particle fluxes at each cell in the layer.

The current system shown in Fig. 2 is equivalent to the Chapman-Ferraro current system of the earth. At the upwind, low-latitude magnetopause it runs in a direction which cancels the original magnetic field on the upwind side, and doubles the field at the downwind side. At the cusp regions the current changes polarity with the magnetic field, as expected. The magnetopause in the tail also has negative J_y, with a positive J_y in the neutral sheath. The current in the neutral sheath is carried by the very few particles located here.

The ion density and magnetic field in the yz plane are shown in Fig. 3. The values are those of the layer which contains the center of the dipole and the dipole axis. The direction of the solar wind is out of the plane toward the viewer. Note that the density is asymmetric, with more ions located at the left side. This is caused by ions grad-B drifting toward this side as they move around the magnetic obstacle. The current density J_z in the yz plane containing the dipole axis is shown in Fig. 4. The current is running in a belt around the dipole with a polarity that cancels fields on the outside, thereby creating a magnetopause.
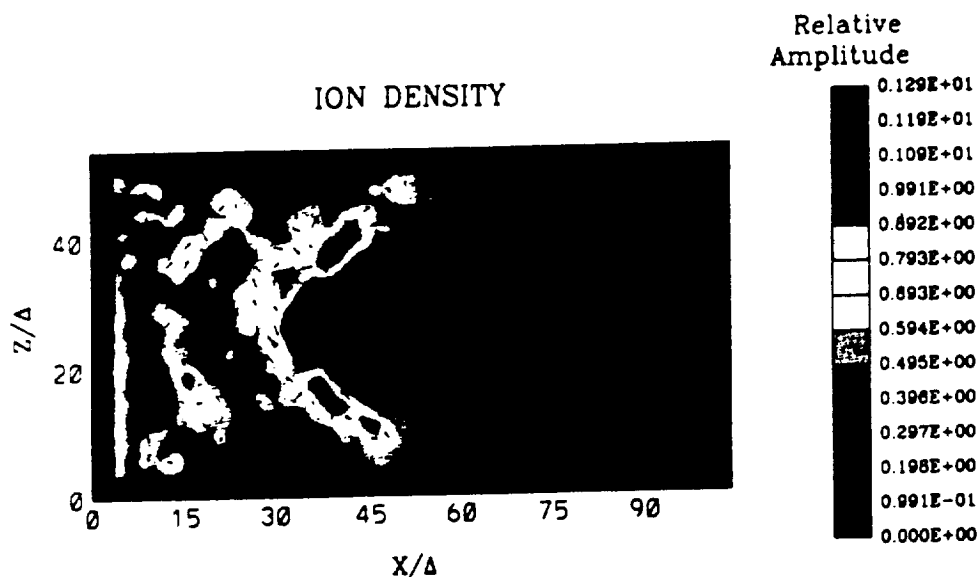
ION DENSITY

Fig. 1.   Ion density in the center xz layer containing the dipole center. "Relative amplitude" on color bar signifies simulation units.
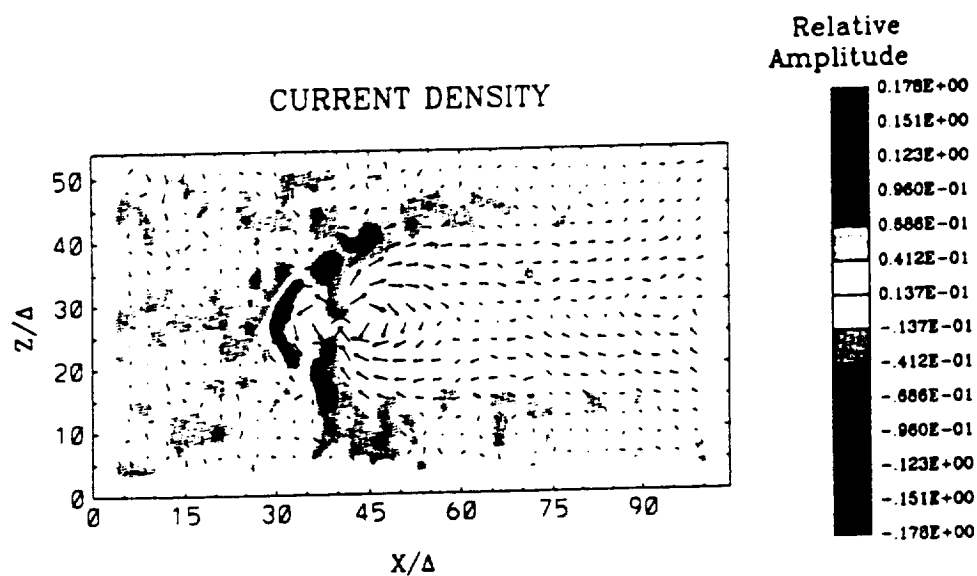
CURRENT DENSITY

Fig. 2.   Current density J_y in the center xz layer containing the dipole center. Positive currents flow into the plane and negative out of the plane.
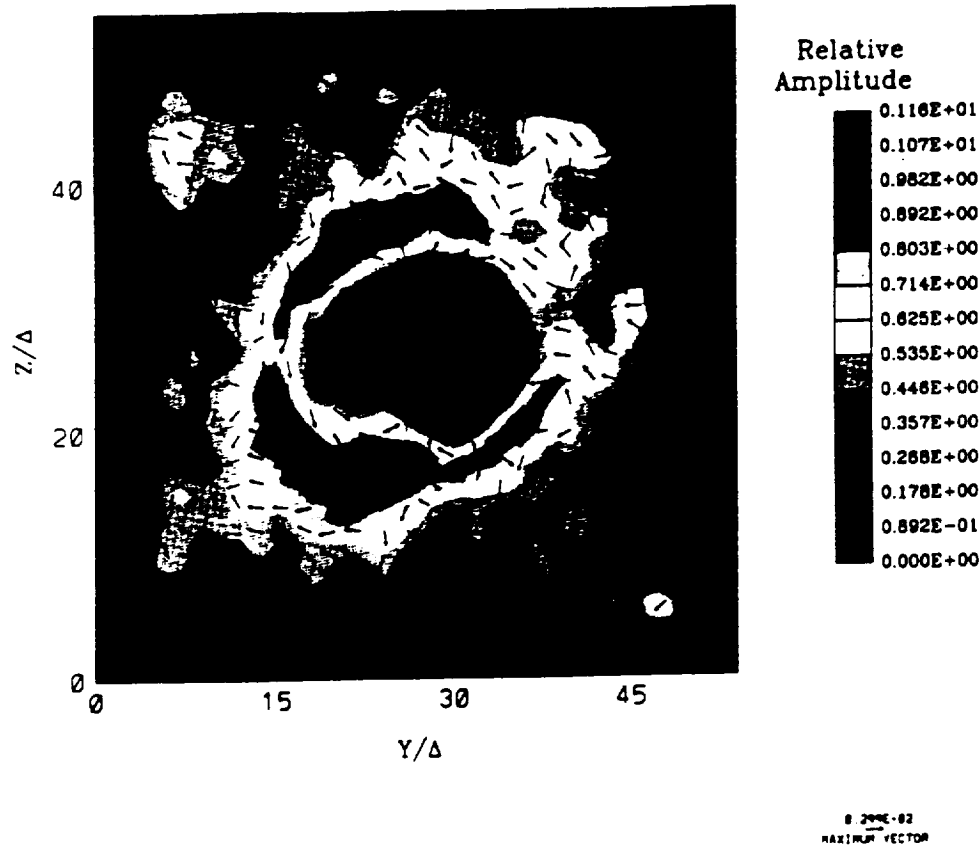
ION DENSITY

Fig. 3. Ion density in the center yz layer containing the dipole center.

Some key parameters are shown in Fig. 5 as functions of x, for center y and center z (sun-earth line). These are the ion density (top panel), the ion thermal pressure (second panel), the ion dynamic pressure (third panel), the magnetic pressure (fourth panel), and the ion Larmor radius (bottom panel). The magnetic field is small in the wind and in the tail, and rises to a peak at the location of the dipole center. Upwind, the increase is quite sudden and corresponds to the magnetopause. Upwind of the magnetopause, the density is high and some oscillations in the density are present here. The nature of these oscillations has not yet been investigated. At the magnetopause the density drops, but recovers and reaches a local maximum at $x = 39$. This maximum is associated with cusp particles that have penetrated to the center of the dipole (there is no planet to stop them). At $x = 46$ a second maximum is reached which correspond to the radiation belt-type particles mentioned earlier. Finally, the density increases slowly with distance in the tail.

The thermal pressure increases dramatically in a region upwind of the magnetopause. The location of this maximum corresponds to the location of the third of the three density maxima found upwind. Through the shock, the wind is slowed down, as seen by combining the plots of density and dynamic pressure. Thus the structures at the upwind side of the magnetopause bear much resemblance to the structures of the earth's bow shock. The ion Larmor radius has large variations with location, as does the magnetic field. In the wind and in the tail (we are in the neutral sheath) the Larmor radius is of the order of 10–30, with peaks in places where the magnetic field becomes small. The magnetic fluctuations in the tail are caused by the tail waving like a flag. (In regions of rapidly varying low field strength, "Larmor radius" loses its meaning.)

IV. DISCUSSION

The results presented in Figs. 1 through 5 show that even with the modest grid size of 105 by 55 by 55 cells, our 3-D fully kinetic model is able to generate the complete magnetosphere with its basic characteristics. This encourages us to continue our work using finer grids (larger array sizes) and including such features as an IMF, a tilt of the magnetic axis, and an inner conducting surface simulating the ionosphere. Larger dimensions will allow finer resolution of fields. The number of particles should also be increased. Longer runs would allow us to enhance realism by using smaller m_e/m_i and larger c/v_p. On presently available single processor computers the grid resolution could be increased by a factor of 3 in all dimensions. Multiprocessor machines in the future will allow even greater improvement, since the code allows simultaneous updating of many cells.

Some important issues that with advantage can be addressed with a kinetic code are as follows:
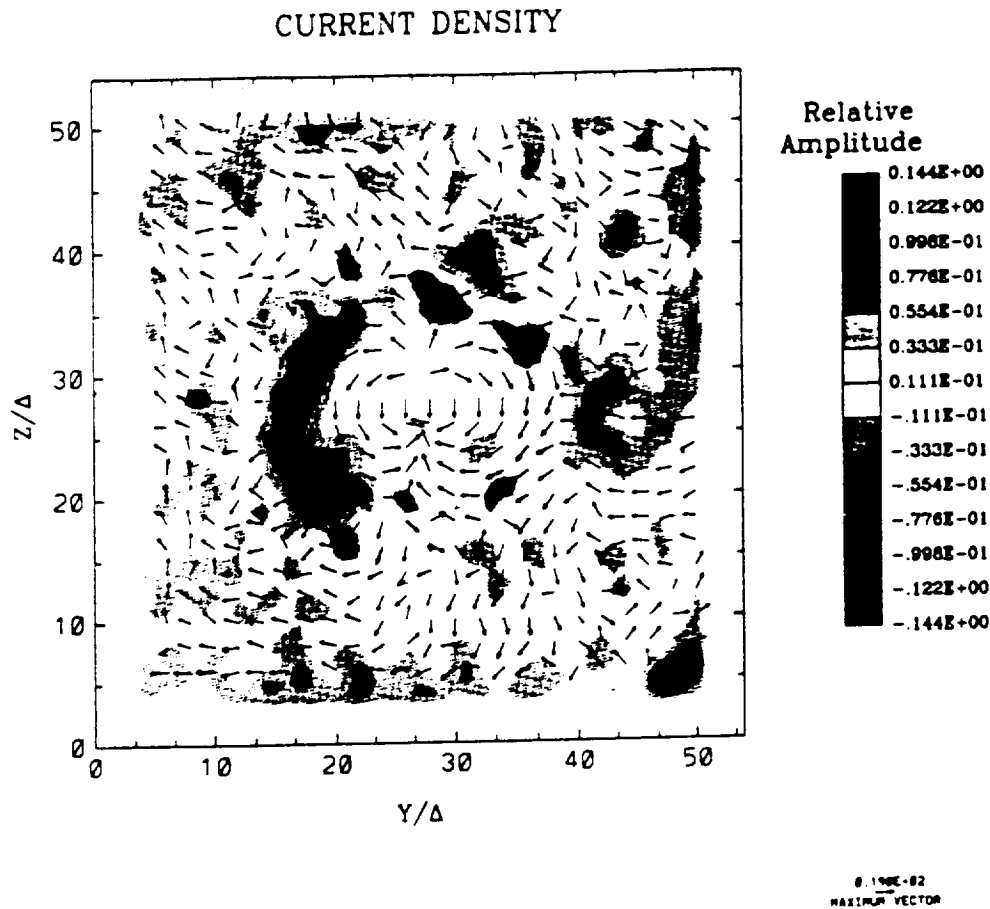
CURRENT DENSITY

Fig. 4. Current density J_x in the center yz layer containing the dipole center. Positive currents flow out of the plane and negative into the plane.

1) In MHD simulations reconnection phenomena are sometimes studied using artificial numerical dissipation to drive the process [16]. Furthermore, artificially high diffusion coefficients are often used in order to achieve a stable solution [11]. With a full kinetic code such problems may be addressed directly.

2) The motions of individual particles are tracked. In many regions of the magnetosphere, such as the magnetopause and the tail, gradients in the magnetic field are of such magnitude that the magnetic field changes significantly during a particle gyration. This gives rise to nonisotropic, non-Maxwellian distribution functions which drive the physics of those regions. The recent research into chaotic particle orbits in the magnetotail [35], [36] is an example. The complex particle motion gives rise to such phenomena as collisionless electron viscosity [37]–[39] and collisionless conductivity [40]. Furthermore, a particle code calculated the particle dynamics in self-consistent rather than model magnetic fields.

3) The complete wave dynamics from low-frequency magnetohydrodynamic modes (Kelvin–Helmholtz instabilities at the magnetopause and ULF pulsations) to electron waves (Langmuir oscillations) are included. An example where electron kinetics is important is illustrated by recent studies of the dynamics of the magnetopause

current layer [25] and the dynamics of expanding plasma clouds [41]. It is thought that a generalized lower hybrid drift instability is generated, which in the case of the magnetopause has the effect of broadening the current layer and causing filamentation of the current.

4) Any complicated magnetic field configuration can be simulated by a simple modification of the source current. This makes it straightforward to simulate not only other planetary magnetospheres such as that of Uranus, but also the effect of the diurnal rotation of the earth's dipole axis with respect to the direction to the sun.

Questions that need to be addressed in the future are those of scaling from the microworld of the simulation to the real macroworld, in particular, the scaling of the ion to electron mass ratio, the Larmor radii, and the Debye length to the earth's radius or other characteristic dimensions. An example is that in our simulation the Debye length is a significant fraction of the earth's radius or the thickness of the bow shock. The earth's radius itself can be determined by the distance from the dipole center to the upwind magnetopause. This distance is typically equal to ten earth radii. In the test simulation described earlier an earth radius is of the order of one grid spacing.

However, some form of scaling is usually needed in particle simulations, even in one and two dimensions, and still such simulations are able to reveal much of the physics behind
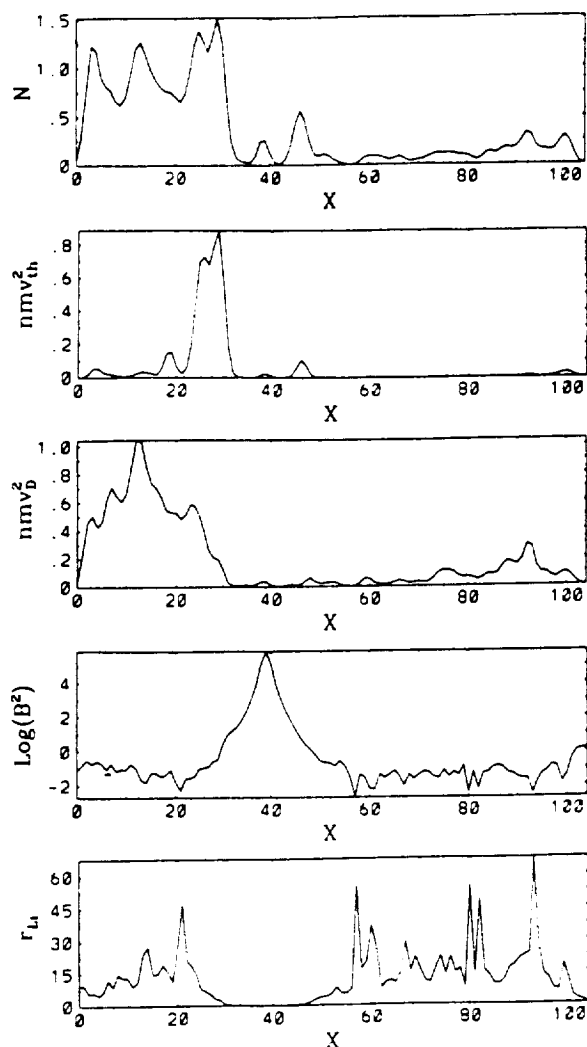
6

Fig. 5. Key parameters as a function of x at center y and center z (along the sun-earth line). From top to bottom are: density, the thermal pressure, the dynamic pressure, the magnetic pressure, and the ion Larmor radius.

natural phenomena. Similar problems are also encountered, and to some degree overcome, in laboratory plasma simulations of macroscale space plasma phenomena. Examples include the study of magnetic field line reconnection [42], [43] and the interaction of a magnetized plasma flow with a dipole magnetic field [44]. We propose, therefore, that a kinetic particle model will be a useful tool for the study of the earth's and other planetary magnetospheres in the solar wind, by supplementing present models that do not contain the complete particle dynamics.

REFERENCES

[1] G. Haerendel and G. Paschmann, *Magnetosphere Plasma Physics*, A. Nishida, Ed. Dordrecht: Reidel Publishing, 1982.
[2] R. C. Elphic, *Rev. Geophys.*, vol. 25, p. 510, 1987.
[3] C. Y. Huang, *Rev. Geophys.*, vol. 25, p. 529, 1987.
[4] B. H. Mauk and L. J. Zanetti, *Rev. Geophys.*, vol. 25, p. 541, 1987.
[5] S. H. Brecht, J. Lyon, J. A. Fedder, and K. Ham, *Geophys. Res. Lett.*, vol. 8, p. 397, 1981.
[6] J. N. Leboeuf, T. Tajima, C. F. Kennel, and J. M. Dawson, *Geophys. Res. Lett.*, vol. 8, p. 257, 1981.
[7] C. C. Wu, R. J. Walker, and J. M. Dawson, *Geophys. Res. Lett.*, vol. 8, p. 523, 1981.
[8] S. H. Brecht, J. G. Lyon, J. A. Fedder, and K. Ham, *J. Geophys. Res.*, vol. 87, p. 6098, 1982.
[9] R. J. Walker, T. Ogino, and M. Ashour-Abdalla, *Magnetotail Physics*, A. T. Y. Lui, Ed. Baltimore, MD: Johns Hopkins University Press, 1987, p. 183.
[10] T. Sato, T. Shimida, M. Tanaka, T. Hayashi, and K. Watanabe, *Geophys. Res. Lett.*, vol. 13, p. 801, 1986.
[11] T. Ogino, R. J. Walker, M. Ashour-Abdalla, and J. M. Dawson, *J. Geophys. Res.*, vol. 90, p. 10553, 1985.
[12] T. Ogino, R. J. Walker, M. Ashour-Abdalla, and J. M. Dawson, *J. Geophys. Res.*, vol. 91, p. 10029, 1985.
[13] T. Ogino, *J. Geophys. Res.*, vol. 91, p. 6791, 1986.
[14] J. A. Fedder and J. G. Lyon, *Geophys. Res. Lett.*, vol. 14, p. 880, 1987.
[15] K. Watanabe and T. Sato, *Geophys. Res. Lett.*, vol. 15, p. 717, 1988.
[16] J. A. Fedder, C. M. Mobarry, and J. G. Lyon, *Geophys. Res. Lett.*, vol. 18, p. 1047, 1991.
[17] K. Watanabe and T. Sato, *J. Geophys. Res.*, vol. 95, p. 75, 1990.
[18] K. B. Quest, *J. Geophys. Res.*, vol. 93, p. 9649, 1988.
[19] D. Burgess, *Geophys. Res. Lett.*, vol. 16, p. 345, 1989.
[20] N. Omidi, K. B. Quest, and D. Winske, *J. Geophys. Res.*, vol. 95, p. 20717, 1990.
[21] V. A. Thomas, D. Winske, and N. Omidi, *J. Geophys. Res.*, vol. 95, p. 18809, 1990.
[22] V. A. Thomas and D. Winske, *Geophys. Res. Lett.*, vol. 17, p. 1247, 1990.
[23] D. N. Winske, N. Omidi, K. B. Quest, and V. A. Thomas, *J. Geophys. Res.*, vol. 95, p. 18821, 1990.
[24] S. Gary and A. G. Sgro, *Geophys. Res. Lett.*, vol. 17, p. 909, 1990.
[25] J. Berchem and H. Okuda, *J. Geophys. Res.*, vol. 95, p. 8133, 1990.
[26] K. R. Moore, V. A. Thomas, and D. J. McComas, *J. Geophys. Res.*, vol. 96, p. 7779, 1991.
[27] S. H. Brecht and J. R. Ferrante, *J. Geophys. Res.*, vol. 96, p. 11209, 1991.
[28] O. Buneman, C. W. Barnes, J. C. Green, and D. E. Nielsen, *J. Comput. Phys.*, vol. 38, p. 1, 1980.
[29] A. L. Peratt, J. Green, and D. Nielsen, *Phys. Rev. Lett.*, vol. 44, p. 1767, 1980.
[30] J. Villasenor and O. Buneman, *Comp. Phys. Comm.*, in press, 1992.
[31] E. L. Lindman, *J. Comp. Phys.*, vol. 18, p. 66, 1975.
[32] A. L. Peratt, *IEEE Trans. Plasma Sci.*, vol. 14, p. 639, 1986; also A. L. Peratt, *IEEE Trans. Plasma Sci.*, vol. 14, p. 763, 1986.
[33] T. Neubert, R. H. Miller, O. Buneman, and K.-I. Nishikawa, *J. Geophys. Res.*, vol. 97, p. 12057, 1992.
[34] O. Buneman, *Proc. ISSS-4* (Kyoto, Japan), 1992.
[35] J. Chen, P. Palmadesso, *J. Geophys. Res.*, vol. 91, p. 1499, 1986.
[36] G. R. Burkhart and J. Chen, *J. Geophys. Res.*, vol. 96, p. 14033, 1991.
[37] J. W. Dungey, *European Space Agency Special Report*, vol. ESA SP-285 (II), p. 15, 1988.
[38] B. U. O. Sonnerup, *Comput. Phys. Commun.*, vol. 49, p. 143, 1988.
[39] L. R. Lyons and D. C. Pridmore-Brown, *J. Geophys. Res.*, vol. 95, p. 20903, 1990.
[40] W. Horton and T. Tajima, *J. Geophys. Res.*, vol. 96, p. 15811, 1991.
[41] D. Winske, *J. Geophys. Res.*, vol. 93, p. 2539, 1988.
[42] W. Gekelman and R. L. Stenzel, *J. Geophys. Res.*, vol. 89, p. 2715, 1984.
[43] W. Gekelman and H. Pfister, *Phys. Fluids*, vol. 59, p. 2017, 1988.
[44] H. U. Rahman, G. Yur, R. S. White, J. Birn, and F. J. Wessel, *J. Geophys. Res.*, vol. 96, p. 7823, 1991.

Torsten Neubert was born in Copenhagen, Denmark, on August 16, 1950. He received the M.Sc. degree in electronic engineering from the Technical University of Denmark in 1976, and in 1981 the Ph.D. degree from the University of Copenhagen for studies carried out at the Danish Space Research Institute.

After his thesis work, he continued at the Danish Space Research Institute, studying natural and spacecraft induced plasma wave and particle phenomena. In 1984 he joined the Space Telecommunications and Radioscience Laboratory at Stanford University, first as a postdoctoral fellow and, in 1987, as an Associate Research Scientist. At Stanford he studied plasma wave radiation and particle dynamics as observed in active electron beam, plasma and neutral gas ejection experiments flown on the space shuttle (STS-3, Spacelab 1 and 2) and on sounding rockets (CHARGE-2). In 1990 he accepted a position as Associate Research Scientist at the Space Physics Research Laboratory, University of Michigan, where he continues studies related to active experiments. His current interests include PIC simulations of electron beams and plasma flows.

Dr. Neubert is a member of the American Geophysical Union.

Ken-Ichi Nishikawa was born in Shiga-ken, Japan, on April 27, 1949. He received the B.S., M.S., and Ph.D. degrees in theoretical plasma physics from Nagoya University, Nagoya, Japan, in 1973, 1975, and 1981, respectively.

After completing his degree, he studied particle simulations with space plasma physics applications with Hideo Okuda at the Princeton Plasma Physics Laboratory for two years. In 1984 he joined the Department of Physics and Astronomy, University of Iowa, as an assistant research scientist, and he became an associate research scientist in 1990. He has investigated several topics based on the observations available at Iowa City using 2-D electrostatic and 3-D magnetostatic particle codes. Recently, he has worked to develop a 3-D electromagnetic particle code with Oscar Buneman and Torsten Neubert. Based on his experience with a 3-D magnetostatic particle code he has been investigating several topics using the newly developed 3-D electromagnetic code.

Simulation of electron beam-driven instabilities by a 3-D electromagnetic particle code

by

K.-I.Nishikawa, O. Buneman, and T. Neubert
(submitted to GRL)

Abstract We have restudied electron beam driven whistler waves with a 3-D electromagnetic particle code. In the initialisation of the beam-plasma system, "quiet start" conditions were approached by including the poloidal magnetic field due to the current carried by beam electrons streaming along a background magnetic field. The simulation show electromagnetic whistler wave emissions and electrostatic beam modes like those observed in the Spacelab 2 electron beam experiment. It has been suggested in the past that the spatial bunching of beam electrons associated with the beam mode may directly generate whistler waves. However, the simulation results indicate several inconsistencies with this picture: (1) the parallel (to the background magnetic field) wavelength of the whistler wave is longer than that of the beam instability, (2) the parallel phase velocity of the whistler wave is smaller than that of the beam mode, and (3) whistler waves continue to be generated even after the beam mode space charge modulation looses its coherence. The complex structure of the whistler waves in the vicinity of the beam suggest that the transverse velocity (gyration) of the beam electrons in the combined poloidal and background magnetic fields is involved in the generation of the whistler waves.

1. Introduction

During the Spacelab 2 flight, launched on July 29, 1985, a spacecraft called the Plasma Diagnostics Package (PDP) performed a fly-around of the shuttle at distance of up to 300 meters while an electron beam was being ejected from the shuttle in a steady (d.c.) mode [*Gurnett et al.*, 1986]. The plasma waves observed as the PDP approached and crossed through the beam took the appearance of a well-defined, funnel-shaped feature when displayed on frequency-time spectrograms. The waves were observed over a broad frequency range extending up to the electron cyclotron frequency ($f_c \approx 1$ MHz) with the center of the funnel coinciding with the passage through the beam. The mode was identified as the whistler mode, propagating with the wave normal close to the resonance cone. At even higher frequencies (3.1 MHz), intense narrowband emissions were observed inside the beam. These emissions are believed to be either at the local electron plasma frequency, f_p or the upper hybrid resonance frequency, $f_{UHR} = (f_c^2 + f_p^2)^{1/2}$ [*Gurnett et al.*, 1986].

The generation of whistler waves by natural and artificially injected electron beams has been studied extencively in the past by means of space experiments, analytical theories, and particle simulations. A review of recent work is given by *Neubert and Banks* [1992]. However, the relationship between the electrostatic beam mode (bunched beam electrons) and the whistler waves is not yet clearly understood. The early work by *Bell* [1968] proposed that Langmuir turbulence in natural auroral electron beams provided a means for quasi-coherent Cherenkov radiation needed to explain the relatively high level of whistler

1

wave radiation observed in the auroral regions. In the Spacelab-2 experiment it was also found that some mechanism creating quasi coherence was needed to explain the observed signal levels. Employing 1-dimensional electrostatic particle simulations, *Farrell et al.* [1989] found that Langmuir turbulence in the beam created a spatial modulation of the current structure, and therefore enhanced the the ability of the beam to radiate. The estimates of the radiation levels based on the simulations were found to be in good agreement with observed levels of radiation. Electromagnetic simulations in 2 dimensions confirmed this picture [*Pritchett et al.*, 1989]. Here it was found that even with no initial net current (background electrons drift opposite to beam electrons thereby providing a return current to a spacecraft), instabilities are generated inside the beam creating a current structure which allow for the radiation of electromagnetic waves.

The outstanding question is really the generation mechanism of the radiating current structure, its dynamics, and how it depends on ambient and beam plasma conditions. Several studies have appeared which imply that the simple picture of an electron beam, space charge modulated by Langmuir turbulence, is not the means through which whistler radiation is generated, although it may be an important "seed" mechanism to get the process started. These works include *Goerke et al.* [1990] who, in a sounding rocket experiment, found no evidence to support the hypothesis that electrostatic bunching at the plasma frequency was responsible for the enhancement of the whistler mode radiation. Furtheremore, simulation results have pointed out that the wavelength of the electrostatic beam turbulence differs from the wave length of the whistler wave [*Omura and Matsumoto*, 1988a].

In this work we attempt to establish more insight into the generation mechanism of whistler waves using a newly developed 3-dimensional, electromagnetic, and relativistic particle code [*Buneman*, 1992; *Buneman et al*, 1992; *Neubert et al.*, 1992]. It extends the 3-dimensional simulations of *Nishikawa et al.* [1989] by using a larger system, by including all components of the magnetic fields as well as relativistic effects, and by including a self-consistent poloidal magnetic field as an initial condition.

2. Simulation Results

The system size used for the simulations is $L_x = L_y = 85\Delta, L_z = 160\Delta$, where L_x, L_y, and L_z are the lengths of the system in the three dimensions and $\Delta(= 1)$ is the grid size. Periodic boundary conditions are used along the ambient magnetic field (z-direction), while radiating boundary conditions [*Lindman*, 1975] are used in the x- and y-directions.

The electron beam is initially in a column with radius, $r_{eb} = 4.47\Delta$, and the axis at the center of the domain ($x = y = 43$) oriented in the z-direction. The plasma density within the beam column is the same as outside and the beam is initially

charge neutral. The location of beam electrons within the column are randomly chosen and is about half of the total electron density. The total number of beam electrons is 4899. The beam drift velocity, $V_d = 3.5v_{et}$, where v_{et} is the electron thermal velocity. The beam electron temperature, $T_{eb} = 0.09T_e$, where T_e is the temperature of the background electrons. In this study the ion drift velocity, V_i is zero. To approximately simulate ionospheric conditions we chose the following parameters: $m_i/m_e = 64$, $T_e/T_i = 1$, $\Omega_e/\omega_{pe} = 0.4$, $c/v_{et} = 10.67$, $\omega_{pe}\Delta t = 0.10$, $\beta = 0.111$, $\lambda_{De} = 0.469\Delta$, $\rho_e = 1.17$, $\rho_i = 9.38$, $c/\omega_{pe} = 5.00$.

As a new feature, quiet start conditions are achieved by including an initial poloidal magnetic field (IPMF) consistent with the current J_z carried by the beam electrons at $t = 0$. The IPMF is calculated from the curl of the vector potential, $\mathbf{A}$, where $\mathbf{A} = (0, 0, A_z)$ and A_z is given by,

$$A_z(i, j) = A_{zo} \log(r^2/r_{eb}^2); r \geq r_{eb} , \qquad (1)$$

$$A_z(i, j) = A_{zo}(\log(1.0) + r^2/r_{eb}^2 - 1.0); r < r_{eb} , \qquad (2)$$

where $A_{zo} = -J_z/(4\pi c)$, r is the radius from the beam column axis, and J_z is the current in the column.

As mentioned earlier, *Pritchett et al.* [1989] also simulated a quiet start ($J_z = 0$). A quiet start avoids a transient stage where a strong return current is induced as reported by *Omura and Matsumoto* [1988a,b].

In Figure 1a, B_x, B_y (with the IPMF subtracted) is shown in the center plane perpendicular to the beam axis at $\omega_{pe}t = 25.6$. The length of the vectors have been scaled to enhance weaker signals in order to better illustrate the field structure. A complicated wave pattern resembling a honeycomb structure is seen rather than simple concentric wave fronts. This structure oscillates in time (not shown) constituting an outward propagating electromagnetic wave.

Figure 1 b shows the magnetic field components B_x, B_z in the center (x, z) plane. The ambient magnetic field B_{zo} has been subtracted. Waves are clearly created near the beam and propagating out in a complicated manner. If the parallel current is uniform, as for the initial conditions, the values of B_x, B_z should be zero in this plane. The fact that these components take on finite values in the center of the beam leads to the idea that a spiral structure of the current is produced in addition to the current along the z-direction, as will be discussed below. Obviously, the B_z - component is created by the electron motions perpendicular to the ambient magnetic field, which also creates transverse electric fields E_x, E_y. This is essential to whistler waves.

The beam electrons in phase space $z - v_z$ is shown in Figure 2a. The electrons are bunched, accelerated, and decelerated,

fundamentally due to the excited electrostatic waves. The background electrons, initially in the column, also show bunching and acceleration in and around the beam column (not shown). As a result, a perturbed current structure is generated which acts like an antenna and emits whistler waves as suggested by [*Farrell et al.*, 1989; *Pritchett et al.*, 1989; *Wong and Lin*, 1990]. The J_z-component of the current is shown in Figure 2b. However, new to our study is that altough the beam initially was directed along the ambient magnetic field with no transverse component, transverse motion (J_x, J_y) develop which are essential to the whistler wave generation.

The time evolution of the charge density and the magnetic field component B_x along the beam axis is illustrated in Figure 3. The charge density shows sporadic waves structures propagating in the beam direction (towards larger z). The phase velocity is of the order of $2.6v_{et}$ for $12 < \omega_{pe}t < 21$. The averaged drift velocity of the beam electrons varies at the same time from $3.26v_{et}$ to $2.56v_{et}$. The phase velocity of the wave is less than but of the order of the averaged drift velocity. Therefore, this wave is excited by the beam electrons and is identified as a beam mode. On the other hand, the magnetic field component B_x, which represent a whistler wave, shows a longer wavelength and a more clear coherent structure. The phase velocity is about $2.22v_{et}$ for the same time period, which is slower than for the beam mode.

The space charge modulation at the earlier time $(\omega_{pe}t < 10)$ does not excite whistler waves. From this fact we may draw the idea that the bunching of beam electrons becomes the seed of the excitation of whistler waves, and only when the electrons are affected by the poloidal magnetic field, which create a transverse velocity, are whistler waves excited. This process was first suggested by *Bell and Buneman* [1964].

Although difficult to conclude from Figure 3a, a closer inspection of the simulation results indicate that the space charge oscillations later get randomized while whistler waves continue to be generated. This means that the whistler wave and the beam mode are well separated, a conclusion reached also by *Omura and Matsumoto* [1988a] and *Goerke et al.*, [1990], as mentioned earlier. It is also consistent with the idea that the self-quenching of the electrostatic instability by creation of an enhanced (turbulent) velocity spread may still allow the whistler mode to take over eventually [*Bell and Buneman*, 1964]. *It suggests that some current structure still exist in the 3-dimensional system (helically).*

In Figure 4 the accumulated spectra along the x direction is plotted for the magnetic field component B_x. The color scale is logarithmic in wave intensity. High-intensity waves are seen below the hybrid frequency within the electron beam, and lower intensity whistler waves below the electron cyclotron frequency propagateing outside the beam.

The dispersion of the electromagnetic waves just outside of the beam column is shown in Figure 5. The plot has been created by performing a 2-dimensional Fourier transformation

(one space and one time) of B_x along the z-direction for the first 512 time steps. The whistler branch extents from the origin toward the horizontal line at the electron cyclotron frequency Ω_e with additional, lower amplitude radiation generated at higher frequencies along a line with a slope corresponding to the velocity of light.

3. Discussion

We have attempted to establish a clearer picture of the generation mechanism of whistler waves. The simulation results show an electrostatic mode contained within the beam collumn and whistler emissions propagating from the beam into the ambient plasma. These results agree qualitatively with observations obtained by PDP during the Spacelab 2 mission. As expected, the simulation results have many similarities with those of previous 1- and 2-dimensional simulations. The initial homogenous parallel current is perturbed through the beam mode, developing spatial inhomogeneities, which stimulate whistler radiation [*Farrell et al.*, 1989; *Pritchett et al.*, 1989]. On the other hand, we found that the beam mode is well separated from the whistler mode as also pointed out by 2-dimensional simulations [*Omura and Matsumoto*, 1988a] and sounding rocket experiments *Goerke et al.* [1990].

Because the beam mode must be instrumental in the perturbation of the beam current, we are faced with the challenge of unifying seemingly contradictory evidence. We suggest a solution along the lines first discussed by *Bell and Buneman* [1964]. Here it was found that a spread in the beam electron velocity in the transverse direction leads to an instability of the stream-plasma system in the whistler mode, with the transverse electron gyrations serving as an energy source. As shown in Figure 1b, the magnetic componenet B_z is produced by the transverse electron motion which is consistent with this finding.

While the electrostatic modes are saturated and quenched due to the slowdown and heating of beam electrons (around $\omega_{pe}t = 25$), whistler waves are still being excited. At this stage the bunching of beam electrons has disappeared in the $z - v_z$ phase space. Phase mixing through longitudinal velocity spread can suppress the electrostatic instability without suppressing whistler growth as pointed out by *Bell and Buneman* [1964]. Therefore, a 3-dimensional spiral bunching structure of the beam (background) electrons may be responsible for this prolonged excitation of the whistler mode. Further discussions will be reported in a separate publication.

References

Bell, T. F. and O. Buneman, Plasma instability in the whistler mode cased by a gyrating electron stream, *Phys. Rev., 133*, A1300, 1964.

Buneman, O., TRISTAN: The 3-D E-M Particle Code, *Proceeding of ISSS-4*, Kyoto, Japan, 1992 (in press).

Buneman, O., T. Neubert, and K.-I. Nishikawa, Solar-wind-magnetosphere interaction as simulated by a 3D, EM particle code, accepted to *IEEE Trans Plasma Sci.*, 1992.

Farrell, W. M., D. A. Gurnett, P. M. Banks, R. I. Bush, and W. J. Raitt, An analysis of whistler-mode radiation from the Spacelab-2 electron beam, *J. Geophys. Res., 93*, 153, 1988.

Farrell, W. M., D. A. Gurnett, and C. K. Goertz, Coherent Cerenkov radiation from the Spacelab 2 electron beam, *J. Geophys. Res., 94*, 443, 1989.

Goerke, R. T., P. J. Kellogg, and S. J. Monson, An analysis of whistler mode radiation from a 100 mA electron beam, *J. Geophys. Res., 95*, 4277, 1990.

Gurnett, D. A. W. S. Kurth, J. J. Steinberg, P. M. Banks, R. I. Bush, and W. T. Raitt, Whistler-mode radiation from the Spacelab 2 electron beam, *Geophys. Res. Lett., 13*, 225, 1986.

Lindman, E. L., Free-space boundary conditions for the time dependent wave equation, *J. Comput. Phys., 18*, 66, 1975.

Neubert, T. and P. Bsnks, Recent results from studies of electron beam phenomena in space plasmas, *Planet. Space Sci., 40*, 153, 1992.

Neubert, T., R. H. Miller, O. Buneman, and K.-I. Nishikawa, The dynamics of low$-\beta$ plasma clouds as simulated by a 3-dimensional, electromagnetic particle code, *J. Geophy. Res., 97*, 12,057, 1992.

Nishikawa, K.-I., L. A. Frank, and C. Y. Huang, Three-dimensional simulation of whistler mode excited by the Spacelab 2 electron beam, *J. Geophys. Res., 94*, 6855, 1989.

Omura, Y. and H. Matsumoto, Computer experiments on whistler and plasma wave emissions for Spacelab-2 electron beam, *Geophys. Res. Lett., 15*, 319, 1988a.

Omura, Y. and H. Matsumoto, Electromagnetic and electrostatic emissions from a thin electron beam in space plasma, in *Numerical Simulation of Space Plasma* edited by B. Lembège and J. W. Eastwood, p. 133, North-Holland, Amsterdam, 1988b.

Pritchett, P. L. H. Karimabadi, and N. Omidi, Generation mechanism of whistler waves produced by electron beam injection in space, *Geophys. Res. Lett., 16*, 883, 1989.

Winglee, R. M. and P. J. Kellogg, Electron beam injection during active experiments 1. Electromagnetic wave emissions, *J. Geophys. Res., 95*, 6167, 1990.

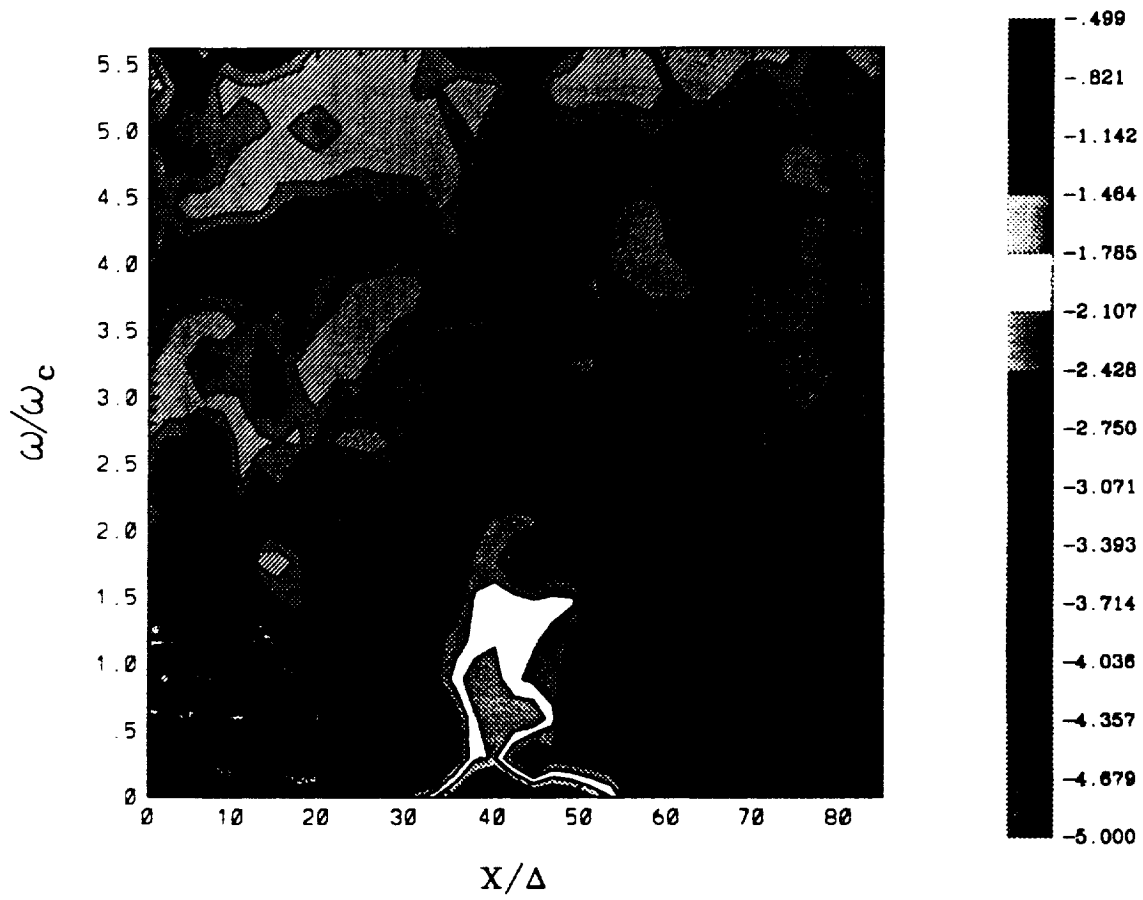Wong, H. K. and C. S. Lin, Plasma instabilities of a finite-radius electron beam in a uniform plasma, *Radio Sci., 25*, 277, 1990.

(a)

(b)

BXCX DISPERSION

Fig. 4

BXSZ DISPERSION

Fig. 5

Fig. 2